1. Report No.	2. Government Accession No.	3. Recipient's Catalog No.
FHWA/TX-10/0-5106-3		

4. Title and Subtitle	5. Report Date
LABORATORY AND FIELD EVALUATION OF CONCRETE PAVING CURING EFFECTIVENESS	November 2008 Published: December 2009
	6. Performing Organization Code
7. Author(s)	8. Performing Organization Report No.
Dan Ye, Anal Mukhopadhyay, and Dan G. Zollinger	Report 0-5106-3
9. Performing Organization Name and Address	10. Work Unit No. (TRAIS)
Texas Transportation Institute The Texas A&M University System College Station, Texas 77843-3135	11. Contract or Grant No. Project 0-5106
12. Sponsoring Agency Name and Address	13. Type of Report and Period Covered
Texas Department of Transportation Research and Technology Implementation Office P. O. Box 5080 Austin, Texas 78763-5080	Technical Report: September 2003-August 2006
	14. Sponsoring Agency Code

15. Supplementary Notes

Project performed in cooperation with the Texas Department of Transportation and the Federal Highway Administration.
Project Title: Evaluation of Curing Membrane Effectiveness to Reduce Evaporation
URL: http://tti.tamu.edu/documents/0-5106-3.pdf

16. Abstract

Ensuring that sufficient water is available in hydrating concrete is of great importance to produce durable concrete and achieve both short- and long-term performance of concrete pavement. Excessive early-age evaporation from the surface of concrete pavement often results in high porosity delaminated and low strength concrete. Application of curing compounds in concrete paving is widely used to minimize evaporation. However, the Texas Department of Transportation (TxDOT) standard specifications for pavement construction (Item 526) only defines the use of the membrane curing in terms of key characteristics such as percent solids, density, viscosity, color, and the application rate, but does not specify curing performance or limits on the rate of evaporation.

This research utilized several techniques to evaluate curing effectiveness from both a moisture retention and physical properties standpoint, to develop a laboratory-based curing evaluation protocol that has application to the field.

A series of tests were carried out to identify factors controlling curing quality under field conditions.

17. Key Words	18. Distribution Statement
Curing Evaluation Method, Portland Cement Concrete Pavement, Moisture, Physical Properties	No restrictions. This document is available to the public through NTIS: National Technical Information Service Springfield, Virginia 22161 http://www.ntis.gov

19. Security Classif. (of this report)	20. Security Classif. (of this page)	21. No. of Pages	22. Price
Unclassified	Unclassified	196	

LABORATORY AND FIELD EVALUATION OF CONCRETE PAVING CURING EFFECTIVENESS

By

Dan Ye
Graduate Assistant Research
Texas Transportation Institute

Anal Mukhopadhyay
Associate Research Scientist
Texas Transportation Institute

and

Dan G. Zollinger
Associate Research Engineer
Texas Transportation Institute

Report 0-5106-3
Project 0-5106
Project Title: Evaluation of Curing Membrane Effectiveness to Reduce Evaporation

Performed in cooperation with the
Texas Department of Transportation
and the
Federal Highway Administration

November 2008
Published: December 2009

TEXAS TRANSPORTATION INSTITUTE
The Texas A&M University System
College Station, Texas 77843-3135

DISCLAIMER

The contents of this report reflect the views of the authors, who are responsible for the facts and the accuracy of the data presented herein. The contents do not necessarily reflect the official view or policies of the Texas Department of Transportation and/or the Federal Highway Administration. This report does not constitute a standard, specification, or regulation. The engineer in charge of the project was Dan G. Zollinger, Texas P.E. #67129.

TxDOT does not have plans to implement the test procedure developed in this research project at this time.

.

ACKNOWLEDGMENTS

The authors wish to express their appreciation to the Texas Department of Transportation personnel for their support throughout this project, as well as the Federal Highway Administration. We would also like to thank the project director Maureen Wakeland and the members of the project monitoring committee, Jennifer Moore, Johnny Miller, and Dennis Warren for their valuable technical comments during this project.

TABLE OF CONTENTS

Page

TABLE OF CONTENTS (continued)

Page

TABLE OF CONTENTS (continued)

LIST OF FIGURES

LIST OF FIGURES (continued)

LIST OF FIGURES (continued)

LIST OF FIGURES (continued)

LIST OF FIGURES (continued)

LIST OF FIGURES (continued)

LIST OF TABLES

CHAPTER 1
INTRODUCTION

Excessive early-age water evaporation from the surface of concrete pavement may induce detrimental impacts, i.e., high porosity, delamination (leading to spalling), and loss of strength on long-term performance of the pavement. Spalling involves the breakdown or dislodging of concrete segments along a joint or crack in a concrete slab within 0.6 m (2 ft) of a joint or crack (Miller and Bellinger 2003), and it affects the quality of concrete pavement smoothness and riding quality.

The Texas Department of Transportation (TxDOT) has recently experienced cases of spalling and delamination failures, which may be related to excessive early age evaporation worsened under the influence of certain field conditions such as high temperature, low relative humidity, high solar radiation, and high wind speed. To mitigate early-age unexpected water loss, application of curing compounds in concrete paving has been widely used to minimize evaporation. However, the TxDOT standard specifications for pavement construction (Item 360) only defines the use of the membrane curing in terms of key characteristics such as percent solids, density, viscosity, color, and the application rate, but does not specify curing performance or limits on the rate of evaporation. The current laboratory curing membrane effectiveness evaluation method ASTM C 156 has some intrinsic deficiencies, i.e., irrelevance of the test conditions to field performance, mortar's hardening effect, and questionable basis for the moisture loss limits. Therefore, a new laboratory test protocol is needed to evaluate the curing membrane effectiveness in controlling evaporation.

CHAPTER 2
LITERATURE REVIEW

First, a discussion will be given regarding what is concrete curing and what happens when cement hydrates. Second, a synthesis of current curing membrane effectiveness evaluation will be summarized. Last, the current lab evaluation protocol ASTM C 156 will be reviewed and its limitations noted.

CONCRETE CURING MECHANISM

Ensuring sufficient water availability in hydrating concrete is of great importance to achieve the ultimate degree of hydration so as to produce delamination resistant concrete for both short-term and long-term performance of concrete pavement. Excessive early-age evaporation from the surface of concrete pavement may result in high porosity concrete, delamination, and loss of strength.

The minimum amount of water needed for cement to achieve the ultimate degree of hydration is about 0.44 g of water per gram of cement (Powers 1947). This amount of water will provide room for the hydration products. Good curing practice should keep the concrete as nearly saturated as possible until the originally water-filled space has been filled with hydration products to some desired extent (Powers 1947).

A key aspect relative to curing quality focuses on what the minimum water content is required for hydration to occur. One researcher (Lasseter 1931) mixed 17 g of cement with 1 g of water, and months later half of the water was still evaporable. Similarly, another attempt (Power and Brownyard 1947) mixed 8 g of cement with 1 g of water, and both free water and unhydrated cement were found after four years curing underwater. Therefore, even in the presence of free water, some cement may remain unhydrated. Accordingly, a unit volume of cement takes up at least 2.14 unit volumes of water to achieve full hydration. The equivalent water cement ratio for full hydration is 0.42 by weight, and the lack of sufficient moisture is also a factor for partially hydrated mixtures.

Relative humidity is a good indicator of the saturation condition of concrete mix. Researchers (Gause and Tucker 1940) placed fresh cement pastes in sealed bottles while

tracking the relative humidity in the bottle. The test results are shown in Figure 2-1. It was noted that the vapor pressure inside the bottle dropped at a progressively diminishing rate. The phenomenon where the water vapor pressure drops due to cement hydration is called self-desiccation (Powers 1947). Accordingly, the volume change due to self-desiccation is called autogenous shrinkage (Davis 1940; Swayze 1942). Mixes with lower water cement ratios ended up with lower "level-off" relative humidity, which is the indication of cessation of hydration. Therefore, it is evident that the hydration of cement under sealed conditions can lower the water vapor pressure to 0.75 or 0.80 prior to the cessation of hydration.

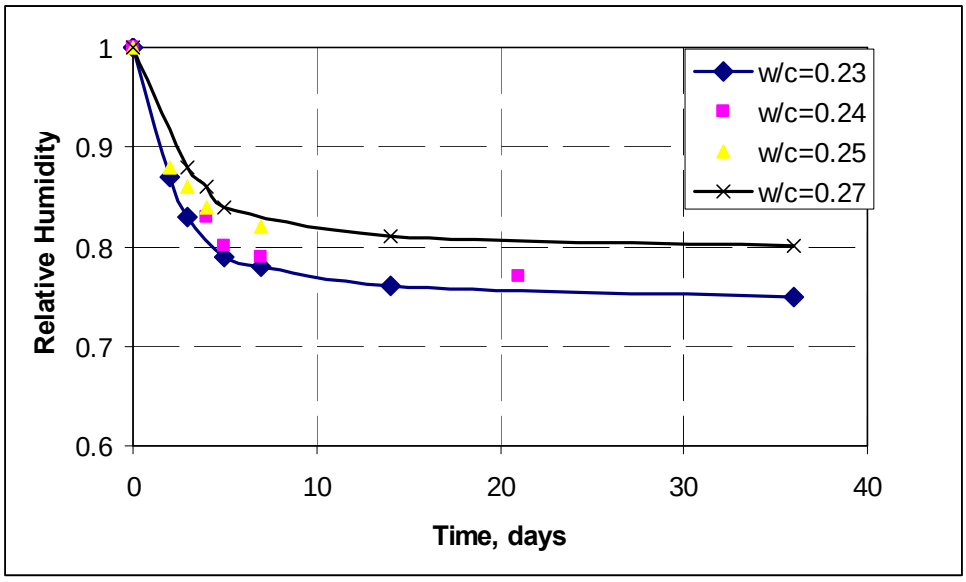

Figure 2-1. Reduction of Vapor Pressure over Sealed Pastes (Gause and Tucker 1940).

In another interesting experiment (Powers 1947), several portions of cement were stored in chambers with different moisture conditions. The amounts of total and non-evaporable water were determined. The results after six months of exposure are shown in Figure 2-2. The water taken up by cement when water vapor pressure was below 0.8 was comparatively low. When the water vapor pressure was above 0.8, the cement took much more water, which indicates the hydration rate was quite higher. These results are in agreement with previous tests. Accordingly, researchers began to

believe that the vapor pressure must be maintained at a comparatively high value (relative humidity 0.8) in order to ensure hydration proceeds at an appreciable rate.

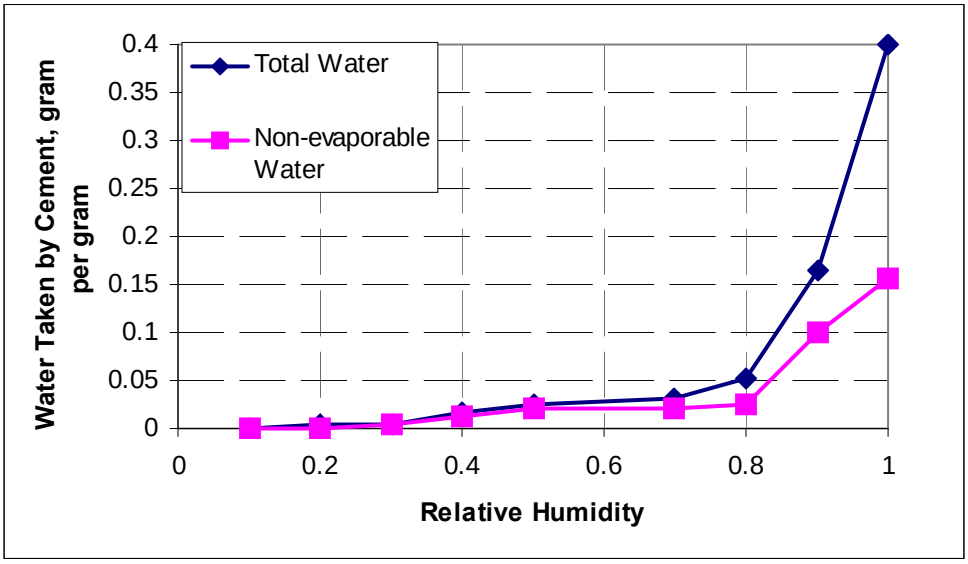

Figure 2-2. Amounts of Water Taken Up by Dry Cement Exposed to Water Vapor for Six Months (Powers 1947).

As stated earlier, hydration products can only take up the water-filled space. In porous media, the relationship between water content and vapor pressure is well defined by Kelvin's equation. When cement grains are exposed to water vapor such as in the experiment previously mentioned, capillary condensation will occur. Condensation occurs at the points of contact between grains. For a simple case, a ring of water is condensed around a point where two identical spheres contact, as shown in Figure 2-3. Under an equilibrium situation, water vapor in the voids is balanced with the saturated pressure above the capillary water by the tension of the water. The Kelvin equation for this case given by equation (2-1) states from a curing perspective, that the higher the vapor pressure is, the greater the amount of condensed water (or the lower the tension in the water), which allows more hydration products to form.

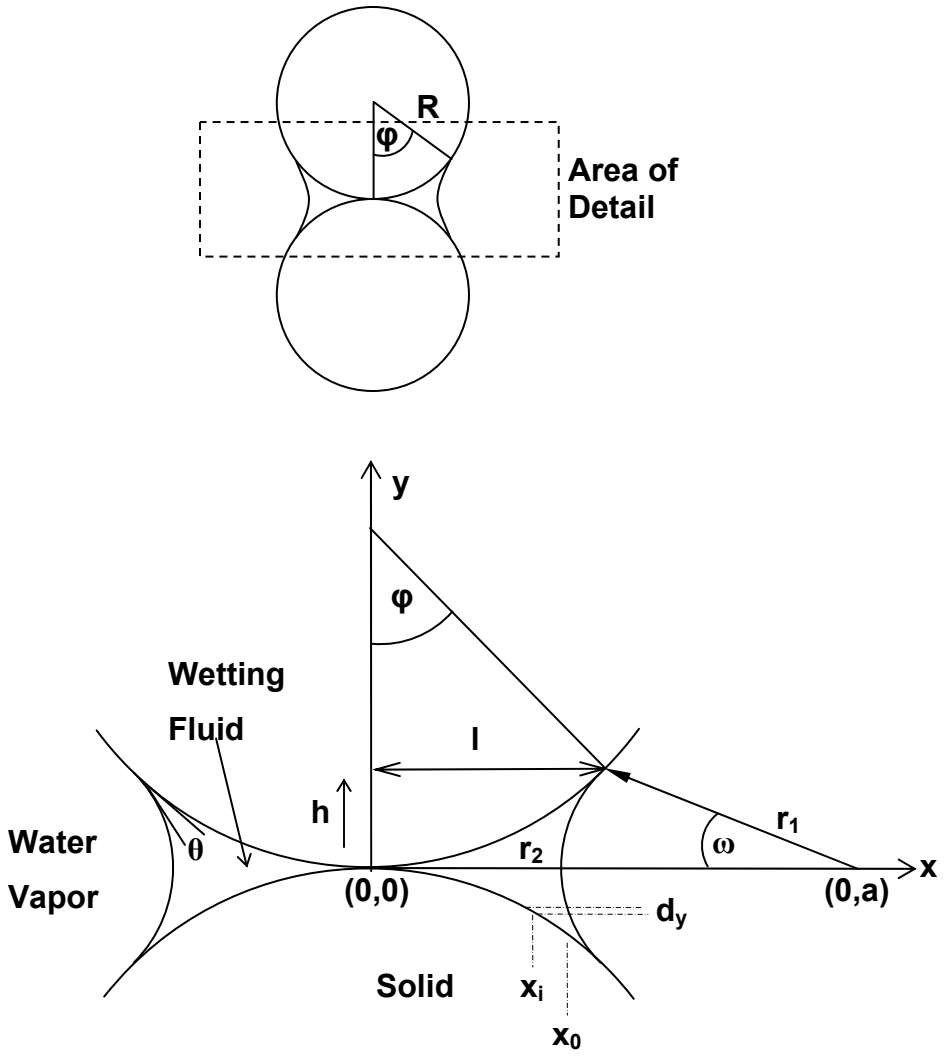

Figure 2-3. Diagram of Water Ring around the Contact Point of Two Spheres (Powers 1947).

$$\frac{1}{r_1}+\frac{1}{r_2}=-\frac{RT}{Mv_f\gamma}\ln\left(\frac{p}{p_s}\right) \tag{2-1}$$

where:

r_1 = radius of concavity,
r_2 = radius of convexity,
γ = surface tension of the water,
v_f = specific volume of water,
M = molecular weight of water,
R = gas constant,
T = absolute temperature,
p = vapor pressure, and
p_s = pressure of saturated vapor.

CLASSIFICATION OF CURING COMPOUND

According to ASTM C 309-03 (2003), the following types of liquid membrane-forming compounds are included:

- Type 1 – Clear or translucent without dye,
- Type 1-D – Clear or translucent with fugitive dye, and
- Type 2 – White pigmented.

The solids dissolved in the vehicle shall be one of the following classes:

- Class A – No restrictions, or
- Class B – Must be a resin as defined in Terminology D 883.

TxDOT utilizes Type 2 (white pigmented) and some Type 1-D curing compound products. Figures 2-4 and 2-5 illustrate the compositions of resin-based and wax-based curing compounds, respectively.

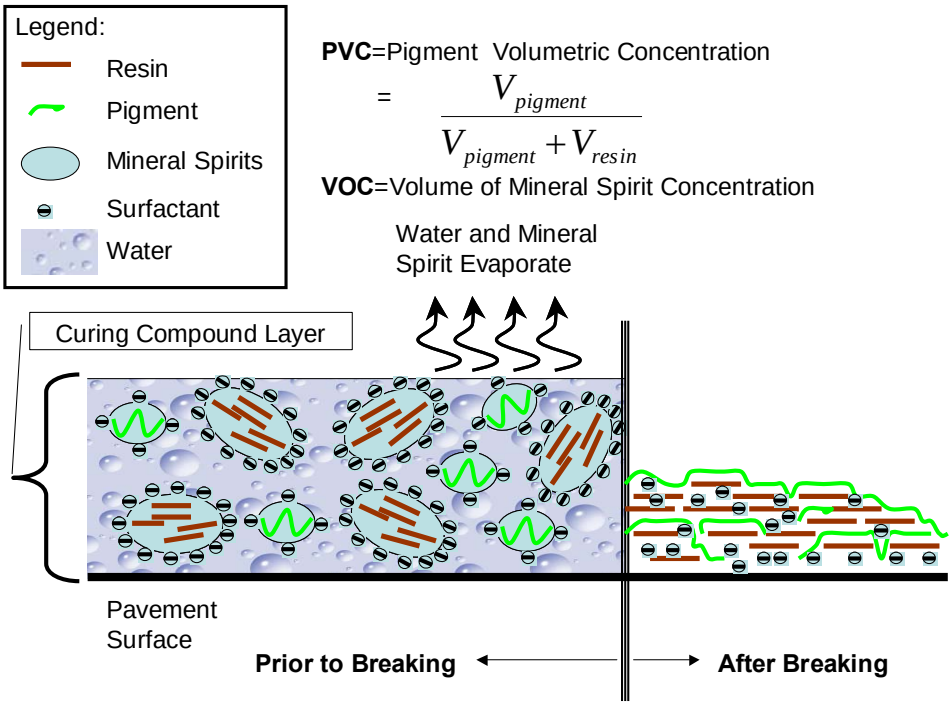

Figure 2-4. Diagram of Resin-Based Curing Compound (Type 2 Class B).

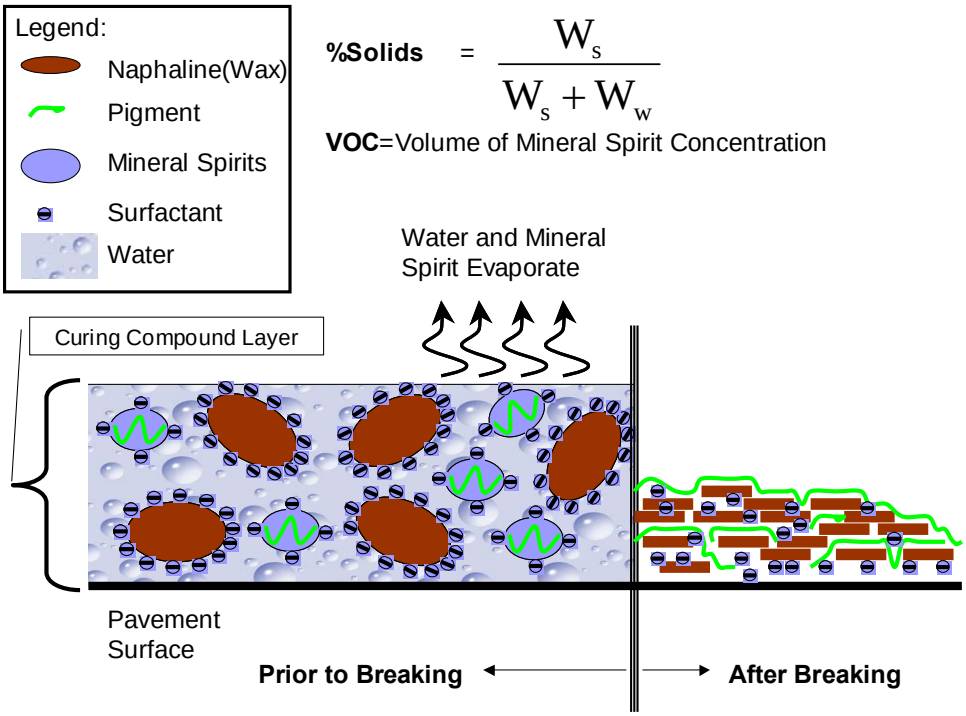

Figure 2-5. Diagram of Wax-Based Curing Compound (Type 2 Class A).

SYNTHESIS OF CURING MEMBRANE EFFECTIVENESS

Some investigations into the effectiveness of curing membranes have tended to measure special concrete properties (i.e., oxygen permeability, electrical conductivity, porosity, etc.) that are caused by or related to the availability of hydration of water and comparing those parameters to evaluate the effectiveness of a curing compound. Although these parameters do have some utility in this regard, their use in curing specifications has some practical limitations since it is difficult to evaluate the curing membrane effectiveness in this manner under field conditions. Some researchers have concluded that maturity is not a good indicator of curing effectiveness. However, this is because only temperature-based maturity was considered. Research under Project 0-1700 (Mukhopadhyay et al. 2006) found that moisture-based maturity was very effective in this manner. The following provides a review of current literature on evaluating curing membranes, effectiveness and briefly summarizes the work done in Research Project 0-1700 regarding assessment of curing effectiveness.

Researchers (Carrier and Cady 1970) evaluated the effects of various application rates of membrane-curing compounds on concrete using a laboratory test in which slab specimens were subjected to curing compound rates ranging from zero to 100 ft^2/gal. To evaluate the effectiveness of the application rate, the moisture changes were characterized in terms of changes in relative humidity (RH) and changes in relative surface strengths using the Schmidt hammer. The test specimens were made with five application rates of curing compound: 0, 50, 100, 150, and 200 percent of the standard coverage (200 ft^2/gal) with a white-pigmented type compound commonly used in Pennsylvania. The RH measuring points were positioned at depths ranging from 0.25 to 2 in. below the concrete surface. The field environment simulated in the lab was that of a hot summer day where the air temperature was cycled daily over a 4 (at 110 ± 2°F) and 20 (at 75 ± 2°F) h period where the wind speed was held constant at 4 ± 1 mph (during the heating phase), and the RH was maintained at 20 ± 5 percent. The RH of specimen was measured at 1, 2, 3, 5, 7, 9, 11, and 14 days of age with the surface strength of the cured specimen was measured with the Schmidt hammer after 14 days. Petrographic examination of the surface concrete determined the differences in the extent of hydration. The following conclusions were found:

- In the measurement of RH, while the zero coverage specimens dried quickly, the specimen sprayed with 200 percent application (100 ft^2/gal) loses as much moisture as those sprayed with 50 percent (400 ft^2/gal).
- Hydration virtually ceases when concrete dries below an RH of about 80 percent at which the water-filled capillaries are emptying. Therefore, the effective curing time is the period that the RH in concrete is maintained above 80 percent.
- The effective curing time increases with increasing application rates; that is, the curing period with zero application rates is very short, while the others increase progressively with increasing application rates.
- The result of strength test appears to be similar to that of the RH test. The result indicates that while the zero percent coverage surfaces are much weaker than any others, the specimens with different application rates have almost the same strengths within the accuracy of the Schmidt hammer. The surface strengths of the sprayed specimens appeared to be similar regardless of the time of curing.
- Petrographic examination shows similar qualitative results; that is, while the surface mortar of the sprayed specimens appears much stronger than that of the unsprayed specimens, there are no differences between the sprayed specimens.
- For a depth of more than 1 in. below the membrane, the concrete maintained an RH of 80 percent even at 28 days of age; that is, the surface membrane did not affect the internal concrete curing. However, for the upper 1 in. of concrete, the moisture distribution increased as the application rate of curing compound increased.

Curing efficiency was evaluated based on oxygen permeability and moisture loss measurements as shown in Table 2-1. The curing efficiency from oxygen permeability was statistically better than that determined from moisture loss measurements. The oxygen permeability tests may be a good method to assess the traditional methods of curing.

Table 2-1. Comparison of Curing Efficiency Results (Carrier and Cady 1970).

Curing Membrane	Solvent-Borne Resin	Wax Emulsion	Solvent-Borne Acrylic	Acrylic Emulsion
Curing efficiency from moisture loss (%)	87.0 (3.8)*	90.1 (3.0)	81.3 (7.2)	56.2 (11.1)
Curing efficiency from oxygen permeability (%)	82.2 (1.8)	92.8 (2.2)	84.6 (2.9)	52.6 (6.8)

* Moisture loss

The efficiency of selected curing compounds to cure concrete was also assessed by Wainwright and Cabrera (1990) using a type of laboratory test that monitored the rate of evaporation of water from mortar specimens under controlled environmental conditions. Four types of curing compounds were evaluated in terms of compressive strength, total porosity, degree of hydration, rate of moisture loss, and oxygen permeability. Concrete slabs of 23.62 x 11.81 x 73.94 in. and mortar slabs of 11.81 x 5.91 x 1.97 in. were cast and kept at 35 ± 1ºC, 45 ± 5 percent RH under a 3 m/s wind velocity. The four compounds tested were solvent-borne resin (resin-based), wax emulsion (wax-based), solvent-borne acrylic, and acrylic emulsion. The compounds were applied at a rate of 0.2 liter/m^2 (0.88 gal/180 ft^2).

Compressive strength was measured at 3, 7, and 28 days age using 3.94 in cubes. The 28-day strength of non-cured specimens was about 22 percent and 19 percent lower than those water-cured for three days and those cured with a wax emulsion membrane, respectively. Moisture loss was measured by monitoring the weight change with time. The water loss trends were similar to those of compressive strength, but the difference between curing types was greater. However, all curing methods produced significant reduction in moisture loss. The wax emulsion compound performed the best and was almost three times less than that of non-cured concrete.

Porosity was also measured at various depths beneath the surface of the concrete slabs. The trends were similar to the test results noted above. The difference between curing methods decreased as the depth below the surface increased. However, since the concrete more than 50 mm below the surface is rarely affected by curing conditions at the

surface, the differences between curing methods become insignificant at depths more than 1.97 in. The measurement of the pore size distribution was conducted using samples taken within 0.47 in. from the surface for both cured and non-cured mortar slabs. The results show that the volume of the capillary pores greater than 3.93×10^{-6} in. is significantly reduced for the cured specimens.

Oxygen permeability was measured on samples taken at various depths beneath the surface of the concrete slabs. The results were similar to those of the porosity test. Near the surface, the non-cured concrete was 8 to 10 times more permeable than cured concretes. Similar to the measured porosities, the difference was insignificant at depths more than 1.97 in. below the surface.

The study shows that although all test results present a similar trend, the oxygen permeability test is most sensitive to curing quality, and the wax emulsion is the most effective curing membrane. The concrete at a depth more than 1.97 in. is barely affected by the method of curing. The permeability test was recommended as a means of durability and curing efficiency assessment since permeability reflects upon the potential durability of concrete, which is largely a function of the method of curing.

Cable, Wang, and Ge (2003) carried out a research project sponsored by Iowa Department of Transportation (DOT) to evaluate curing compound materials, application methods, and effects of curing on concrete properties. The research consisted of laboratory testing and field evaluation of identified products and application rates. The research showed that curing materials and application methods have a critical effect on the properties of the near-surface concrete, particularly in hot weather conditions. Concrete cured with curing compounds that were indexed with a high curing efficiency had lower sorptivity, higher conductivity, higher degree of hydration, and higher compressive strength. Among these tests, the sorptivity test is the most sensitive indicator for quality, whereas the compressive and flexural strengths were not. The sorptivity showed a close relationship to moisture content and degree of hydration, while the conductivity showed a strong correlation to moisture content of the concrete.

Curing compound materials and related application methods were evaluated in the field relative to the properties of field concrete pavement. The curing compounds tested are listed in Table 2-2 according to Iowa DOT designations and their rated qualities. The

1600-white series (1645 white and 1600 white) are wax-based, white-pigmented concrete curing compounds with selected white pigments. The difference between 1645 and 1600 concrete curing compounds is the solid content where 1645 has 29.2 percent and 1600 has 17.1 percent. The 2200-white series concrete curing compounds are high solids, white pigmented, and polyalphamethylstryene-based (resin-based).

Table 2-2. Typical Properties of the Curing Compounds.

Curing Compounds	Efficiency Index	Estimated Cost ($/gal)
1645-White	95.9	2.0
1600-White	89.0	1.0
2255-White	98.1	6.5

The compounds at two application rates were compared to no curing and wet curing in terms of measured conductivity, permeability, and maturity at the surface of a concrete slab. The conductivity is a measure of water retentivity of a curing compound; the maturity is an indication of the degree of hydration, and the permeability an indication of durability of the near-surface concrete. The efficiency index used in this study was defined as:

$$Efficiency = \frac{E_o - E_c}{E_o - E_w} \tag{2-2}$$

where:

E_o = moisture loss for no curing,

E_c = moisture loss for certain curing compound, and

E_w = moisture loss for wet curing.

Maturity testing did not prove to be beneficial. The temperature-based maturity was apparently insufficient to evaluate the effectiveness of curing and was not sensitive to environmental effects such as the air temperature, humidity, wind, or rainfall.

Permeability testing was conducted at the top, middle, and bottom of cores taken from the pavement. The test data showed little difference in the middle and bottom measured permeability, and there seemed to be no difference between different curing methods; the without curing condition, however, yielded higher permeability at the top. The sections with curing compound and with wet curing had almost the same permeability. The permeability also decreased as the depth increased.

This research showed that electrical conductivity is statistically related to moisture content of the concrete, and that the method of curing affected the surface concrete more than portions deeper below the surface. Deep sections had higher conductivity than at the top because of evaporation. Accordingly, the effectiveness of a given curing method is ascertained by comparison between the initial and current conductivity values. The conductivity results followed the same trends as those shown with the efficiency index of the curing compounds listed in Table 2-1. No sorptivity test or moisture content results were provided, but the degree of absorption of water is thought to be closely related to the pore structure characteristics of concrete as a potential test for the curing effectiveness. The moisture content readings with time showed a large variation due to several factors such as texture of the pavement, measuring position, and environmental variation.

This research concluded that only slight differences existed among wet curing, compound curing, and no curing, while the maturity test could not identify the difference between different curing compound materials. The permeability test showed that curing compounds provide the same quality as wet curing, and that the compound materials tested were ranked as: wet curing, 2255 single layer, 1645 double layer, 1645 single layer, and 1600 double layer.

The Minnesota Department of Transportation (MnDOT) examined and evaluated curing compounds used in the state projects relative to any needed changes in their curing specification (Vandenbossche 1999). Some of the work focused on the application of the compound to the pavement surface. The MnDOT requirement is 4 m^2/gal (163 ft^2/gal) regardless of the type of pavement surface such as tinning or texturing, which increases the surface area. The application rate should be determined based on surface texture and

application device in order to obtain uniform coverage. The five factors listed below affect the curing compound application:

1. nozzle type: spray pattern, droplet size, pump pressure, spray angle, flow rate;
2. nozzle spacing and boom height: adjusting for 30 percent overlap of spray pattern edge;
3. nozzle orientation;
4. cart speed; and
5. windshield.

It was concluded that non-uniform coverage is mainly caused by damage to the nozzle or orifice. Nonetheless, MnDOT showed that the desired coverage can be achieved by the proper nozzle selection, cart speed, pump pressure, flow rate, etc. The study proposes the following recommendations for applying a curing compound:

- The application of the curing compound should be calculated based on the type of surface texture maintaining a minimum of 4 m^2/gal (163 ft^2/gal).
- Thirty percent of the spray overlap should be obtained.
- The coverage should not be controlled by the pump speed but by the cart speed.
- The cart speed should be calculated using the following equation.

$$v = \frac{coeff. \times F}{C \times w} \tag{2-3}$$

where:

v = cart speed (km/h, or miles/h),
coeff. = 6 for SI units, or 0.13636 for English units,
F = flow rate (L/min, or gal/min) per nozzle,
C = desired coverage (L/m^2, or gal/ft^2), and
w = nozzle spacing (cm or in.).

In another MnDOT related study, Whiting and Snyder (2003) evaluated the effectiveness of high and low volatile organic compound (VOC) curing compounds by examining the moisture-retention capacity of them. A modification of ASTM C 156-98, Standard Test Method for Water Retention by Concrete Curing Materials, was used for this evaluation. In addition, compressive strength, permeability, and capillary porosity of hardened mortar samples were also determined. Three different curing methods, ponded water (Treatment W), no curing (Treatment N), and polyvinyl sheeting (Treatment P), were also examined for reference. The curing compounds used for the test were low VOC (L-1, 2, 3) and three of high VOC (H-1, 2, 3). Infrared fingerprinting, characteristic of surface coverage, and percentage of solids were examined to understand this aspect of each curing compound tested.

The moisture retention was measured by monitoring the mass loss of each mortar specimen. The curing compound was applied as soon as the bleed water had disappeared, and the application rates were based on the minimum rate recommended by the manufacturers. The specimens were cured in the test chamber at a specific temperature, RH, and evaporation rate.

As expected, the result of the moisture retention test showed that Treatment P was the most effective. However, generally speaking, the high VOC compounds showed a lower rate of moisture loss than the low VOC compounds, but moisture loss was high within the first 24 hr and then gradually stabilized. Although ASTM requires the moisture loss after 72 hr to be less than 0.55kg/m^2, only Treatment P met that requirement. Moisture retention capacity of the curing compounds was evaluated relative to the moisture loss for the Treatment N:

$$\%Effectiveness = \frac{Mn - Ms}{Mn}(100) \qquad (2\text{-}4)$$

where:

Mn = average moisture loss of specimens from Treatment N, and

Ms = average moisture loss of specimens from treatment being considered.

The percent effectiveness decreases with time for all treatments where Treatment P had the highest percent effectiveness.

In terms of compressive strength, mortar specimens cured with high VOC compounds gained strength more quickly than those cured with low VOC compounds. The 28-day strength of Treatment N cured mortar was about 54 percent of that of Treatment W. The 28-day strength of specimens with curing compounds ranged from 55 percent to 75 percent of the strength achieved using Treatment W. The result showed that curing method has a greater impact on long-term strength development than early-age strength. A high correlation existed between the average moisture loss and the compressive strength. There was also a strong correlation between the percentage of solids and compressive strength. However, the percentage of solids is apparently only a good indicator if the compounds are chemically similar.

The relative permeability of the specimens was also estimated using the rapid chloride penetration (RCP) test at 3, 10, and 28 days. After 3 and 10 days of curing, the estimated permeability of all specimens was high, exceeding 4000 coulombs. After 28 days of curing, all test results range from moderate to high permeability. The low VOC samples had the highest permeability value, and Treatment W and Treatment P had the lowest values.

In conclusion, the specimens with high VOC compounds show less moisture loss, higher strength, and lower permeability than those with low VOC compounds. The specimens cured with plastic sheeting show better moisture retaining ability, long-term strength, and lower permeability than any other curing compounds. However, early strength is higher in some specimens with a high VOC compound than in those with plastic sheeting. Thus, the VOC content does not appear to be the best indicator of how a curing compound will perform.

REVIEW OF ASTM C 156

Current TxDOT specification for curing membrane application practice requires two applications, each of which has an application rate of 180 ft^2/gallon. The factors for selecting curing compounds for paving activities are: water retention, pigments, drying time, type and amount of solids, VOC, and compatibility with coatings.

The standard test, ASTM C 156-98, *Standard Test Method of Water Retention by Concrete Curing Materials*, is focused on water retention and requires a controlled environmental chamber that can potentially evaporate water ranging from 0.65 to 1.1 $kg/m^2/hr$ (0.133 to 0.225 $lb/ft^{2/}hr$). The standard water loss limit according to ASTM C 309 and American Association of State Highway and Transportation Officials (AASHTO) M 148 is 0.55 kg/m^2 (0.113 lb/ft^2) for a duration of 72 hr, and TxDOT specifications require that the total water loss with respect to the total weight of specimen is less than 2 percent at 24 hr and less than 4 percent at 72 hr. This standard water loss limit is based on the strength of stripped and coated cylinders and dates back to the 1930s and 1940s.

The method is relatively straightforward, but apparently, the reported precision between laboratories is poor, and several deficiencies can be pointed out. The method is also rather limited as far as field application since it is conducted under fixed ambient conditions (temperature, relative humidity, and wind speed) and a single application rate, while field environmental conditions represent a variety of condition combinations. Second, ASTM C 156 specifies the use of mortar specimens to conduct the evaporation test, which exhibits a high evaporation rate initially while the specimen is still fresh and then decreases as the mortar hardens. The majority of moisture loss occurs during the initial hardening stages but very little takes place after that 72-hr test period. Third, the dimension of the strength test specimen is too large to capture the subtlety induced by different curing methods; in order for the difference in strength to be noticeable, the difference of the physical properties of the exposed concrete at the top of the specimen versus that of the interior concrete would need to be enormous. Nowadays, curing is key to achieving quality concrete within the top few inches of the exposed surface. The following discussion will elaborate on these aspects relative to ASTM C 156 as a curing compound effectiveness evaluation method.

SINGULAR EXPERIMENTAL CONDITIONS

ASTM C 156 is carried out under a singular set of curing conditions and with only a single curing compound application rate. Since ambient weather conditions encompass huge variations, curing effectiveness should be defined over a range of

humidity and wind conditions. As a result, the final curing effectiveness is the combination of the effect of curing practice and ambient conditions, as shown in Figure 2-6. Curing practice includes the type of curing compound, application rate, and uniformity. Ambient conditions consist of temperature, relative humidity, and wind speed.

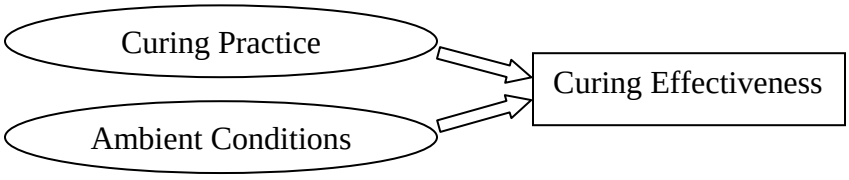

Figure 2-6. Factors on Curing Effectiveness.

Table 2-3 lists the required test conditions described in ASTM C 156. There is no specific requirement for wind, which is a crucial factor affecting the rate of evaluation. The American Concrete Institute (ACI) nomograph (ACI 308) can be used to characterize the effect of weather on evaporation potential. It calls for the input of air temperature, air relative humidity, concrete temperature, and wind velocity, as shown in Figure 2-7. This nomograph can also be represented in Equation (2-5), which has variables of air temperature, air relative humidity, and wind speed.

Table 2-3. ASTM C 156 Environmental Conditions.

Temperature	37.2 ±1.1ºC (99.0±2.0ºF)
Relative Humidity	32±2%

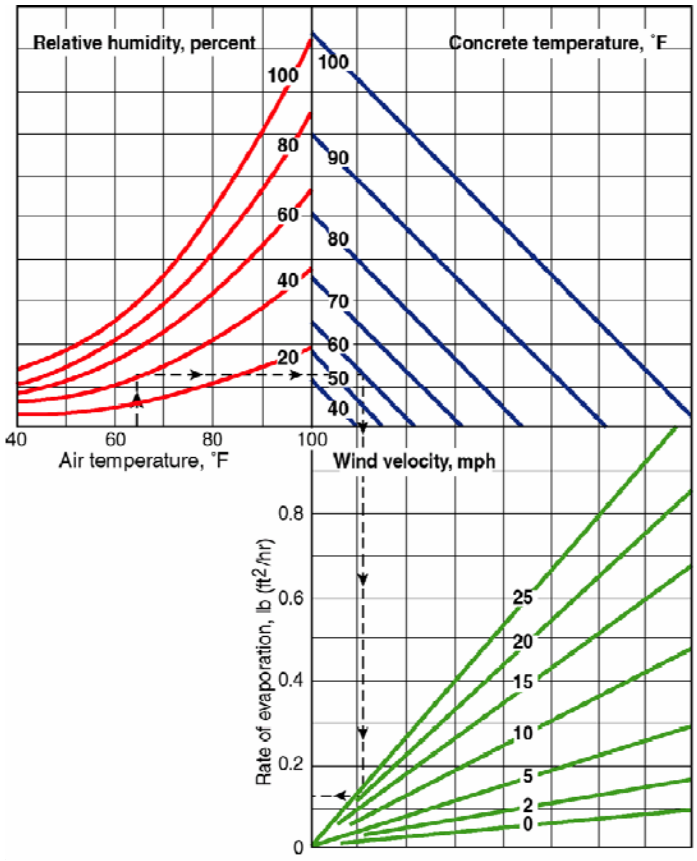

Figure 2-7. Nomograph in the American Concrete Institute Guide (ACI 308).

$$PE = [T_c^{2.5} - (R *\times T_a^{2.5})] [1 + 0.4 V] * 10^{-6} \qquad (2\text{-}5)$$

where:

PE = potential of evaporation rate, lb/ft^2/hr;

T_c = concrete temperature, ^{o}F;

T_a = air temperature, ^{o}F;

R = (relative humidity percent)/100; and

V = wind velocity, mph.

According to this equation, the weather severity index for ASTM C 156 is 0.066 lb/ft^2/hr. In Texas, the air temperature often goes as high as 105ºF, and with the effect of the wind, the potential of evaporation rate may exceed 0.600 lb/ft^2/hr; on the

other hand, the potential of evaporation is as low as 0.020 lb/ft^2/hr with an air temperature of 70ºF, relative humidity of 50 percent, and no wind. Whatever test conditions are utilized for curing compound evaluation, it appears it would be useful to understand the manner in which the test conditions relate to field conditions and the needed rate of application to achieve quality curing.

MORTAR SPECIMEN

ASTM C 156 describes a method to evaluate water retention as a measure of curing effectiveness. The method involves the measurement of evaporation from a mortar specimen over a period of 72 hr. The mortar exhibits a high rate of evaporation while it is fresh and a lower rate when it is hardened. Following this procedure, it is nearly impossible to separate the water retention capacity of curing membrane from that due to the hardening of the mortar. Consequently, the evaluation of the water retention capability of a curing compound is compromised to some extent.

A special lab test was conducted to demonstrate the extent the hardening of the mortar contributes to the reduction of water loss. Four short cylindrical specimens with a diameter of 6 in. and a thickness of 2 in. shown in Figure 2-8 were prepared. The environmental conditions are listed in Table 2-4.

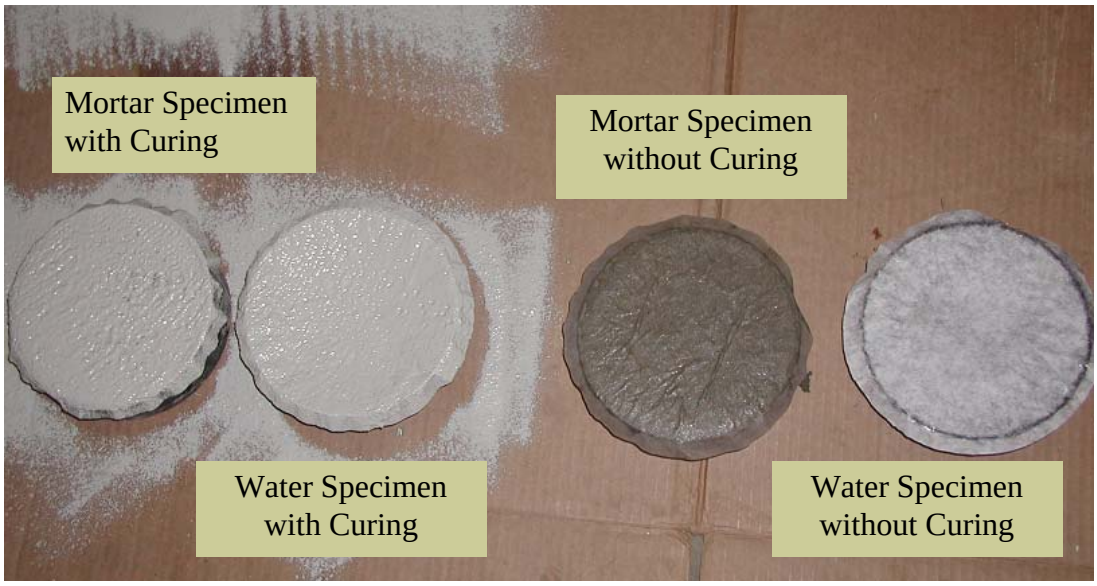

Figure 2-8. Specimens for the Special Test.

Table 2-4. Environmental Conditions.

Temperature	104ºF (40ºC)
Relative Humidity	30 percent
Wind Speed	10 mph
PE	0.395 lb/ft^2/hr

The environmental conditions for these tests were set according to Table 2-4, and a wind flow of 10 mph was applied. The weight losses for mortar specimens and water specimens are shown in Figures 2-9 and 2-10, respectively.

As shown in Figure 2-9, the weight loss for the mortar specimens exhibit a high initial moisture loss rate, but the total moisture loss gradually levels off, while water specimens show a constant moisture loss rate (Figure 2-10). The constant moisture loss rate indicates that the curing compound is stable under constant ambient conditions. Figure 2-10 shows that the rates of moisture loss for water specimens were constant throughout the testing period, which indicates the properties of the curing membranes remained unchanged.

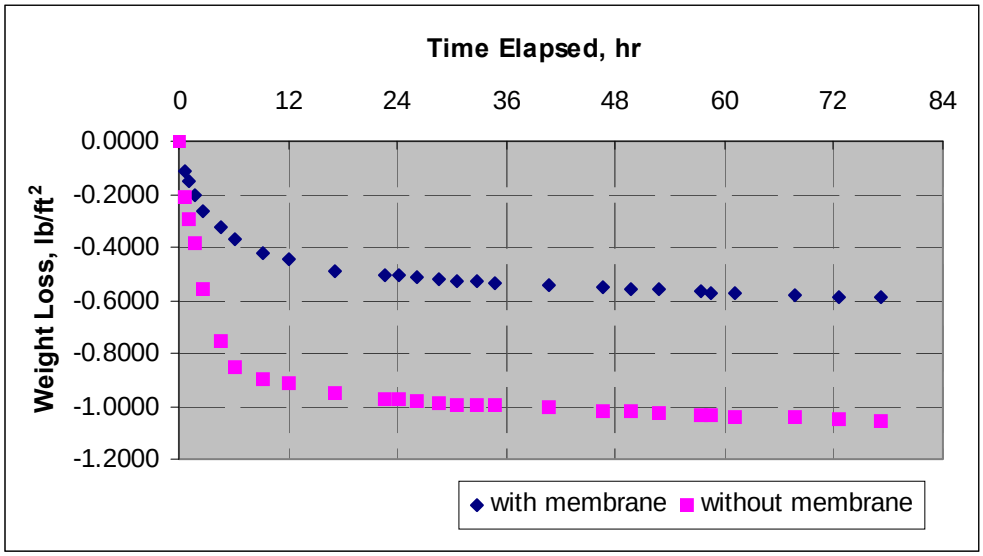

Figure 2-9. Weight Loss for Mortar Specimens.

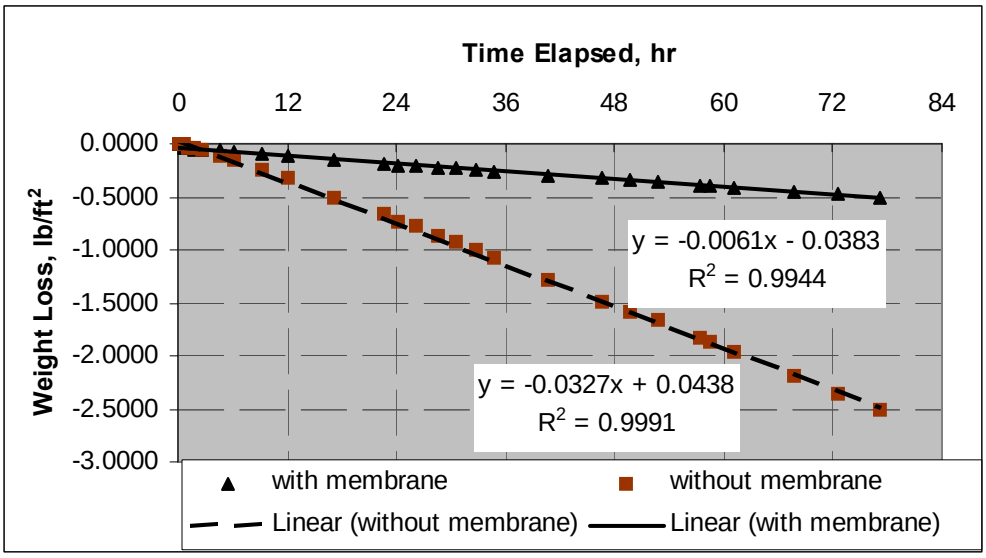

Figure 2-10. Weight Loss for Water Specimens.

Figure 2-11 shows a comparison of mortar specimen water loss at different stages. The first 12-hr stage is the only one in which the non-cured sample moisture loss is evidently larger than that of the cured sample. For the remaining stages, the moisture loss differences between cured and non-cured samples are very small. However, in the first stage, the most evaporated water is that associated with bleeding, which could cause a loss of strength if bleeding was excessive, although this may not be easily verified. In any event water loss due to bleeding constitutes a large amount of the total loss. In the other three stages, the moisture loss from the two specimens were about the same. This evidence suggests that the rate of moisture loss due to the hardening of the mortar is nearly equivalent to the rate of moisture loss of the membrane-cured mortar. The early water loss, during the first stage may have a greater impact on strength and lesser impact on stress development in the concrete (at later ages). Furthermore, the starting point of recording moisture loss is when bleeding stops. However, it is very difficult to identify the stoppage point, which results in a variation of moisture loss in the first stage possibly accounting for poor precision in this method.

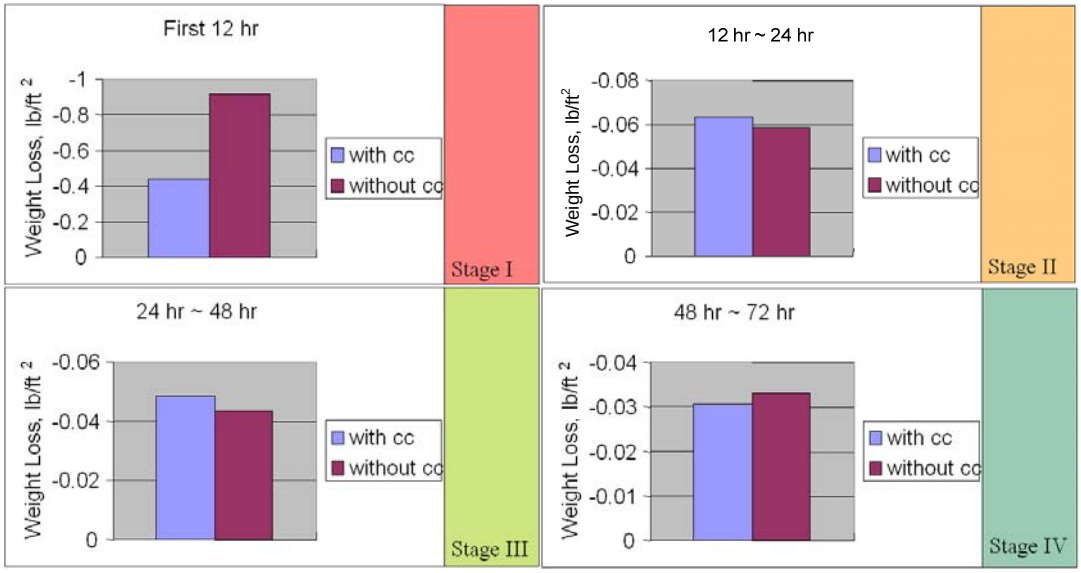

Figure 2-11. Weight Loss at Different Stages.
Note: cc=curing compound.

LIMITS ON MOISTURE LOSS

The standard water loss limit according to AASHTO M 148 and ASTM C 309 is 0.55 kg/m^2 (0.113 lb/ft^2) for a duration of 72 hr. The water loss limit is based on the strength of stripped and coated cylinders dating to the 1930s and 1940s. The question is whether the strength of the overall cylindrical specimen is affected by the strength of the surface concrete. The limit should, perhaps needs, to be lower in order to overcome composite effect of the large volume of the fully cured concrete. As shown in Figure 2-12, it would be more meaningful to investigate the properties of the top part of the specimen rather than taking the compression strength of the whole cylinder specimen, which comprises a large volume of well-cured concrete.

Curing mainly affects only the very top part of the exposed concrete. It is perhaps inappropriate to use compression strength of the entire cylindrical specimen as a means to substantiate curing effectiveness. Physical properties (such as total porosity and permeability) of the top part of the concrete specimen may be more desirable when evaluating curing effectiveness.

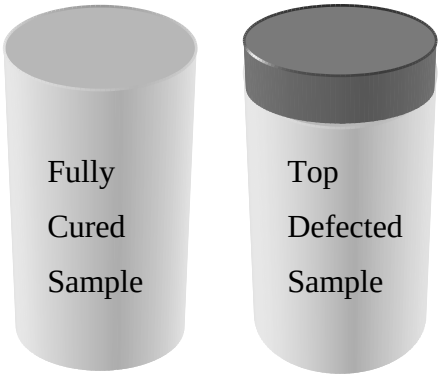

Figure 2-12. Diagram of Cylinder Samples of Different Top Conditions.

SPRAY TECHNOLOGY

The new laboratory protocol, which will be presented in the next chapter, features linkages between curing practice (application rate) according to the actual ambient conditions (potential of evaporation) and type of curing compound (ranking of curing compound). These linkages instill a greater level of versatility in the curing equipment technology. This section reviews present technologies pertinent to curing compound spraying.

Typical sprayers used in the field consist of nozzles, lines, pumps, tanks, pressure regulators, pressure gauges, strainers, shutoff valves, and agitators. Some sprayers are equipped with pressure-activated shutoff valves at each nozzle to stop nozzle flow without dripping. The pump moves the material from the tank and pumps it to the spray nozzles. Pressure at the spray nozzles is determined by the setting of the agitator control valve and the pressure regulator, the capacity of the pump, and the pressure loss in the lines, and fittings between the pressure gauge and the nozzles. For slip form pavers, sprayers use a boom with nozzles spaced uniformly along the boom as shown in Figure 2-13.

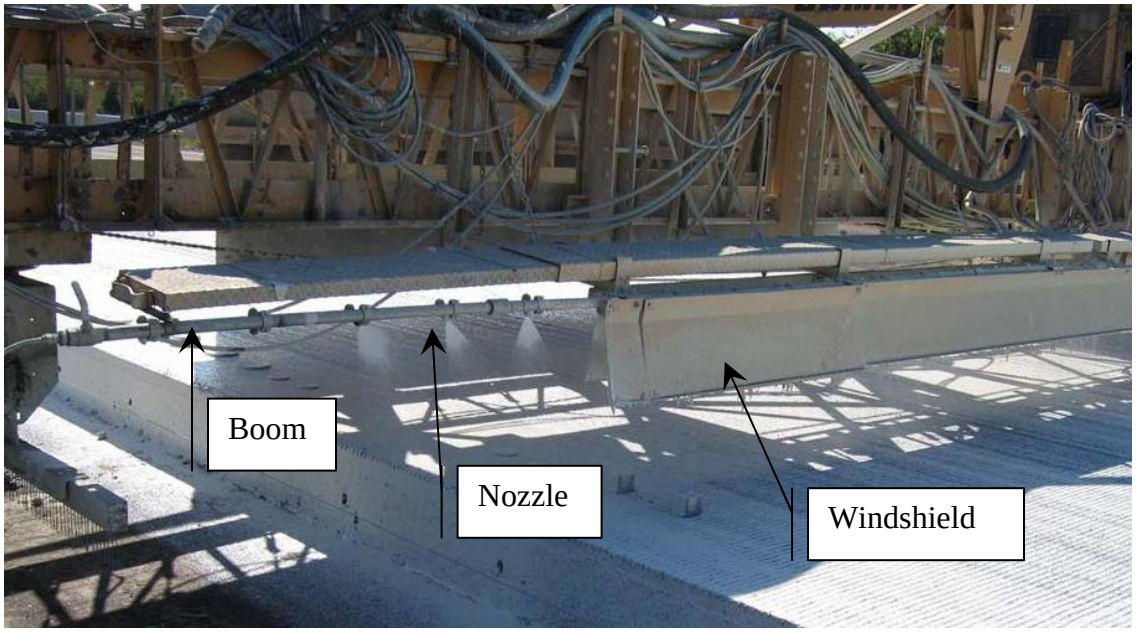

Figure 2-13. Curing Application by Slip Form Paver.

In the chip seal industry, designated application rates of the asphalt binder on the pavement surface are rechecked periodically by placing either buckets or absorbent pads across the width of the pavement (as depicted in Figure 2-14). Before and after pad weights are taken so that the weights of the binder applied can be obtained. The application rates on each pad are then calculated based on the weight gained and the pad area. Since the pads are placed across the width of the pavement, the application rate distribution transversely can also be obtained. The control of application process is also automated and metered; however, the purpose of the metering is mainly to control the initial rate of application and the application pressure. The application is also checked for spray height and nozzle orientation particularly if "drilling" or improper spray distribution occurs.

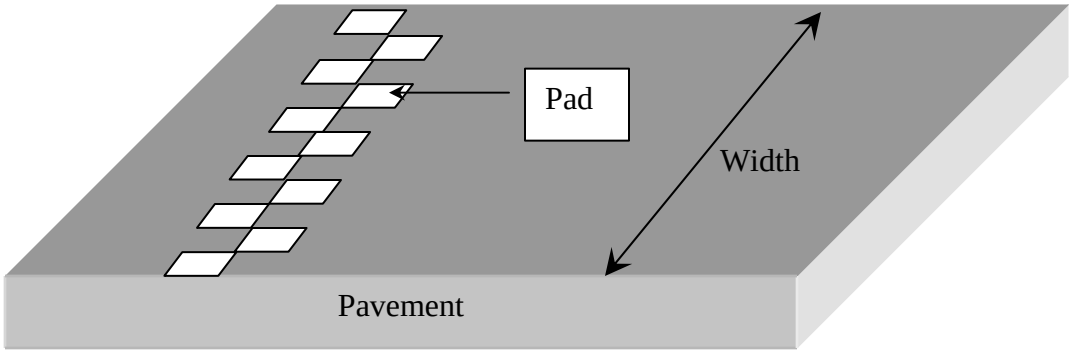

Figure 2-14. Setup of Pads on Pavement Surface.

NOZZLE TYPE

Nozzle selection is one of the most important factors affecting curing quality. The type of nozzle determines not only the amount of spray applied, but how the uniformity of the applied spray is controlled, the coverage obtained on the sprayed surfaces, and the amount of drift that can occur. Each nozzle type has specific characteristics and capabilities and is designed for use under certain application conditions.

Each type of nozzle has a specific spray angle, flow rate, spray pattern, and droplet size. The most prevailing patterns are hollow cone, full cone, and flat fan, as shown in Figure 2-15. For curing compound application, a flat spray nozzle is often used.

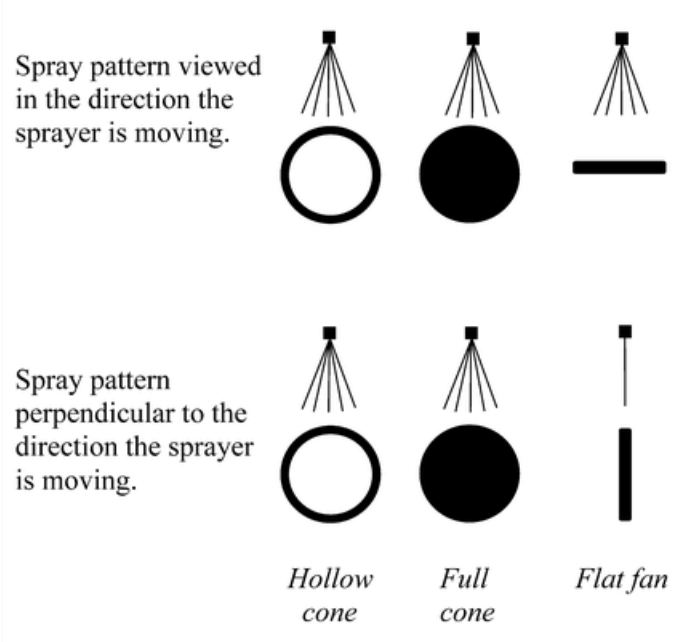

Figure 2-15. Typical Spray Patterns (Catalog 45A 1997).

Spray nozzles used for broadcast spraying do not always deliver a uniform quantity of material over the width of the spray pattern (see Figure 2-16). The distribution pattern is determined by nozzle design, wear, clogging, and pressure at the nozzle.

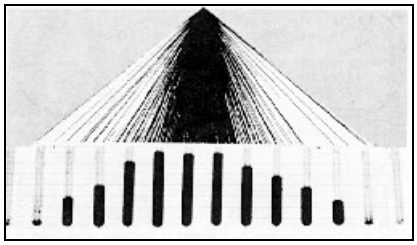

Figure 2-16. Typical Distribution (Catalog 45A 1997).

The dimension of the droplet created by the nozzle is critical for successful curing application. It is difficult to achieve uniform coverage with large droplets; however if the droplets are too small, they increase the drift potential. Droplets with a diameter smaller than 200 microns are susceptible to drift. Nozzle manufacturers often provide volume median diameters for nozzles at different pressures. Each type of nozzle has a designated

four-digit number. The first two digits represent the spray angle in degrees, and the last two represent the flow rate (gallons per minute).

UNIFORMITY OF DISTRIBUTION

Several factors are important to achieve uniformity of distribution, nozzle and boom height, pump pressure, and rate of application.

Nozzle Spacing and Boom Height

As stated earlier, spray nozzles used for broadcast spraying do not deliver a uniform quantity of material over the width of the spray pattern. When a number of nozzles are spaced on the boom, the individual nozzle spray patterns must overlap to obtain more uniform distribution over the entire boom width. Nozzle manufacturers normally provide recommendations for boom height for each particular nozzle and nozzle spacing. Improper boom height will result in uneven distribution patterns (see Figure 2-17). Anything that changes boom height will affect the distribution pattern.

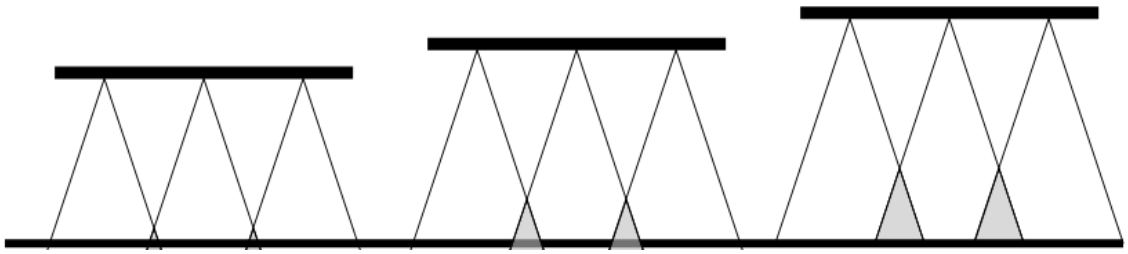

(a) Insufficient Overlap (b) Correct Overlap (c) Excessive Overlap

Figure 2-17. Boom Height vs. Overlap (Catalog 45A 1997).

Effect of Pressure

Pressure is another important factor that affects the distribution pattern. When pressure goes up, the size of droplets tends to decrease so that a more uniform coverage can be obtained; when pressure goes down, the size of droplets increases, which results in a less-uniform coverage. Coverage obtained is determined primarily by droplet size and the volume of material applied. As droplet size is decreased, better coverage is obtained

with a given volume of material. If the diameter of spray droplets is reduced by one-half, the number of droplets produced with a given volume is increased by eight times. Conversely, doubling the diameter will reduce the number produced by eight times. Using small droplets to achieve good coverage can result in problems due to drift. Thus, the pressure and boom height need to be checked to ensure uniform coverage.

APPLICATION RATE

The quantity of curing compound applied per unit of area by a sprayer depends on the shape and size of the hole (orifice) in the nozzle, pressure, nozzle spacing on the boom, and speed of travel.

Nozzle Size

Nozzles are selected that deliver the correct amount of material per unit of time and desirable droplet size under certain pressure. However, during use, the size of the hole in the nozzle may change rather rapidly due to wear, plugging (due to dirt or residue of the curing compound), and damage caused by trying to clean a plugged nozzle with wire, etc. The rate of nozzle wear depends on the type of material being sprayed, the amount of dirt in the water, and the material from which the nozzle is made.

The Prairie Agricultural Machinery Institute in Canada has found nozzle tip wear sufficient to cause a 10 percent increase in nozzle delivery after only 50 hr of use. This is the major reason for checking the flow rate of a nozzle frequently.

Pressure

As the pressure of the nozzle increases, the flow rate through the nozzle increases. The flow rate is directly related to the square root of the pressure. Thus, doubling the pressure increases the nozzle flow rate by 1.4 times; tripling the pressure increases the flow rate by 1.73 times; and increasing the pressure by four times doubles the flow rate.

Normally, nozzle manufacturers publish flow rate in gallons per minute (GPM) versus pressure for their nozzles. Nozzles might not deliver the amount specified by the manufacturer if there is an inaccurate pressure gauge. It could also be caused by the fact that the actual pressure at the nozzle is less than that indicated by the pressure gauge. Such pressure losses can be caused by restrictions in the line, buckling of supply hoses,

or partially clogged nozzle strainers. Using nozzles larger than those for which the sprayer was designed may cause a reduction in pressure at the nozzle.

Nozzle Spacing

For a given nozzle size, increasing spacing on the boom will reduce the application rate (typically expressed in gallons per square feet). For example, spacing nozzles (of the same size) at 40-in. intervals instead of 20 in. apart on the boom reduces the application rate by one-half.

Speed of Travel

Application rate varies inversely with the cart speed. That is, if the speed of travel in miles per hour is doubled, the application rate is reduced by one-half. If the miles per hour is reduced to one-half, the application rate is doubled. Thus, speed of travel is very important in obtaining the proper application rate. Otherwise, if the chosen miles per hour is not maintained, improper application rates result.

CALIBRATION PROCEDURES

The following procedures are to be followed in order to obtain a uniform distribution of the designed application rate:

1. Select the proper nozzle size.
2. Determine the application rate (AR).
3. Select an appropriate speed of travel.
4. Determine the effective spray width (W) per nozzle. For boom type sprayers, W is equal to the nozzle spacing on the boom.
5. Determine the cart speed to obtain the required GPM for each nozzle from Equation (2-3).

CHAPTER 3
LABORATORY EVALUATION OF CURING EFFECTIVENESS

Ensuring sufficient water availability in hydrating concrete is of great importance to produce durable concrete at the surface to achieve both short- and long-term performing concrete pavement. Excessive or extensive early-age evaporation can often result in high porosity, delaminated, or low strength concrete at the surface of a concrete pavement. Properly conducted curing ensures the potential for young concrete to transform into strong and durable product. On the other hand, improper curing can result in low strength concrete at the evaporative surface susceptible to drying shrinkage induced damage manifest as delaminated and spalled concrete.

As stated in previous chapters, current laboratory curing effectiveness evaluation protocols have certain limitations that inhibit complete engineering relative to field management of the curing process or its sensitivity to different ambient conditions. In this chapter, a new laboratory curing membrane effectiveness evaluation protocol is presented that has the additional capability to guide field curing practice. Even though curing compound efficiencies vary among commercially available curing compounds, a specified application rate is expected to achieve the same level of curing effectiveness irrespective of the prevailing ambient weather conditions or type of curing compound used in the field. Since construction weather conditions can be rather variable, certainly a consideration as far as a variant application rate should be adopted as it would apply to different conditions, which requires a more comprehensive approach to curing compound characterization.

DEVELOPMENT OF EVALUATION INDEX TO ASSESS CURING COMPOUND

During the early stages of concrete hydration, bleed water appears and dissipates from the surface of concrete due to evaporation. Furthermore, the rate of evaporation will vary according to ambient wind and relative humidity conditions inducing moisture variations within the concrete immediately below the surface. If evaporation at the surfaced is minimized by a given curing method, the RH profile immediately below the

surface will be relatively stable with time and will have little variation due to ambient effects above the concrete because of the isolative effects of the curing medium. It is clear that the effect of ambient conditions on the moisture levels immediately below and at the surface of concrete needs to be considered to improve characterization of curing compound efficiency and its sensitivity to the ambient curing conditions of the concrete.

Generally, after placement of concrete, the RH at the surface and inside the concrete increases for a few hours regardless of ambient conditions because of bleeding action. Bleed water forms on the concrete surface even in the presence of high evaporative conditions during the bleed period. As the bleeding rate subsides, the surface RH eventually diminishes over time to approximately the level of the ambient relative humidity. An example of RH and moisture weight loss curves are presented in Figure 3-1 where the ambient RH and the wind speed are fixed at 30 percent and 10 mph. The surface RH experienced an increase, correspondingly to bleeding action, and then gradually decreases as the rate of bleeding subsides. In other words, the rate of water loss from the concrete surface was initially high and then decreased with time.

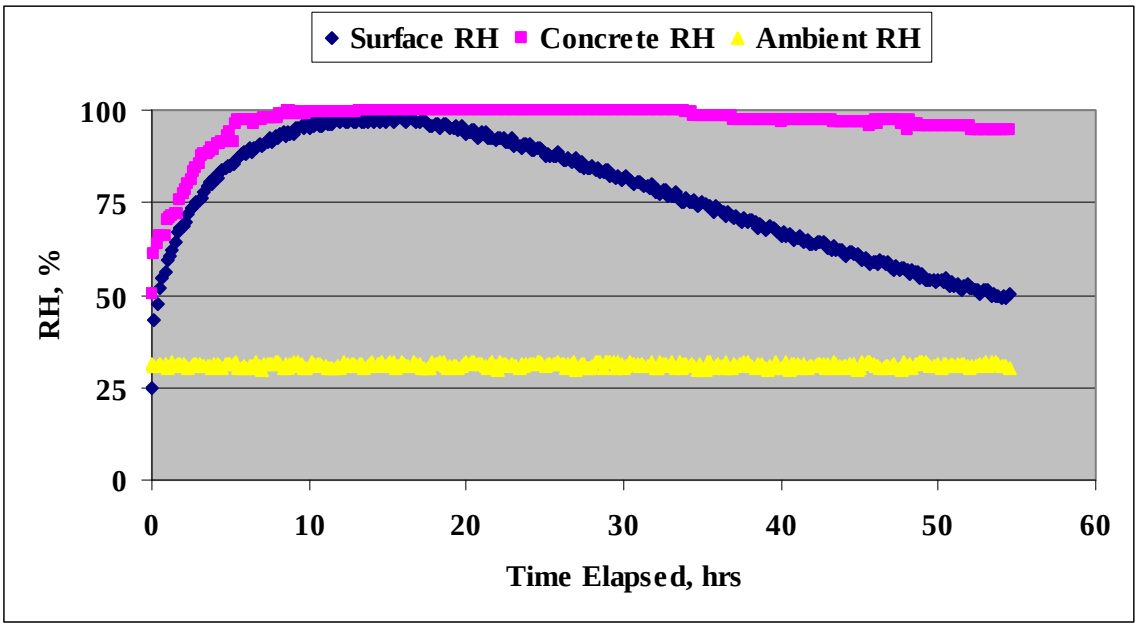

Figure 3-1. Typical Relative Humidity Curve: High Bleeding at Initial Stage (WRM 2250).

In order to maximize the overall utility of a curing membrane evaluation index, it should have application under both laboratory and field conditions. Relevant to previous discussions on moisture loss, a method of evaluating curing compound effectiveness could be based on the total moisture loss, particularly if it were determined relative to the moisture loss of uncured or unprotected hydrating concrete Moisture loss measures are of course obtainable under laboratory conditions but impractical under field conditions, unless calibration procedures are implemented to adjust the calculated evaporation as a prediction that is a function of variable weather conditions in the field. Predictive models for evaporation are often based on energy concepts.

Gibbs' free energies per unit mass of water in the concrete and in the environment, which are related to the concrete and ambient RH, respectively govern the rate of moisture exchange between concrete and the ambient air. It can be described by Equation (3-1) (Bažant and Najjar 1972) as:

$$\vec{n} \cdot \vec{J} = -B\left(\ln(RH_a) - \ln(RH_s)\right) \tag{3-1}$$

where:

B = surface emissivity, which is the property of curing membrane;

$\vec{n}$ = unit outward normal at the concrete surface;

RH_a = ambient relative humidity;

RH_s = surface relative humidity; and

$\vec{J}$ = water evaporation rate.

Using laboratory measured moisture loss data, the parameter B can be calculated using a revised form of Equation (3-1):

$$B = -\frac{\vec{n} \cdot \vec{J}}{\left(\ln(RH_a) - \ln(RH_s)\right)} \tag{3-2}$$

The parameter $\vec{J}$ can also be expressed (Bažant and Najjar 1972) as:

$$\vec{J} = -c \cdot grad\ RH \tag{3-3}$$

and by rewriting Equation (3-1):

$$c \cdot grad(RH)\vec{n} = B(\ln(RHa) - \ln(RHs)) \tag{3-4}$$

Accordingly, a parameter c/B can be defined (Bažant and Najjar 1972) by rewriting Equation (3-4), as shown in Equation (3-5):

$$c/B \cdot = \frac{(\ln(RHa) - \ln(RHs))}{grad(RH)\vec{n}} = ECT \tag{3-5}$$

The units of c/B are of length and is further defined as the effective curing thickness (ECT) as a means to convey the physical meaning of this ratio. Under laboratory conditions, ECT is a direct measure of curing compound effectiveness and in this regard can be described as the equivalent layer of concrete that would provide the same degree of curing as the curing medium. Under constant ambient RH conditions, the effective curing thickness increases as the difference between the ambient and the humidity immediately below the curing membrane increases.

Using the data in Figure 3-2, calculation of instantaneous ECT using Equation (3-5) and the accumulated ECT results in trends shown in Figure 3-3. It is noted that *grad(RH)* parameter can be approximated by taking the difference between the surface and concrete RH divided by the distance between them.

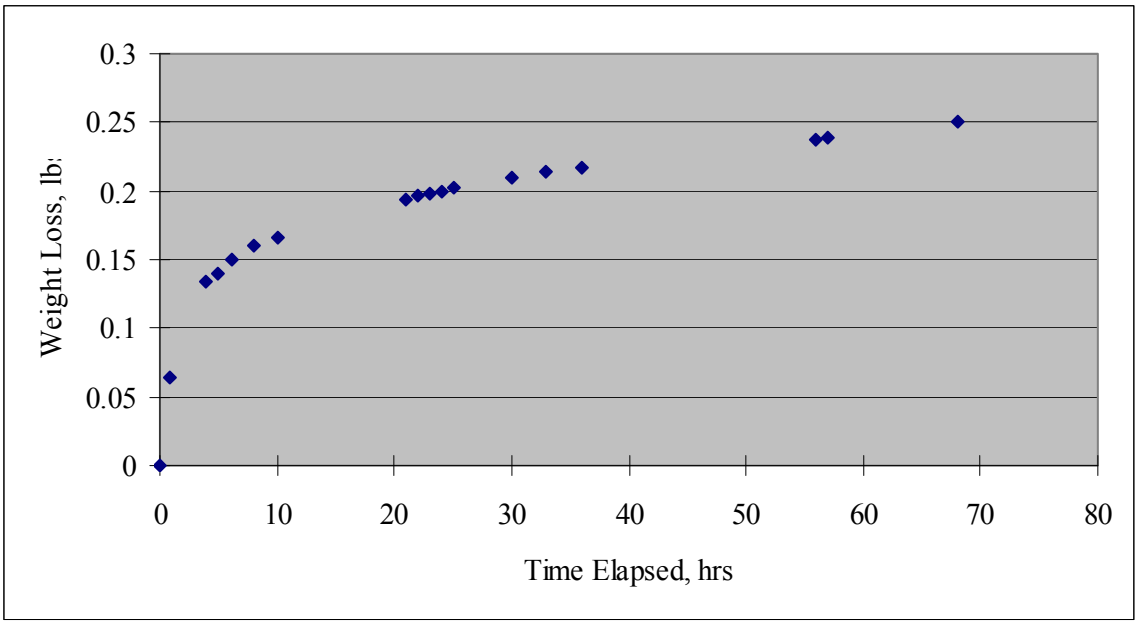

Figure 3-2. Moisture Loss Data (WRM 2250).

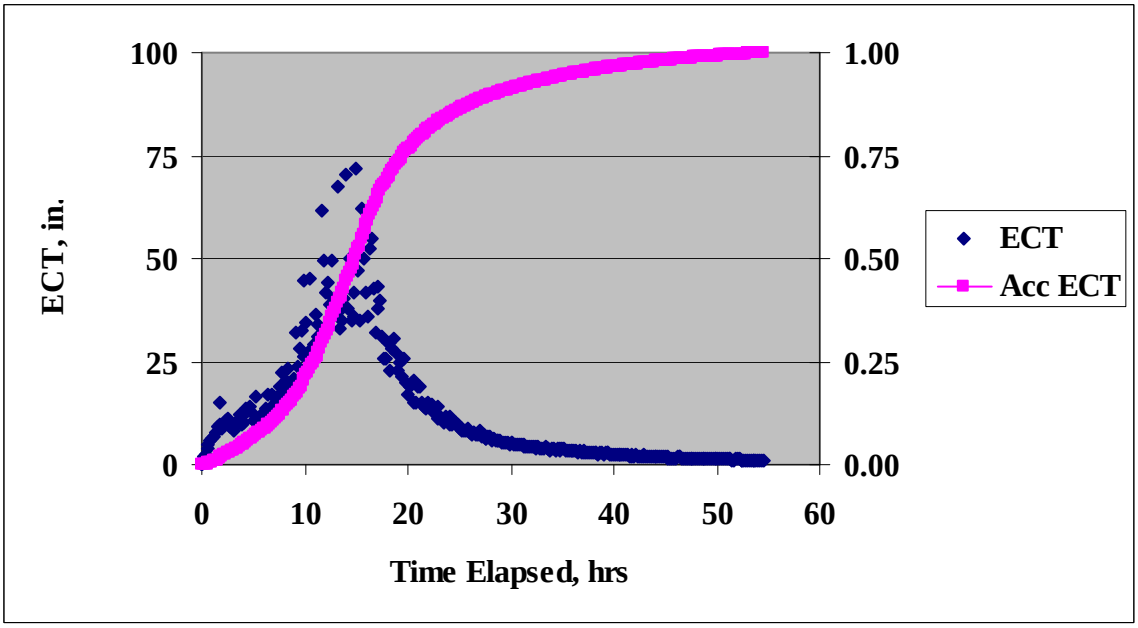

Figure 3-3. ECT vs. Time (WRW 2250).

Research under Project 0-1700 (Appendix A) indicated that the peak of the ECT curve actually coincided with the end of the bleeding period for hardening concrete corresponding to a tapering off of increasing vapor pressure trends. Apparently, there is some similarity between the trend of the accumulative ECT ($\frac{\sum ECT_i}{ECT_{Tot}}$) curve shown in Figure 3-3 and the trend of the moisture loss curve shown in Figure 3-2. Since ECT is both a field and a laboratory determinable parameter, there is utility in it being associated with moisture loss due to evaporation, which unfortunately is only practically measurable under laboratory conditions. Furthermore, since ECT_i and $\sum ECT_i$ are obviously related, the parameter $\frac{ECT_i}{\tau}$ (where τ is the maximum ECT) can advantageously be substituted for $\frac{\sum ECT_i}{ECT_{Tot}}$ in correlations with moisture loss trends. Since $\frac{\sum ECT_i}{ECT_{Tot}}$ is not consistently determinable from the collected humidity data provided by the curing monitoring system (CMS) unit, making this substitution is important. Nonetheless, both the accumulative moisture loss and ECT trends can be represented by a Weibull accumulative distribution (represented by $e^{-\frac{t}{\beta}^{\alpha}}$ where t = time) which has been widely used in many engineering applications due to its versatility. Depending on the values of the Weibull distribution parameters α and β, the Weibull distribution can be used to model a variety of characteristics relative to either the moisture loss or curing compound behavior.

Based on Chapter 2 discussions, an evaluation index (EI) in which to represent curing effectiveness using moisture loss data can be formulated (based on 24-hour moisture loss data) as:

$$EI_{ML} = 1 - \frac{Wt\ loss_{24}}{Wt\ loss_{24-uc}} \tag{3-6}$$

where:

$Wt\ loss_{24}$ = 24-hour weight loss of cured sample, and

$Wt\ loss_{24-uc}$ = 24-hour weight loss of uncured sample.

The ratio $1-e^{-\frac{t}{\beta}^{\alpha}}$ is also used to formulate and index since it can represent the degradation of the curing compound effectiveness as it would be depicted by either the change in moisture loss or ECT over time. In similar fashion using RH trends (as would be depicted in Figure 3-1), Equation (3-7) serves as a means to characterize an ECT-based EI as:

$$EI_{ECT} = \frac{ECT}{\tau} = \left[1 - e^{-\left(t/\beta\right)^{\alpha}}\right] \tag{3-7}$$

where:

τ = maximum ECT,

β = residence time factor, and

α = degradation factor.

The Weibull function relates well to the degradation of the curing compound as it ages (as governed by the α parameter) and the duration or the residence time of the curing (as governed by the β parameter) but at a time of 24 hours, the 24-hour EI_{ECT} can be determined.

EI_{ECT} ranges between 1 and 0 where quality curing would be reflected by a value closer to 1. Equation (3-7) has obvious similarities to Equation (3-6) but does involve two unknowns that require definition based on the calculated ECT data. The mathematics associated with the analysis of the regressed ECT data are elaborated in Appendix B. The determination of EI_{ECT} will be subsequently elaborated following a description of the equipment and procedures to carry out the data collection.

Averaging the 24-hour EI_{ML} and 24-hour EI_{ECT} into an overall evaluation index (EI) forms a parameter that is representative of both laboratory and field performance as well as a means to assess and rank curing compound quality based on 24-hour data. Consequently, the EI parameter will be representative in part of the total history of water loss, which is of course an index of ASTM C 156 but with special emphasis on the 24-hour water loss. Furthermore, EI should prove to ascertain performance differences between different curing compounds with respect, for instance, to the required number and frequency of coats, or the applications of one type of curing compound to achieve equivalency with another type curing compound, or a specification standard of a minimum curing effectiveness. Finally, the EI should be useful to establish the rate of application in the field, necessary to achieve the specified level of curing quality in accordance with a specified degree of strength gain.

LAB TEST PROTOCOL

A new protocol is subsequently described outlining the equipment and procedures to collect both moisture loss and relative humidity data in which to calculate EI_{ML} and EI_{ECT}. Since these parameters relate to the quality of the curing compound (versus the quality of the concrete) they can be used, as subsequently described, to rank curing compound effectiveness. How EI relates to the rate of application under field conditions will be introduced later. The laboratory-based test protocol outlined in Figure 3-4 consists of test procedures, analysis, and curing compound effectiveness evaluation.

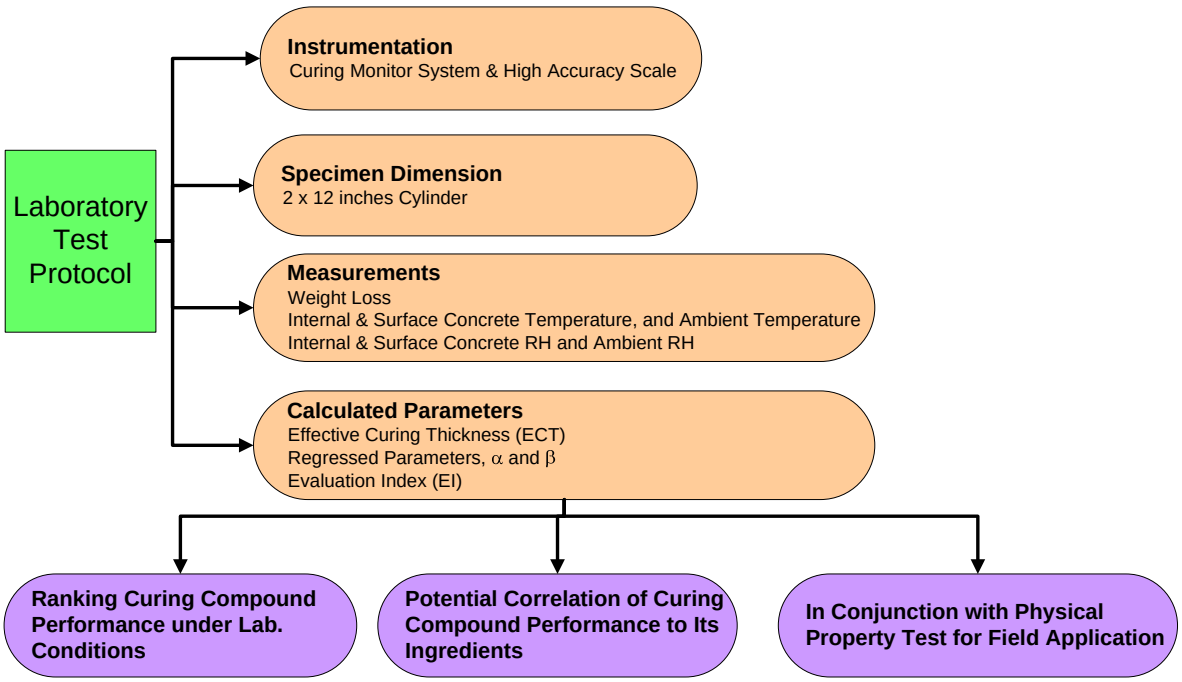

Figure 3-4. Diagram of Lab Test Protocol.

A curing monitor system (CMS) and a high accuracy weighing scale are used to monitor the weight change of a curing specimen in the laboratory using a mortar cast in a mold with a depth of 2 in. and a diameter of 12 in. Weight loss, relative humidity, and temperature at three locations (ambient, surface, and concrete) are recorded. The evaporation rate (as reflected in the weight loss over time) and the ECT are determined from this data as previously described.

Equipment and Instrumentation

Weight loss data and relative humidity data are two primary test measurements. A weighing scale, shown in Figure 3-5, with 0.1 gram accuracy was used while the relative humidity data were measured using the CMS device (manufactured by ATEK Co. in Dallas, Texas). A detailed view of this device is shown in Figure 3-6. The unit consists of three relative humidity sensors arranged to measure the relative humidity above, at, and below the concrete surface. The concrete RH sensor, is a chilled mirror hygrometer type sometimes called an optical condensation hygrometer, is the most

accurate, reliable, and fundamental hygrometer commercially available. As a result, it is widely used as the calibration standard. Since the moisture state inside young concrete is mostly saturated, the chilled mirror hygrometer is the most suitable sensor to measure the relative humidity inside concrete. Recent modifications of the CMS unit added the capacity to monitor wind speed and solar radiation, which are two other important factors to affect evaporation and curing quality under field conditions. Those two sensors are also shown in Figure 3-6.

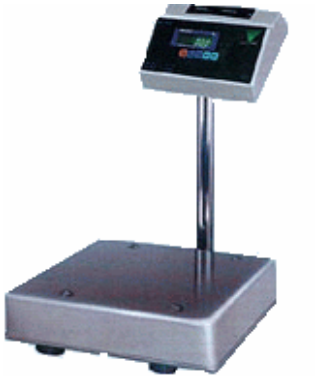

Figure 3-5. Weighing Scale.

The moisture loss specimen consists of a mortar cast in a cylindrical mold with an inside diameter of 2 in. The mold consists of 0.5-in. thick PVC pipe wall and an end plate with a thickness of 0.25 in.

Relative humidity measurements at the concrete surface and 1 in. below require sampling chambers in order for the chamber pressure to equilibrate with the pore pressure inside the concrete. Sampling chambers are shown in Figures 3-7 and 3-8. The chamber for chilled mirror sensor is inserted 1 in. into the concrete. The chamber for concrete surface humidity rests on the surface of the fresh concrete and consists of a filter paper lid (Figure 3-7 [a]) on which a layer of curing compound is sprayed. The relative humidity in the surface humidity chamber consequently represents the humidity of concrete surface immediately below the curing membrane. Figure 3-9 shows the entire test setup for the new protocol.

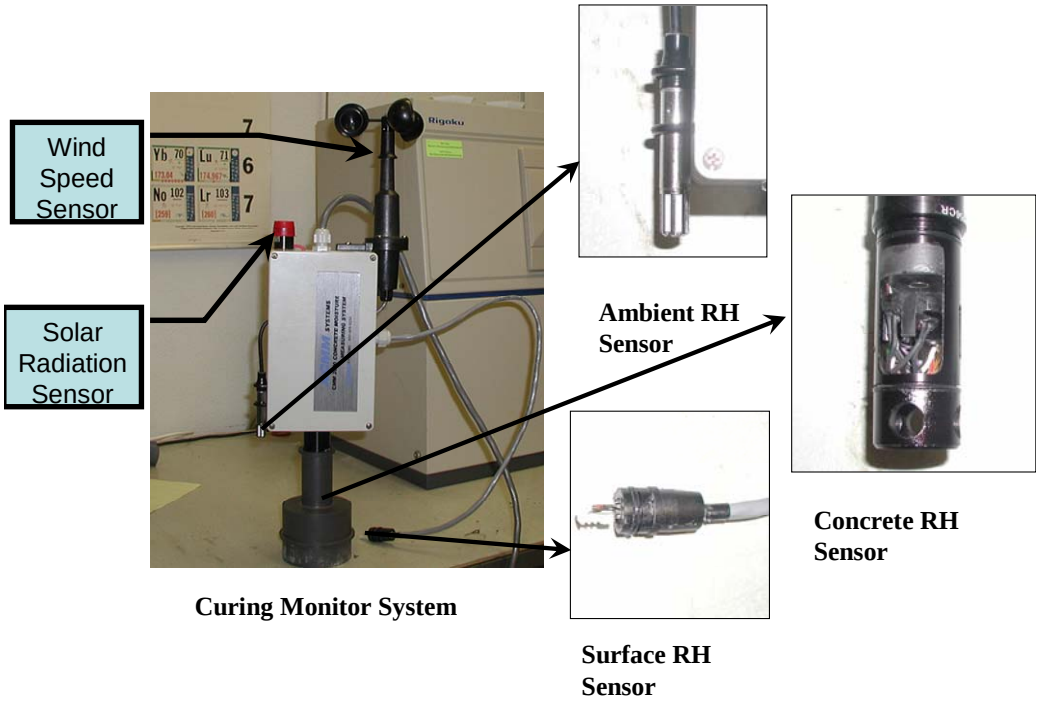

Figure 3-6. CMS Sensors.

(a) Filter Paper Cover (b) Surface Chamber

Figure 3-7. Surface Chamber Setup.

Figure 3-8. Chilled Mirror Chamber.

Figure 3-9. Laboratory Test Setup.

The occurrence of evaporation is mainly due to the vapor pressure difference between air and concrete surface; the bigger the difference, the faster the evaporation rate. Air flow over the mortar specimen continuously replaces the saturated air near the evaporating surface with less saturated air, which maintains the vapor pressure difference and evaporation rate. Ambient relative humidity is a direct indicator of the ambient water

vapor pressure; the lower the ambient relative humidity, the lower the ambient water vapor pressure and the larger the vapor pressure difference across the membrane leading to a higher evaporation rate. As temperature increases, the saturated vapor pressure level and the relative differences in vapor pressure increase. If the water vapor pressure in the air remains the same, the increased concrete temperature would decrease the vapor pressure difference, which decreases the evaporation rate. For consistency purposes, the test is carried out under laboratory testing conditions, shown in Table 3-1.

Table 3-1. Laboratory Standard Testing Conditions.

Wind Speed	Ambient Relative Humidity	Temperature	Application Rate
10 mph	30 percent	104±5°F	180 ft^2/gallon

Since weight loss, concrete relative humidity and temperature near the evaporative surface, concrete surface relative humidity and temperature, and ambient relative humidity and temperature are recorded, the evaporation rate can be calculated, as well as the hourly ECT. The laboratory protocol for curing compound effectiveness testing is provided in Appendix D.

Test Procedure Demonstration

The protocol can be demonstrated by first preparing the moisture loss mortar specimens. Mortar preparation and mixing can be carried out using an electrically driven mechanical mixer according to ASTM C 305, *Standard Practice for Mechanical Mixing of Hydraulic Cement Pastes and Mortars of Plastic Consistency*, using the following sequence:

1. The total amount of water is first placed in the mixing bowl.
2. The cement is introduced and mixed at a slow speed for 30 s.

3. The required amount of aggregate is added to the mixer over a period of 30 s while the mixer continues to operate.
4. The resulting mortar is allowed to mix for an additional 30 s at a medium speed.
5. After a minute rest period, the mixing is continued for an additional minute until a homogeneous mortar with no lumps is obtained. The schematic mixing procedure is given in Figure 3-10.

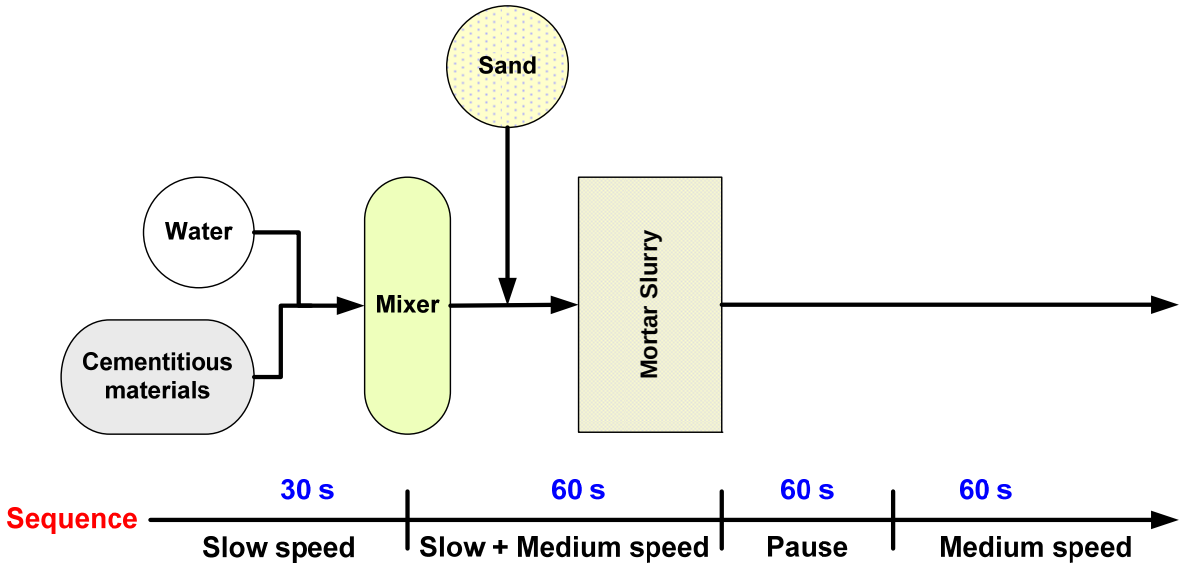

Figure 3-10. Mixing Procedure.

Materials and Mixture Proportion

The Texas Department of Transportation uses a select number of curing compounds. In the lab testing program, 10 different curing compounds, seven of which were resin-based, another was clay-based, and the other two were wax-based, were tested. The classifications of the tested curing compound samples are listed in Table 3-2. Type 2 denotes white-pigmented curing compounds. Class B denotes the solids in the compounds are resin-based, and there is no restriction for Class A.

Table 3-2. Classification of Curing Compounds.

Manufacture/Designation	Type	Comments
WR Meadow 2255	Type 2—Class B	High Reflective
WR Meadow 2250	Type 2—Class B	High Reflective
WR Meadow 1640	Type 2—Class A	Wax-based
WR Meadow 1600	Type 2—Class A	Wax-based
WR Meadow 1250	Type 2—Class B	Normal Resin-based
WR Meadow 1240	Type 2—Class B	Normal Resin-based
WR Meadow 1140	Type 2—Class B	Normal Resin-based
ECO II	Type 2—Class A	Clay-based
TSC 100	Type 2—Class A	Normal Resin-based
Concrete Chemical	Type 2—Class A	Resin-based

An ASTM Type I portland cement and masonry sand meeting the specification of ASTM C 144 was used in the mixture. The oxide composition of cement consisted of 19.12 percent SiO_2, 5.07 percent Al_2O_3, 3.40 percent Fe_2O_3, 64.73 percent CaO, 0.64 percent MgO, 3.13 percent SO_3, and 0.65 percent Na_2O_e. Its specific gravity and loss on ignition were 3.11 and 2.26, respectively. The sand had 100 percent passing the #8 sieve, an absorption capacity of 1.01 percent, and a specific gravity of 2.57.

A total of 30 mixtures were prepared where three mixtures per each curing compound were evaluated. The mixture proportion is given in Table 3-3. Test mixtures were prepared under laboratory conditions.

Table 3-3. Mixture Proportion.

Mixture	W/C	Unit Weight (lb/in.^{3})		
		Water	Cement	Sand
	0.4	2069	828	5689

Measurement of Moisture Loss

Figure 3-11 shows the development of moisture loss over 72 hr of curing. As previously mentioned in Chapter 2, all mixtures exhibited rapid initial loss of moisture followed by a more gradual period of moisture loss. Water loss up to 12 hr occupies a major part of the total moisture loss, which is attributed to bleeding action.

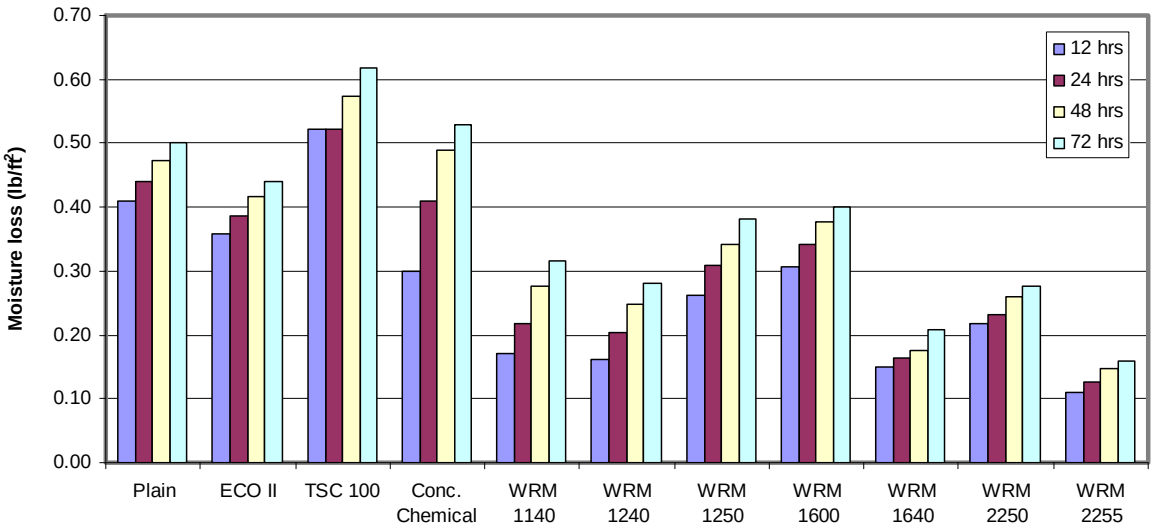

Figure 3-11. Moisture Loss of Different Curing Compound Mixtures.

As expected, the specimens with no curing compound lost water at the fastest rate, except for the mixture with the TSC 100 curing compound. TSC 100 demonstrates poor

curing protection because it loses more water (at 12 hrs) than the unprotected plain mixture. The WRM 2255 mixture had the lowest moisture loss.

Compressive Strength

Although not part of the test protocol, mortar cubic specimens of 2 in. x 2 in. x 2 in. were prepared for compressive strength according to the ASTM C 311 standard. Immediately after casting, curing compound was sprayed on the surface of the mortar specimens and placed in the humidity chamber maintained at 104 ± 1.1°F and 30 percent RH. The compressive strength was then determined at ages 1 and 3 days.

Compressive strength of the cured mortar is useful to evaluate curing quality since it is a reflection of the material porosity as affected by the curing conditions curing method and type of curing compound applied. Ensuring sufficient water availability during hydration by using appropriate curing is important to produce low-porosity and quality-strength concrete. Figure 3-12 shows compressive strength development as a function of different curing compounds (i.e., curing quality).

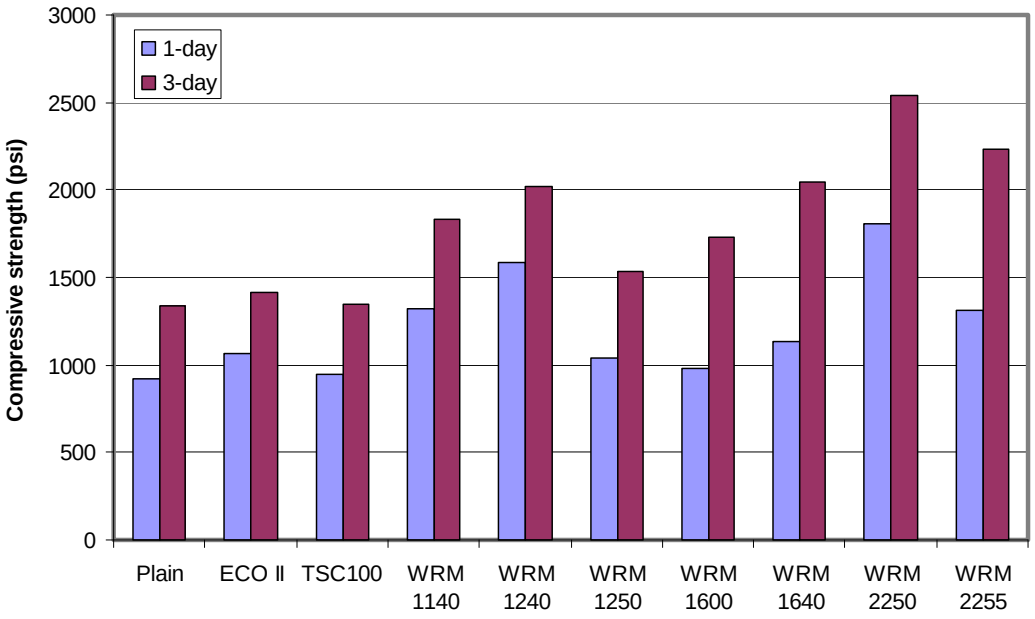

Figure 3-12. Compressive Strength Development of Different Curing Compound Mixtures.

It was observed that mixtures sprayed with WRM 2250 displayed the highest strength while the plain mixture not containing any curing compound showed the lowest strength regardless of age. ECO II curing compound, which is a clay-based membrane, shows relatively lower strength than those of resin-based compounds. Although the TSC 100 mixture had a strength lower than that of the uncured specimen.

Determination of Curing Effectiveness Index Parameters

Using Equations (3-6) and (3-7), EI_{ML}, EI_{ECT}, and EI are calculated and summarized in Table 3-4. Figure 3-13 shows the EI_{ECT} trends for all of the tested curing compounds listed in Table 3-1. Appendix C summarizes the test data in the format of Figures 3-1 to 3-3. Each compound is rated according to EI_{ML} and the EI_{ECT}. Averaging these two EIs forms the EI for ranking purposes as well as provides a tie to field performance previously discussed.

Table 3-4. Ranking of Curing Compounds.**

Type of Curing Compound	24-hr EI_{ML}	α	β	24 hr EI_{ECT}	COV	*Overall EI	Ranking
Plain	0.00	2.66	11.42	0.00	1.36	0.00	10
ECO II	0.12	2.77	10.59	0.00	1.39	0.06	8
TSC 100	0.00	2.57	13.36	0.01	0.03	0.00	10
Concrete Chemical	0.07	-	-	0.00	-	0.03	9
WRM 1140	0.50	3.25	27.37	0.80	0.80	0.65	4
WRM 1240	0.54	2.67	18.37	0.14	0.82	0.34	6
WRM 1250	0.30	3.98	26.30	0.53	0.66	0.41	5
WRM 1600	0.22	3.13	20.74	0.22	0.95	0.22	7
WRM 1640	0.63	3.34	33.30	0.69	0.21	0.66	2
WRM 2250	0.47	2.87	30.59	0.59	0.36	0.53	3
WRM 2255	0.71	3.52	37.81	0.82	0.80	0.77	1

*The overall EI is the average of EI_{ML} and EI_{ECT}.
**The curing compound rankings are listed separately in Appendix E.

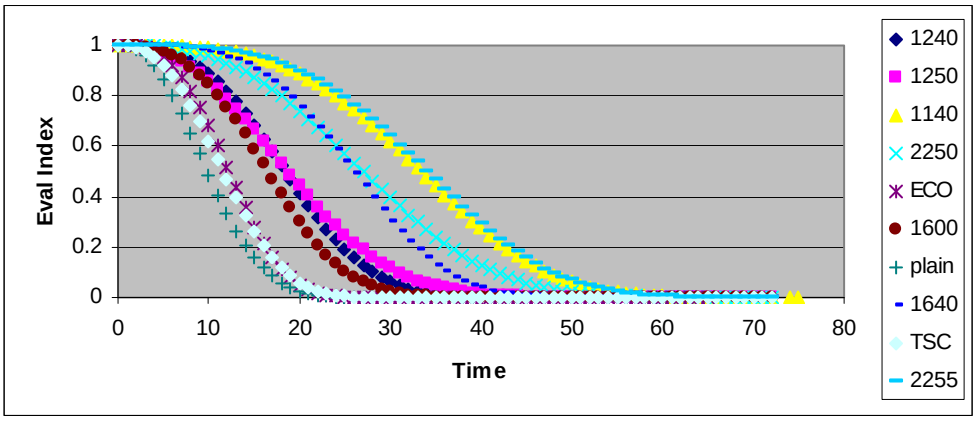

Figure 3-13. ECT Evaluation Index (EI) Results.

Extension of Test Protocol to the Application Rate (AR) under Field Conditions

A series of physical property tests were carried out similar to those identified in ASTM C 156 (which specifies moisture loss limits relative to the compressive strength of concrete as determined by cylindrical specimens (ASTM C 39)) to develop a basis for applying the curing membrane rankings to conditions in the field. Instead of using cylindrical strength specimens, thin specimens were prepared for porsimetry testing to better represent the characteristics of the surface concrete. Measured porosities are not only strength indicators but also indicators of curing effectiveness for a given curing compound. In terms of the application rate achieving a certain level curing quality of the concrete, these tests were conducted through a full factorial of combinations of two factors, the application rate and the potential for evaporation (PE – Equation 2-5).

The measurement of porosity (mainly capillary sized pores) in terms of the two-level factorial of environmental curing conditions, was done on specimens cured using the WRW 1250 curing compound as the referenced compound. The porosity of sealed and exposed specimens were also measured, and with this type of information it was possible to determine a concrete-based (versus a compound-based) evaluation parameter referred to as the curing effectiveness (CE) index calculated on a relative scale to the sealed sample porosity:

$$CE = \frac{S_C - S_E}{S_S - S_E} \quad (3\text{-}8)$$

where:

S_C = 24-hour capillary-sized porosity of cured sample,

S_E = 24-hour capillary-sized porosity of uncured sample, and

S_S = 24-hour capillary-sized porosity of sealed sample.

Mercury intrusion porosimetry (MIP) test was carried out to determine the porosity of testing specimens. As shown in Figure 3-14, MIP specimens were designed to be cured under different potential of evaporation (PE) conditions and curing conditions (application rate).

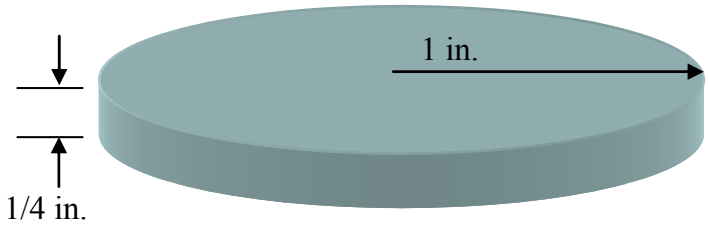

Figure 3-14. Diagram for MIP Test Specimen.

As part of bridging the gap between laboratory test and field exposure conditions, it is important to address the extremes of field conditions that occur in terms of different PE to be replicated in the lab. As stated earlier, temperature, relative humidity, and wind are the three main factors that affect PE. To achieve different PEs, three different wind conditions were used. Under some field conditions, PE could be less than 0.066 lb/ft^2/hr, but the range of the test parameters shown in Table 3-5 encompasses a broad range of field conditions. Table 3-5 lists the potential evaporation according to wind speed as well as a range of curing membrane application rates. Figure 3-15 shows how the specimens were cured under the conditions shown in Table 3-5 subjected to different rates of application.

Table 3-5. Potential Evaporation and Curing Membrane Application Rate.

		Potential Evaporation, lb/ft^2/hr
Wind speed, mph	0	0.066
	10	0.331
	20	0.596
		Curing Membrane Application Rate, ft^2/gallon
Level of application rate	Low	180
	Medium	90
	High	60

(a) High Wind Speed

(b) Medium Wind Speed

(c) No Wind

(d) Sealed Specimen

Figure 3-15. Samples Cured under Different PEs.

Figure 3-16 shows the total porosity for samples under different conditions. As expected, the intruded mercury volume is greater in specimens subjected to high wind speed and low curing application rate conditions.

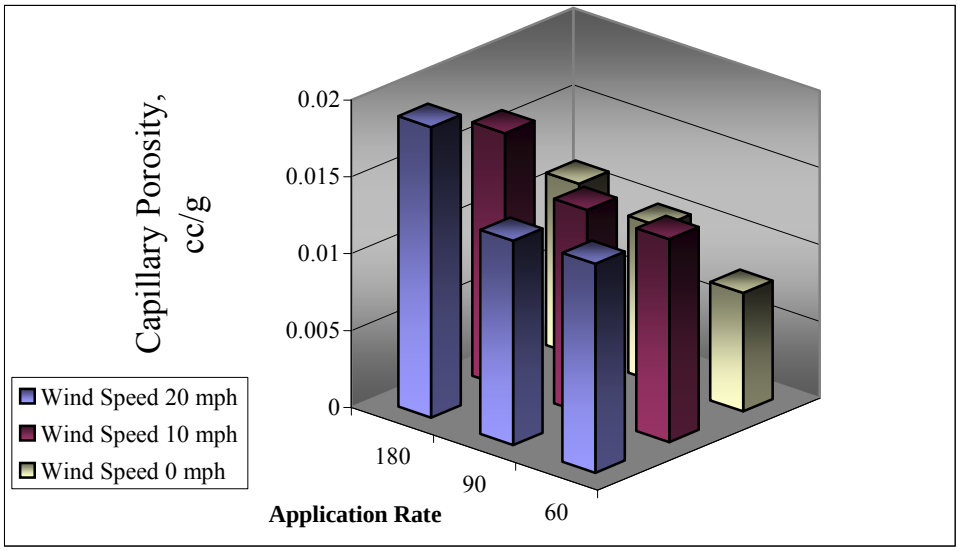

Figure 3-16. Capillary Porosity (cc/g) (WRM 1250).

The curing effectiveness index can be defined in terms of the AR and PE in the form of Equation (3-9). The increase in either AR or PE would cause CE to decrease. The regressed parameters—a, b, c, and d—are determined as 179.744, 4.223, 0.968, and 1.192, respectively.

$$\ln(CE) = -\left(\frac{AR}{a}\right)^{b} - \left(\frac{PE}{c}\right)^{d} \tag{3-9}$$

where:

a, b, c, d = regressed parameters,

AR = application rate, and

PE = potential of evaporation [see Equation (2-5)].

A nomograph is created in part from Equation (3-9) as shown in Figure 3-17. This nomograph comprises two charts. The values on each chart are CE and PE, respectively, but the nomograph needs to include a relationship between both the EI and CE. The average EI is used as the indicator of curing compound quality as determined from the laboratory testing in the nomograph and is related to CE via:

$$\frac{EI_{1250}}{CE_{1250}} = \frac{EI}{CE} \tag{3-10}$$

To use this nomograph, one starts from the EI, draws a vertical line until meeting the designed CE, then draws a horizontal line toward the chart on the right until hitting the curve with the PE value of actually ambient conditions, and then draws a vertical line toward the axis of application rate. The following example describes how to determine AR to satisfy the required CE.

The ambient weather conditions are as follows: temperature = 104ºF (40ºC), relative humidity = 30 percent, and wind speed = 10 mph. Assume 1250 and 2255 types of curing compound to be used and CE to be 0.70. The EIs for 1250 and 2255 are 0.41 and 0.77, respectively. From Equation (3-10), the PE is 0.40 lb/ft^2/hr. As shown in Figure 3-17, the application rates are projected to be 57 ft^2/gal and 160 ft^2/gal, respectively; for curing compounds 1250 and 2255 to achieve 0.70 CE under the ambient conditions, in other words, the PE would need to be no greater than 0.395 lb/ft^2/hr.

Contrast between ASTM C 156 and the New Protocol

A comparison is summarized between ASTM C156 and the new test protocol in Table 3-6. The motivation for the development of the new protocol is based on inherent limitations of ASTM C 156 based test data to serve as a measure of curing compound effectiveness under field conditions. The main limitation is its insensitivity and non-relevance to curing effectiveness under varying combinations of wind, temperature, and relative humidity. This research has demonstrated how a laboratory-measured curing parameter can be tied to field performance. The consequence of this tie is demonstrated

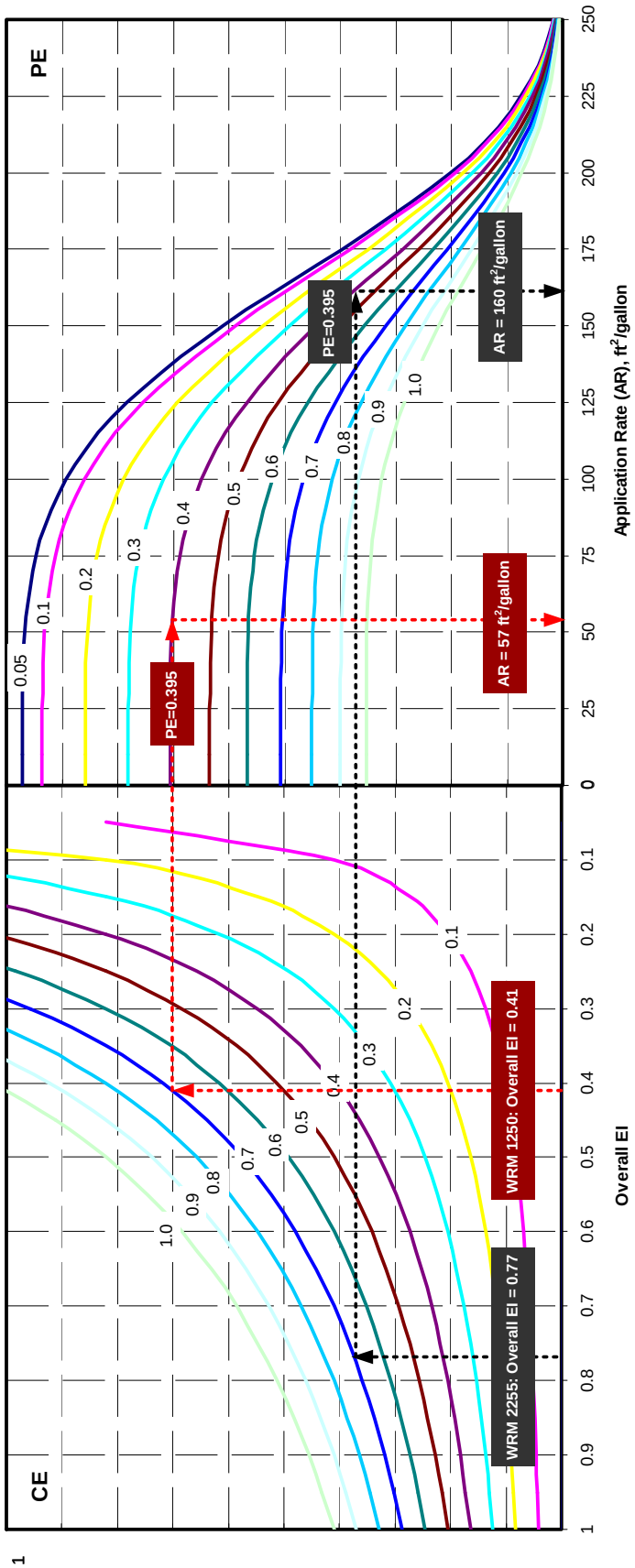

Figure 3-17. Nomograph for AR Determination.

in the differences between the quality of different curing compounds (as reflected in the EI) and the appropriate AR to yield quality curing.

The Table 3-4 data clearly demonstrate the rationale, adequacy, and repeatability of the new lab protocol and the integration of the associated EI with conditions in the field and the required rate of application to ensure adequate strength development during the curing period. The correlation between moisture loss and EI is also evident. With respect to field performance, the new protocol is a step beyond ASTM C 156 and fills a long-needed void between laboratory and field performance.

Table 3-6. Comparison of ASTM C 156 and the New Test Protocol.

	Instrumentation/ Equipment/Rate of Application	Effectiveness Basis of Curing	Dependent Parameters	Standard Conditions	Physical Properties
ASTM C 156/TX219F	Weighing Scale 1 gal/180 SF	24- and 72-hr Moisture Loss	None	Temperature and Relative Humidity	Strength of Thick Cylinders
New Protocol	CMS and Weighing Scale 1 gal/180 SF	RH Measurements at 3 Locations 24-hour Moisture Loss	PE, AR, EI	Temperature, Relative Humidity, and Wind	Porosity of Thin Samples

SUMMARY

This chapter presents a new laboratory protocol and its application to the field. A series of curing compounds were tested and ranked through this protocol. In conjunction with the physical property testing, the new protocol has the potential to guide field curing practice under various ambient weather conditions.

CHAPTER 4
FIELD TESTING ON CURING EFFECTIVENESS EVALUATION

An improved curing practice in the field relative to the use of curing membranes consists of three components: lab qualified curing compound, uniform application, and appropriate rate of application as dictated by ambient conditions, as shown in Figure 4-1.

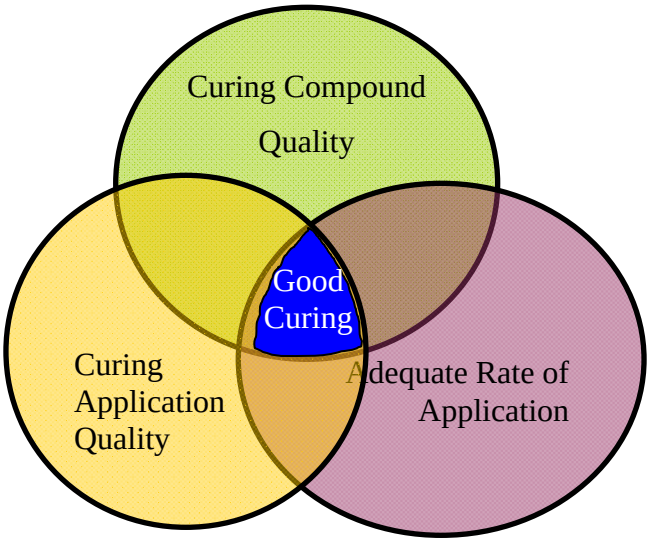

Figure 4-1. Diagram of Good Curing Practice.

A highly ranked curing compound does not guarantee the quality of the curing practice effort in the field particularly if the curing compound is not properly applied. The more severe the ambient conditions, the higher the rate of curing compound application rate should be to achieve the designed curing effectiveness. Therefore, field checks are necessary to identify the levels of key factors that affect the curing effectiveness under field conditions.

A series of field tests have been carried out in this research examining types of curing compounds, application schemes, application method, and ambient condition relative to their effect on curing effectiveness in terms of moisture retention and the resulting physical properties of the concrete.

The eight field tests comprised a wide range of geographical locations and weather patterns in Texas. The geographical distribution of the field tests is illustrated in

Figure 4-2. Figure 4-3 shows the accumulated PE for the all the field tests. The accumulated PE ranges from 3.09 lb/ft^2 (November 2005) to 12.36 lb/ft^2 (August 2006). Synthesis of the field tests and findings will be discussed thereafter in this chapter. Field test data are presented in Appendix F through Appendix M.

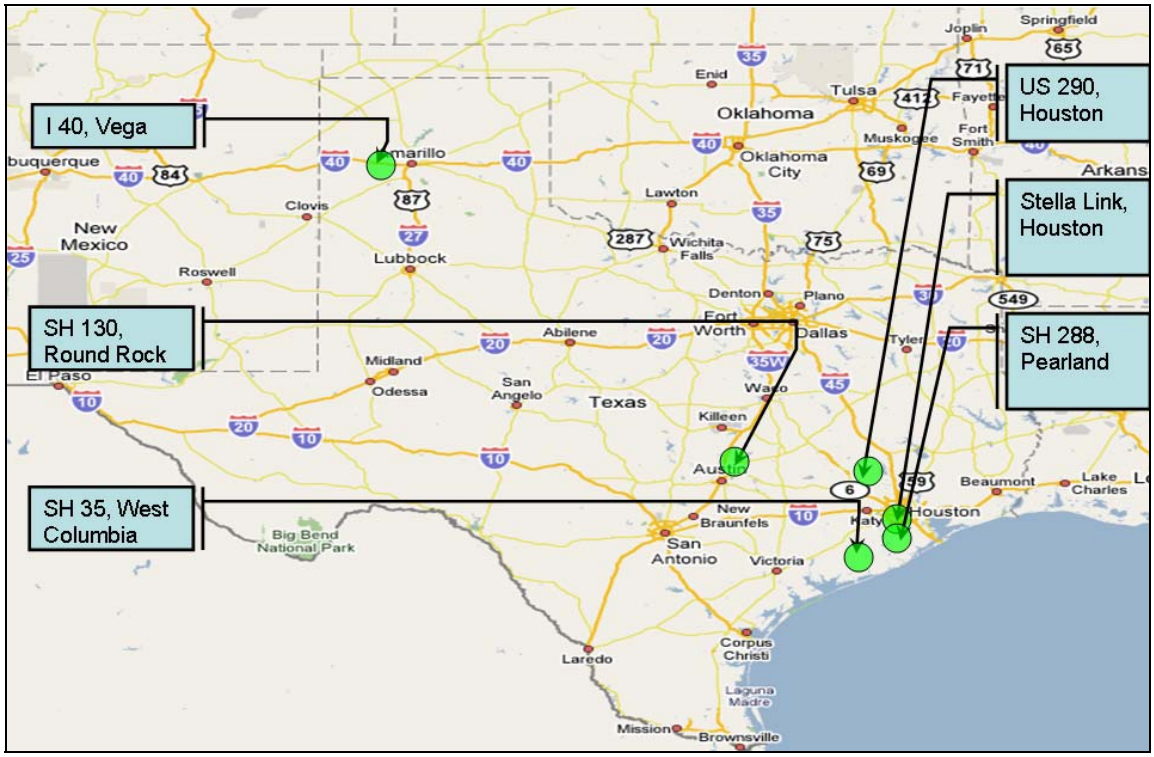

Figure 4-2. Geographical Distribution of All Field Tests.

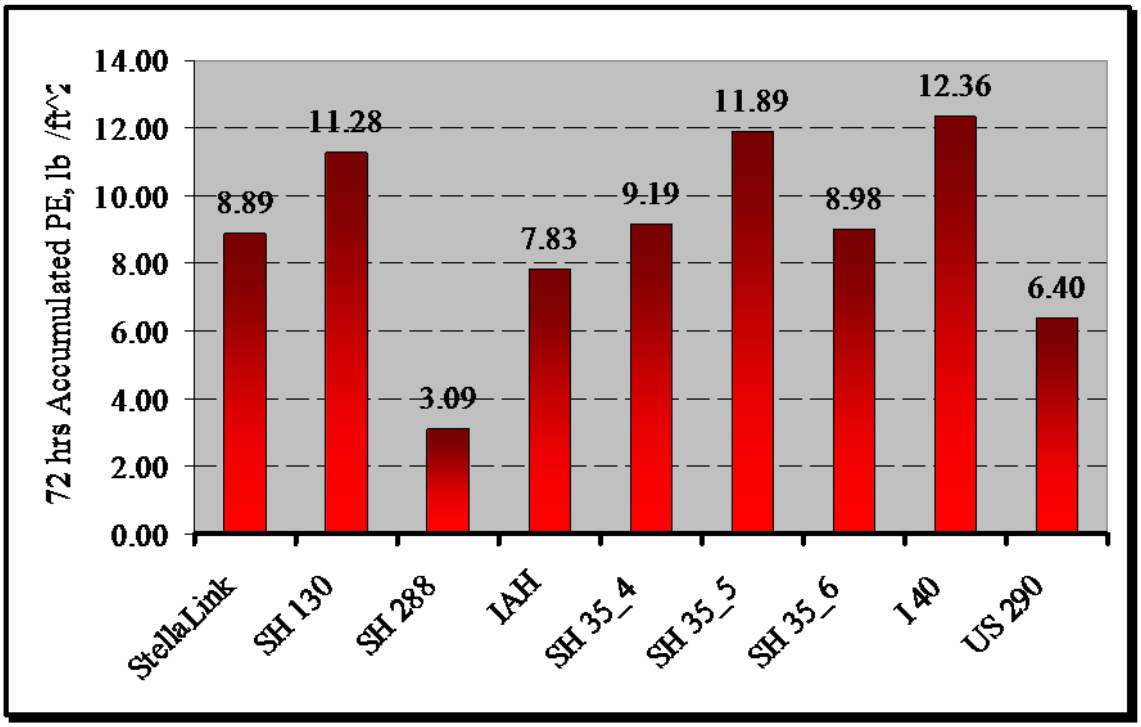

Figure 4-3. Ambient Weather Conditions of All Field Tests.

RELATIVE HUMIDITY MONITORING IN THE FIELD

As stated earlier, the CMS device requires placing two sampling chambers, one for surface relative humidity and the other for concrete relative humidity at 1 in. below the concrete surface. In order to properly install the CMS and not to interfere with the surface finishing and curing compound application operations, certain procedures need to be followed, as shown in Figure 4-4.

(a) Dummy Casing and Filter Paper Cover

(b) Removing Dummy Casing

(c) After Removing Dummy Casing

(d) Filter Paper Cover

(e) Surface Humidity Sample Chamber

(f) Setup of CMS

Figure 4-4. Procedures for CMS Setup in Field.

Procedures:

1. Place dummy casing and filter paper cover when tining is finished; see Figure 4-4 (a).
2. Remove dummy casing and take off paper filter after curing compound application; see Figure 4-4 (b) and (c).
3. Place chilled mirror sensor casing.
4. Insert chilled mirror sensor into casing, and screw the filter paper cover onto surface relative humidity chamber; see Figure 4-4 (d) and (e).

DIELECTRIC CONSTANT (DC) MEASUREMENT

A percometer was used to collect DC values, as shown in Figure 4-5. The relative dielectric constant of a material under given conditions is a measure of the extent to which it concentrates electrostatic lines of flux. It is the ratio of the amount of stored electrical energy when a potential is applied, relative to the permittivity of a vacuum. It is also called relative permittivity. The dielectric constant is represented as ε_r. It is defined as:

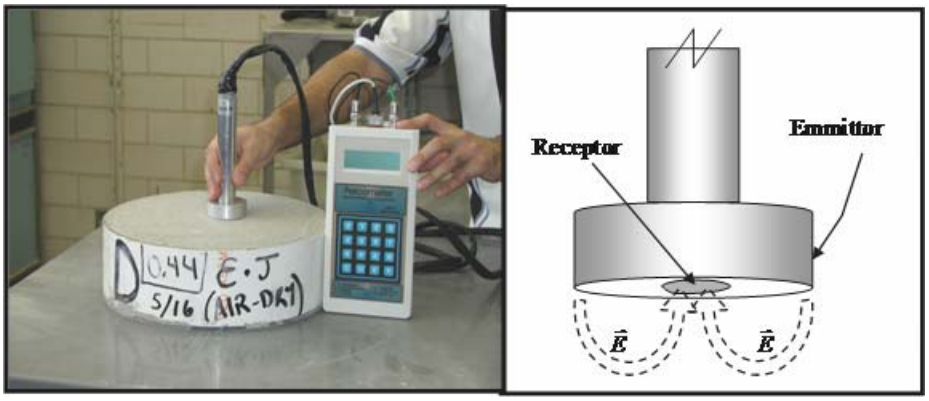

Figure 4-5. Percometer.

$$\varepsilon_r = \frac{\varepsilon_s}{\varepsilon_0} \tag{4-1}$$

where ε_s is the static permittivity of the material, and ε_0 is vacuum permittivity. Vacuum permittivity is derived from Maxwell's equations by relating the electric field intensity E to the electric flux density D. In the vacuum, the permittivity ε is just ε_0, so the dielectric constant is 1.

DC exhibits a decaying trend as concrete hardens. The decrease in dielectric corresponds to the decrease in water content of the concrete. There are two main factors causing this decrease. One is the effect of self-desiccation since hydration process and the other is the loss of water due to evaporation.

The slope in the DC data most likely represents the decaying rate of the available moisture in the capillary pores during the first couple of days after placement. These trends are only indicators of the curing effectiveness, and more research is needed to develop quantifiable parameters as moisture levels on the surface concrete. If DC slopes are intended to evaluate the curing effectiveness under different ambient conditions, normalization is needed to offset the effect of ambient conditions.

SYNTHESIS OF FIELD DATA

As stated earlier, the field curing effectiveness depends upon the curing compound quality, the curing application quality, and the ambient conditions. Each one of the three components needs to be satisfied to constitute a good field curing practice.

The findings are as follows:

- Uniformity of the curing membrane is one of the most important factors affecting curing quality. Manual spraying often resulted in non-uniform application.
- Applying the second coat in the same day when concrete is placed helps to increase curing quality.
- Curing compound application in the second day does not significantly increase the curing quality.

CHAPTER 5
CONCLUSIONS

Ensuring sufficient water availability in hydrating concrete (particularly at the surface) is of great importance to produce delamination resistant concrete for both short-term and long-term performance of concrete pavement. Insufficiently inhibited early-age evaporation from the surface of hydrating concrete pavement can result in highly porous, low strength concrete at the surface susceptible to delamination. Current laboratory curing membrane evaluation method ASTM C 156 has three deficiencies which are 1) test conditions holding little relevance to field performance, 2) confounded mortar specimen weight loss due to hardening effects, and 3) questionable basis for the moisture loss limits. A new laboratory protocol was developed to counter these limitations through a curing compound effectiveness ranking process based on the trend of the curing effectiveness over time under a standard set of testing conditions. A bridge to field performance was illustrated in terms of a nomograph relating concrete surface quality to the curing compound ranking and placement conditions. The nomograph development was carried out with the aid of a factorial design consisting of different application rates and PEs; providing a means to guide curing practice based on the ambient field conditions and the type of curing compound.

Extensive field tests were conducted to investigate the adequacy of the curing effectiveness nomograph from both a moisture retention standpoint and a physical properties standpoint. Researchers found the following items to ensure quality curing:

1. Obtaining uniformity of the application of the curing membrane. This is best achieved using the automatic spraying equipment that follows behind the paving train. Manual spraying can also achieve similar if not better uniformity; however the spray equipment needs to be sufficiently pressurized to vaporize the curing compound to form a finely divided mist ensuring even distribution of the compound.
2. Use of multiple, delayed applications of curing compound. Although the findings from the field testing were inclusive (perhaps because of the method

of placement), the application of at least one delayed or additional coat of curing compound anywhere from a half to a full day after placement of the concrete appears to improve the quality of curing. Future implementation efforts should further validate this aspect of curing with consideration to application rates and type of curing compound.

3. Selecting the rate of application as a function of the prevailing PE conditions. There is no compelling justification to assume the ASTM C156 application rate should yield adequate curing under field conditions. PE will vary from day to day as well as from morning to afternoon but adjustment of the rate of application should be a practical matter for the paving contractor to address based on expected weather conditions. Again, the details and the management of such adjustments should be the focus of future implementation efforts.
4. Use of higher quality curing compounds with an EI of 0.3 or greater. Higher quality curing compounds are more difficult to place due to their greater viscosity but their use would involve fewer or lower rates of application at the same quality of curing. The use of such compound could be predicated upon threshold seasonal increases in PE during the construction period or by not using compound EIs less than 0.3 for PEs greater than 0.4 $lb/ft^2/hr$.

REFERENCES

ASTM C 39 (1999). Standard Test Method for Compressive Strength of Cylindrical Concrete Specimens. Annual Book of ASTM Standards. West Conshohocken, Pennsylvania.

ASTM C 309 (2003). Standard Specification for Liquid Membrane-forming Compounds for Curing Concrete. Annual Book of ASTM Standards. West Conshohocken, Pennsylvania.

Bažant, Z.P., and L.J. Najjar (1972). "Nonlinear Water Diffusion in Nonsaturated Concrete." Materials and Structures 5(25).

Carrier, R.E., and P.D. Cady (1970). "Evaluating Effectiveness of Concrete Curing Compounds." Journal of Materials 5(2).

Catalog 45A (1997). Agricultural Spray Products Catalog. Wheaton, Illinois, Spraying Systems Co.

Davis, H.E. (1940). Autogenous Volume Change of Concrete. Proceedings of the 43rd Annual ASTM Meeting, Atlantic City, New Jersey, June, pp 1103-1113.

Gause, G.R., and J. Tucker (1940). "Method for Determining the Moisture Condition in Hardened Concrete." Journal Research National Bureau of Standards 25: 403-416.

Lasseter, F.P. (1931). "Chemical Reactions in the Setting of Cement," Dissertation (Ph.D.) Columbia University.

Miller, J.S. and W.Y. Bellinger (2003). Distress Identification Manual for the Long-Term Pavement Performance Program. McLean, Virginia, Federal Highway Administration.

Mukhopadhyay, A.K., D. Ye, and D.G. Zollinger (2006). Moisture-Related Cracking Effects on Hydrating Concrete Pavement. College Station, Texas, Texas Transportation Institute.

Powers, T.C., and T.L. Brownyard (1947). Proceedings American Concrete Institute.

Powers, T.C. (1947). A Discussion of Cement Hydration in Relation to the Curing of Concrete. Highway Resource Board, Washington D.C.

Swayze, M.A. (1942). Early Concrete Volume Changes and Their Control. American Concrete Institute.

Vandenbossche, J.M. (1999). A Review of the Curing Compounds and Application Techniques Used by the Minnesota Department of Transportation for Concrete Pavements.

Wainwright, P.J., and J.G. Cabrera (1990). Assessment of the Efficiency of Chemical Membranes to Cure Concrete. Proceedings of an International Conference on the Protection of Concrete, Dundee, Scotland.

Cable, J.K., K. Wang, and Z. Ge (2003). Investigation Into Improved Pavement Curing Materials and Techniques: Part 2 (Phase III). Report Number: CTRE Project 02-77, Iowa State University, Ames, Iowa.

Whiting, N.M., and M.B. Snyder (2003). Effectiveness of Portland Cement Concrete Curing Compounds. Transportation Research Record 1834, Transportation Research Board, National Research Council, Washington, D.C., pp 59-68.

APPENDIX A

TxDOT TECHNICAL MEMORANDUM

CURING AND EVAPORATION ON CONCRETE

TECHNICAL MEMORANDUM
TEXAS DEPARTMENT OF TRANSPORTATION

To: Project 1700 Staff

From: Dan Zollinger and Jin-Hoon Jeong
Texas Transportation Institute

Subject: Project Status Report Date: July 09, 2002
Test Methodology and Model for Curing Effectiveness of Concrete Pavement

Early age moisture loss from the surface of a concrete pavement may induce undesirable effects that play a factor on long-term performance. Early aged detrimental behavior such as slab curling, warping, delamination, and even plastic shrinkage cracking are affected by the amount of evaporation and the effectiveness of the curing medium. The rate of evaporation is a key item relative to monitoring the quality of the curing. However, most approaches for this are largely empirical and are only useful under laboratory conditions. The effective curing thickness concept is introduced as a method to evaluate the curing effectiveness of a curing method.

The surface relative humidity has the biggest influence on both the effective curing thickness and the rate of evaporation. Prediction of the evaporation rate of concrete depends on the surface relative humidity and is important for evaluation of the method of curing. Existing evaporation models including ACI nomograph were evaluated relative to their capability to predict the evaporation from curing concrete. Penman's evaporation model was modified based on data collected in a series of laboratory experiments.

INTRODUCTION

Available moisture in hardening concrete evolves into two types of water—one referred to as evaporable water held in both capillary and gel pores including interlayer pores and the other as non-evaporable water combined structurally in the hydration products *(1)*. The sum of these portions equals the total water content in the paste. Water available in the capillary pores evaporates at the surface of concrete when it is exposed to ambient weather conditions. Because the predominance of moisture movement associated with evaporation occurs in the surface area, moisture variations within the cross-section of the concrete are found mostly near the surface. Typical relative humidity profiles for both a specimen made in laboratory and a test slab made in the field are shown in Figure A-1. These moisture profiles are of concern with respect to the effect on slab deflections and development of delaminations in bonded concrete overlay systems *(2)* at an early age.

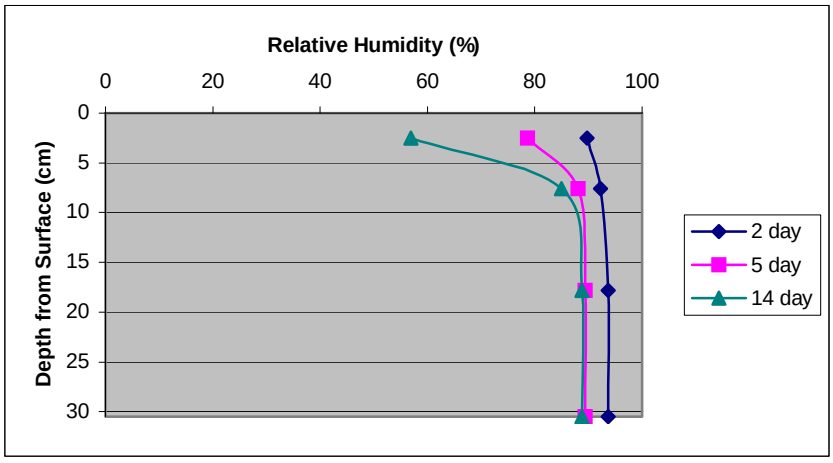

(a)

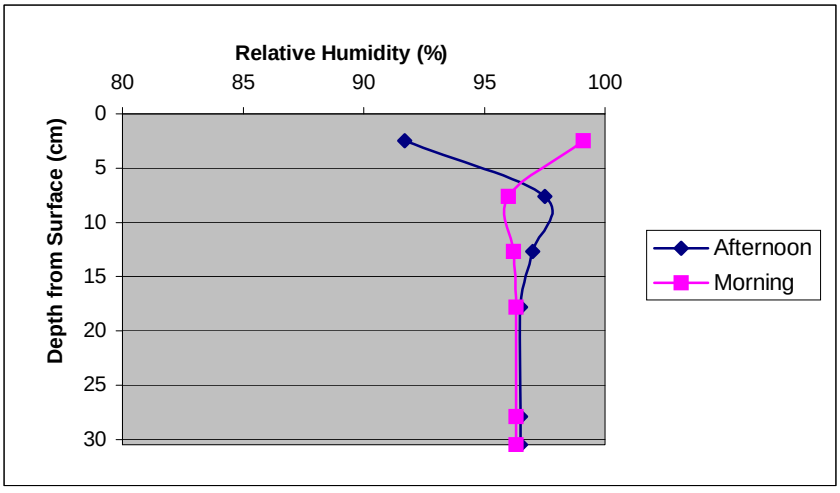

(b)

Figure A-1. Moisture Profiles in Concrete: (a) From a Specimen Cured in 15% Room Relative Humidity; (b) From a Test Slab Cured in Field.

Evaporation at the surface of a concrete slab can be defined as the net rate of vapor transport to the atmosphere *(3)*. This change in state requires an exchange of approximately 600 calories for each gram of water evaporated. Vaporization removes heat

from water near the surface of the concrete slab being vaporized. Therefore, evaporation is another important factor to be considered in the analysis of thermally induced stresses and strains in a concrete slab in addition to conduction, convection, and radiation *(4)*.

Evaporation is controlled by use of the appropriate curing method to minimize potential for undesirable cracking and deformation at early ages. The presence of water serves to enhance both hydration and strength development. As hydration advances and fills the space available in the capillary pores, capillary porosity continues to decrease, and the amount of the gel pores increase. Gel pores tend to limit the movement of moisture through the capillary pores. Thus, the increase of hydrated product and reduced capillary porosity reduces the rate of evaporation. Drying shrinkage, due to evaporation, which leads to cracking or warping is also controlled by minimization of water loss from capillary pores *(1, 5)*. Strength of concrete is affected not only by the total moisture content but also by the moisture variations in the concrete. For an example, test data have indicated that even a short period of drying causes a recognizable decrease in the magnitude of tensile strength in the surface due to the moisture variation *(6)*.

Numerous efforts have been made to develop empirical models to express evaporation as a function of atmospheric factors *(7-12)*. Most of the models are of the Dalton type and have been presented in the form of *(13)*:

$$E = (e_s - e_d)\, f(v) \tag{1}$$

where

E = rate of evaporation ($FL^{-2}T^{-1}$)
e_s = saturation vapor pressure of water surface (FL^{-2})
e_d = vapor pressure of air above water surface (FL^{-2})
$f(v)$ = wind function
v = wind speed (LT^{-1})

The ACI nomograph *(14)* shown in Figure A-2 was based on the Menzel's model *(9)* derived from the Dalton's model *(13)* and the Lake Hefner test results conducted between 1950 and 1952 *(15)*. The Menzel's model, Equation (2), has been accepted as one of the best methods for predicting evaporation of bleed water while it is exposed on the surface of the concrete (which inherently excludes the consideration of curing media).

$$E = 0.44(e_s - e_d)(0.253 + 0.096v) \tag{2}$$

However, since the quantified net radiation was not measured during the Lake Hefner tests, this model also fails to consider the effects of radiation on evaporation. Another shortcoming is related to vapor pressure effects, which can be overcome by considering the many equations that have been suggested to express vapor pressure as a function of temperature *(16-19)*.

Another widely used method for evaporation prediction is Penman's model *(7)*. Penman's model, shown in Equation (3), is also based on Dalton's model but resolves the difficulties of existing Dalton type models relative to wind and surface vapor pressure effects field. This model predicts evaporation by considering both net radiation and aerodynamic effects.

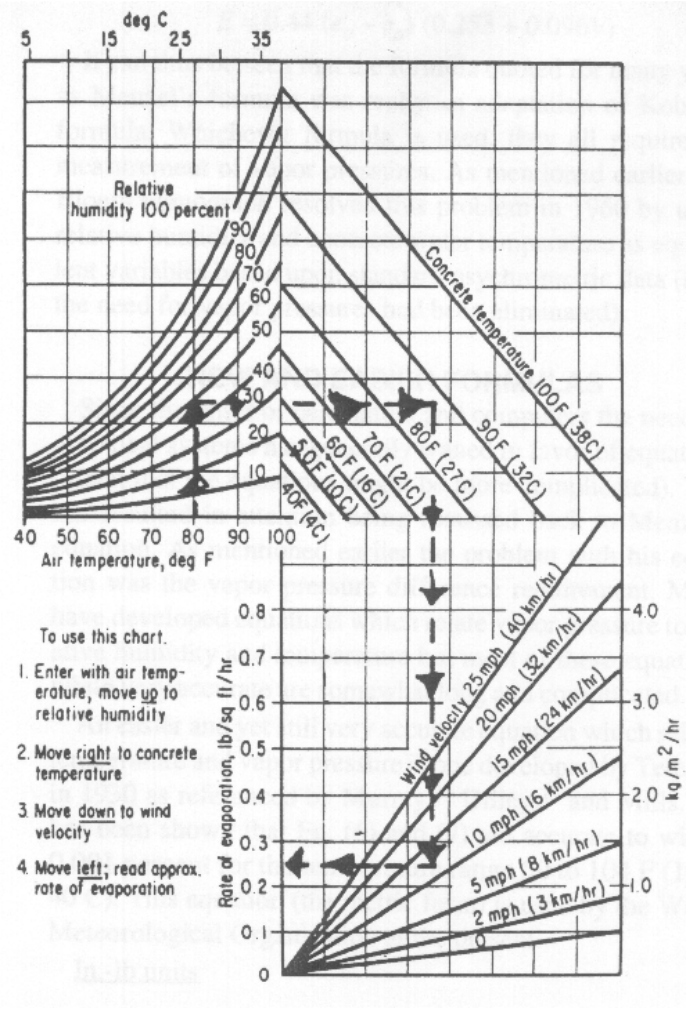

Figure A-2. ACI Evaporation Nomograph *(14)*.

$$E = \frac{\Delta E_q + \gamma E_a}{\Delta + \gamma} \tag{3}$$

where

Δ = slope of the saturation vapor pressure versus temperature curve (FL^{-2})

$$= \frac{e_s - e_a}{T_s - T_a}$$

e_a = saturation vapor pressure of air (FL^{-2})

T_s = surface temperature

T_a = air temperature

E_q = rate of evaporation due to net radiation ($FL^{-2}T^{-1}$)

γ = psychometric constant (FL^{-2})

E_a = rate of evaporation due to aerodynamic effects ($FL^{-2}T^{-1}$)

Both the ACI nomograph and Penman's model are based on evaporation from a water surface but fail to consider the effects of changes of moisture within the concrete with time, and consequently cannot accurately predict evaporation from concrete (particularly, beyond the cessation of bleeding). Therefore, development of a theoretical model for prediction of evaporation from concrete both before and after bleeding is necessary.

LABORATORY TEST PROGRAM

A laboratory test program was carried out to develop a test methodology and a model to evaluate curing methods for concrete pavement construction. A cylindrical mold with inside diameter of 30.5 cm (12 in.) and height of 15.2 cm (6 in.) was prepared. The mold consisted of 1.3 cm (0.5 in.) thick PVC wall and end plate with thickness of 0.6 cm (0.25 in.). Concrete was placed in the mold and was compacted according to ASTM C 192 *(20)*. The concrete mixture for this testing consisted of a crushed limestone coarse aggregate and a natural sand as the fine aggregate. Table A-1 presents the mix proportions. A water cement ratio of 0.46 was used, and the unit weight of concrete was determined using ASTM C 29 *(21)* and was found to be 2422 kg/m^3.

Table A-1. Mix Proportions in 1 m^3 (1.31 Cubic Yard) of Concrete.

Material	Proportions
Coarse Aggregate (Limestone)	1143 kg
Fine Aggregate (Natural Sand)	753 kg
Cement (Type I)	360 kg
Water	166 kg
Water/Cement	0.46
Concrete Unit Weight	2422 kg/m^3

After placing concrete in the mold, a curing monitoring system manufactured by ATEK and an electronic scale with 0.1 gram accuracy was used to collect data from the concrete when it cured. The ATEK system consisted of three sensors to measure the ambient relative humidity,

the relative humidity at the concrete surface, and inside the concrete as shown in Figure A-3. The relative humidity inside the concrete was determined from a chilled mirror type sensor, which measures the dry bulb and the dew point temperature from inside a plastic casing. The relative humidity (H) data is calculated from dry bulb (T) and dew point (T_{dp}) temperature data using the following expression:

$$H = \exp\left[\left(\frac{17.502T_{dp}}{240.97+T_{dp}}\right)-\left(\frac{17.502T}{240.97+T}\right)\right] \quad (4)$$

The ATEK system includes a plastic casing, as noted in Figure A-3, connected to an aluminum stand that supports the weight of the curing monitoring system which is inserted approximately 2 in. into the concrete. There are four holes in the casing 1.9 cm (0.75 in.) below concrete surface to allow the vapor pressure of the concrete to equilibrate inside the casing. The surface sensor measures the relative humidity from inside a PVC cylinder with an inside diameter and height of 6.4 cm (2.5 in.) and 5.1 cm (2 in.), respectively, as shown in Figure A-3 (b). The cylinder is placed on the concrete surface in an area cleared of the curing membrane. During the curing, weight loss of the specimen and relative humidity of ambient, surface, and in the concrete were measured until

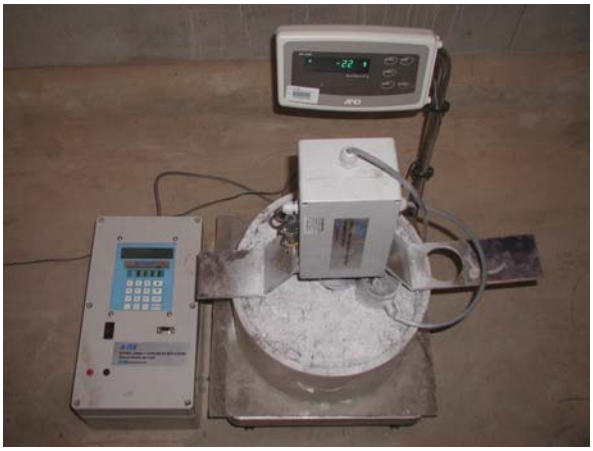

(a)

(b)

(c)

Figure A-3. Instrumentation and Devices: (a) View of Setup; (b) Chilled Mirror Sensors and Reader; (c) Stand and Tip.

the surface relative humidity equilibrated with the ambient relative humidity. Four different wind speeds, 0, 2.08, 2.83, and 5.33 m/s, were used at a room temperature and relative humidity of 40°C and 15 percent, respectively.

Relative Humidity Trends

Other laboratory tests were conducted to observe the trend of relative humidity with time and to use it to back-calculate the moisture diffusivity. A cylindrical concrete specimen with diameter of 20.3 cm (8 in.) and height of 30.5 cm (12 in.) was placed in a PVC wall.

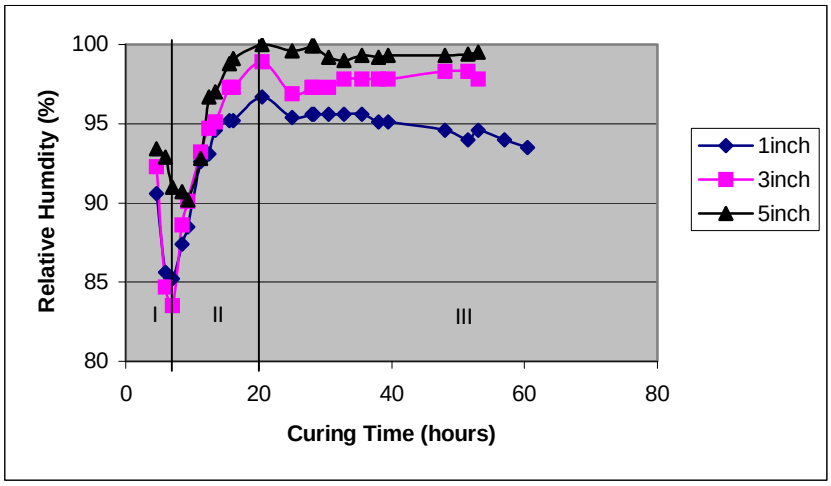

Figure A-4. Relative Humidity History of Concrete (Laboratory Test).

Moisture sensors were located 2.5, 7.6, and 12.7 cm (1, 3, and 5 in.) below the exposed surface. The temperature and relative humidity of curing room were 32°C and 50 percent, respectively.

The initially measured low relative humidity of concrete during the bleeding record in Figure A-4 appears to be due to significantly high values of moisture diffusivity in the concrete while it is in a fresh state as shown in Figure A-5. Low vapor pressure of concrete due to high moisture diffusivity results in low initial relative humidities. On the basis of numerous results from the field and the lab, the trend of relative humidity of concrete can be categorized by three stages as shown in Figure A-4. During the first stage

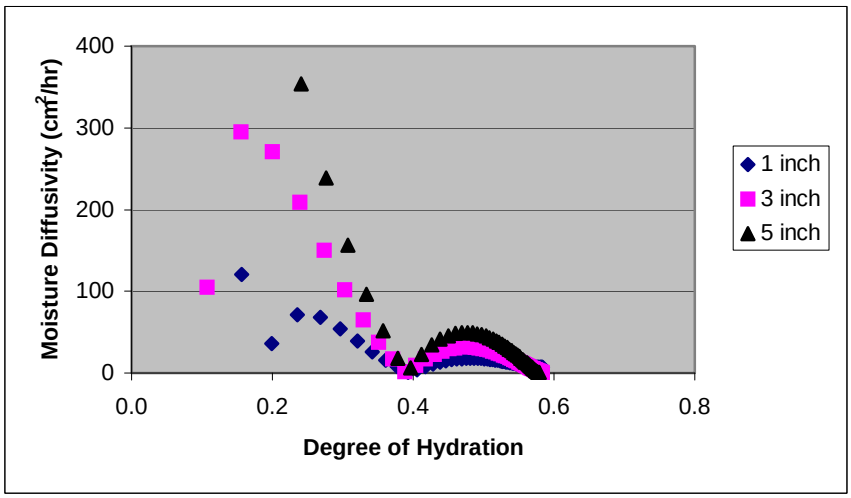

Figure A-5. Back Calculated Moisture Diffusivity.

(placement of concrete), the initially high relative humidity decreases rapidly due to high values of moisture diffusivity of concrete. This may be caused by a condition of non-equilibrium between the vapor pressure inside the concrete and the surrounding atmosphere immediately after placement. In stage II, during the bleeding stage, the relative humidity increases with time and cones to a peak as the initial substantially high moisture diffusivity decreases during this stage. However, the moisture diffusivity is still at a comparatively high level so the evaporation rate is still at a comparatively high rate. During the third stage (after bleeding), relative humidity decreases with time and is equilibrated to ambient relative humidity due to reduced moisture diffusivity of the concrete. The duration of each stage depends upon the prevalent curing conditions and water content of the concrete mixture.

Moisture diffusivity (D), which governs moisture movement with time in concrete, is back calculated from the equation of moisture diffusion based on thermodynamic equilibrium *(22)* as:

$$D = \frac{\frac{\partial H}{\partial t}}{\frac{\partial^2 H}{\partial x^2}} \tag{5}$$

where

D = moisture diffusivity (L^2T^{-1})

H = concrete relative humidity

t = curing time (T)

x = vertical coordinates in concrete (L)

From the relative humidity data in Figure A-4 and Equation (5), diffusivities were back calculated as shown in Figure A-5. Significiant changes occurred in back calculated moisture diffusivity during the early stages of hardening. The diffusivities were significantly high initially, but diminished quickly. Previous research *(22-24)* indicated that the moisture diffusivity has been found to be a function of humidity, concrete age, and paste porosity. Thus, it is reasonable that moisture diffusivity (D) is assumed to vary with relative humidity (H) and degree of hydration (α) in concrete on the basis of the test results as:

$$D = a + \frac{b}{\alpha} + cH \tag{6}$$

where *a*, *b*, and *c* are coefficients for the model of moisture diffusivity and the values of the coefficients are dependant upon mix proportioning. The moisture diffusivity is proportional to relative humidity and is reciprocal to degree of hydration as shown in Equation (6).

Determination of Curing Effectiveness

As concrete dries, free moisture disappears from the surface due to evaporation. Furthermore, higher rates of evaporation induce larger moisture variations within the cross-section of the concrete near the surface. If evaporation is minimized by a given curing method, the relative humidity immediately below the surface will be constant with time and will vary little with respect to the relative humidity inside the concrete. The ambient moisture conditions and the moisture levels at the concrete surface need to be included as a modification to Penman's model to improve its sensitivity to the curing conditions of the concrete. To this end, the effective curing thickness concept originally introduced by Bazant *(22)*:

$$L = \frac{\ln \frac{H_s}{H_a}}{\frac{\partial H_s}{\partial x}} \tag{7}$$

where

L = effective curing thickness (L)

H_s = surface relative humidity

H_a = ambient relative humidity

was adopted. Effective curing thickness can be described as the equivalent layer of concrete that would provide the same degree of curing as the curing medium. Properly cured concrete has an effective curing thickness in the range of 3 to 5 in. In other words, the thicker the effective curing thickness is, the larger the humidity difference between the surface and the point immediately below the surface *(22)*.

For a few hours after placement, the relative humidity of the surface and inside the concrete increases because of bleeding as shown in Figure A-6. Bleed water exists on the concrete surface in spite of the high rates of evaporation over this period of time as shown in Figure A-7. It is after the bleeding is complete that the surface relative humidity eventually diminishes to the ambient relative humidity.

The initial rates of evaporation computed from the test data were clearly affected by wind speeds (v). Higher wind speeds initially increase the amount of accumulative evaporation while there was little effect after a few hours as shown in Figure A-7. ACI committee 305 suggests that there should be precautions for plastic shrinkage cracking when the evaporation rate exceeds 1.0 kg/m^2/hr (0.2 lb/ft^2/hr) *(14)*. At a wind speed of 5.33 m/s, the measured evaporation rate exceeded the critical values for approximately 2 hours and then gradually decreased to zero. The measured evaporation rates during this time had nearly the same values as the evaporation rates obtained from the ACI nomograph. However,

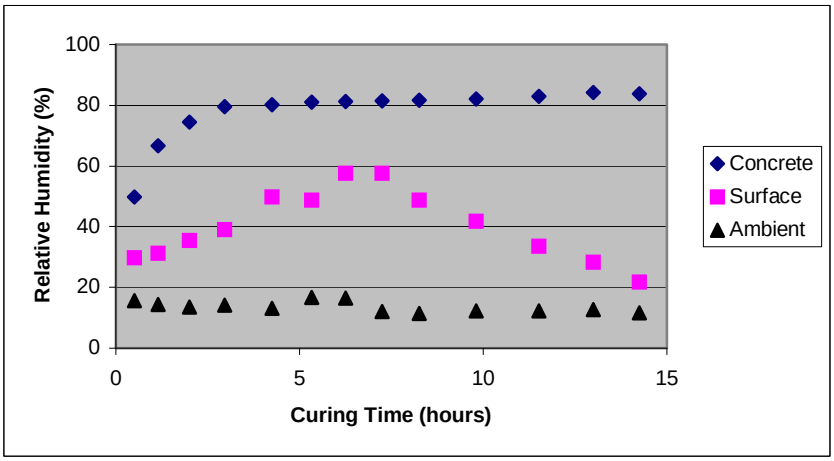

Figure A-6. Relative Humidity with Curing Time at Each Position (No Wind Case).

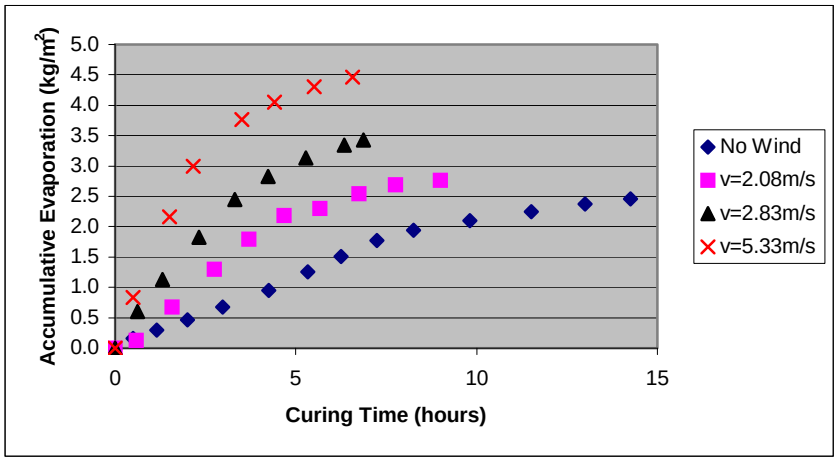

(a)

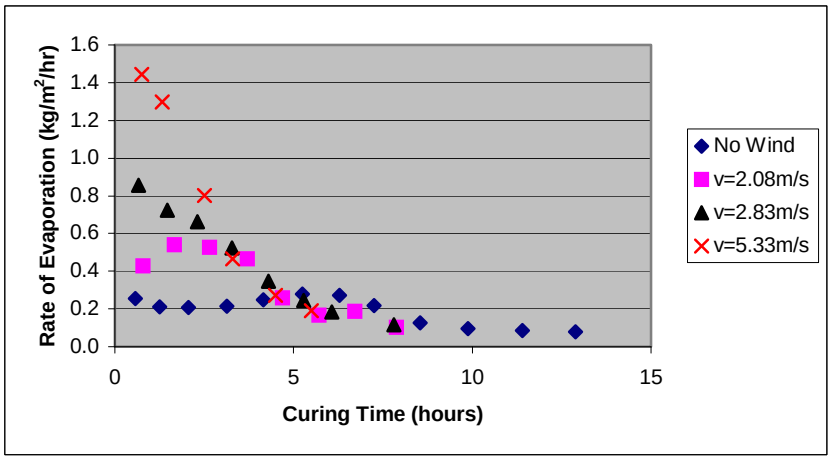

(b)

Figure A-7. Wind Effects on Evaporation: (a) Accumulative Evaporation; (b) Rate of Evaporation.

the measured evaporation rates were much smaller than the evaporation rates predicted by the ACI nomograph after bleeding as shown in Figure A-8. The ACI nomograph is apparently not sensitive to the effects of various curing methods because the nomograph does not consider the moisture condition in concrete. Since most curing methods are applied after the bleeding has stopped, the ACI nomograph may have limitations with respect to the prediction of evaporation for both cured and uncured concrete after the bleeding stage.

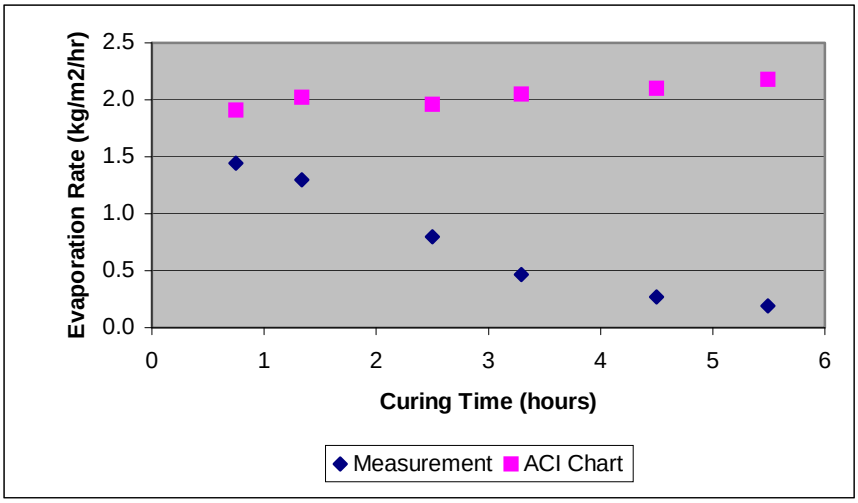

Figure A-8. Comparison of Evaporation Rate between Measurement and ACI Nomograph (v = 5.33 m/s).

The effect of wind speed on the surface relative humidity is shown in Figure A-9. Obviously, the magnitude of peak surface relative humidity and the duration of bleeding decreased as wind speed increased. The peak surface relative humidity occurred 6.3, 4.7, 3.3, and 2.2 hours after placement for 0, 2.08, 2.83, and 5.33 m/s of wind speed, respectively. Interestingly enough, there were little differences in the rate of increase or decrease of surface relative humidity between wind speeds as indicated by the trends shown in Figure A-9.

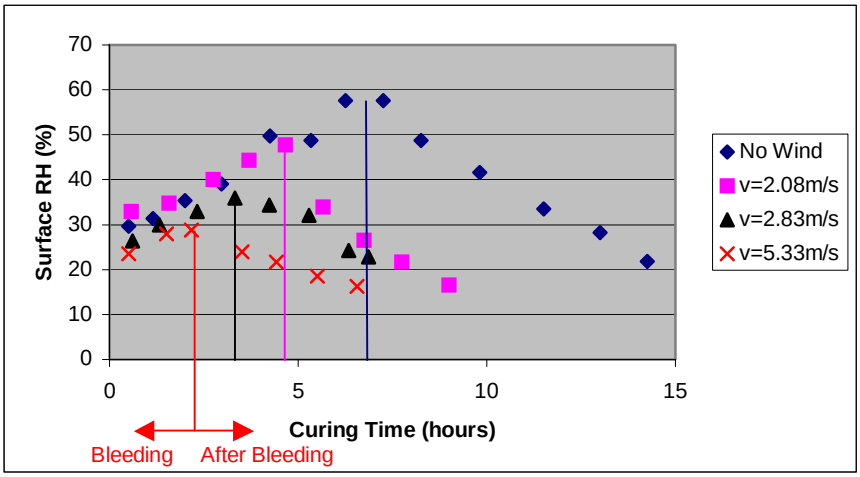

Figure A-9. Wind Effects on Surface Relative Humidity.

The trends of effective curing thickness shown in Figure A-10 were similar to those of surface relative humidity because the effective curing thickness is governed mainly by the surface relative humidity. The effective curing thickness increased throughout the duration of the bleeding as effected by the level of wind speed. The higher wind speed caused a lower effective curing thickness because of the greater loss of moisture from concrete surface by evaporation. Effective curing thickness represents the quality of curing as shown in Figure A-10 and can perhaps be used as an indicator of curing quality under both field and laboratory condition. Rate of evaporation is closely related to the curing effectiveness, and a new evaporation model is developed by the test data presented above.

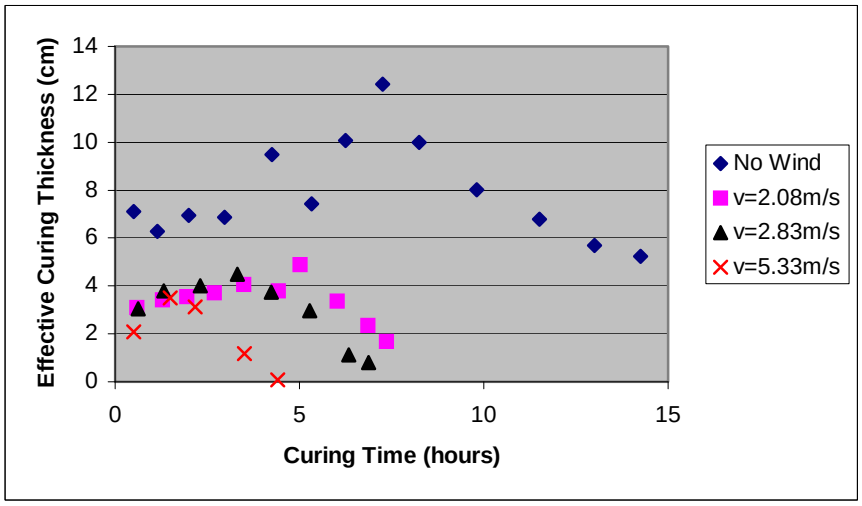

Figure A-10. Wind Effects on Effective Curing Thickness.

NEW EVAPORATION MODEL

Penman's model is modified for predicting concrete evaporation by adding the net radiation and aerodynamic effects as:

$$E = \delta \frac{Q_s}{H_v} + J \tag{8}$$

where

E = rate of evaporation from concrete due to both net radiation and aerodynamic effects (kg/m^2/hr)

δ = calibration factor for moisture condition of concrete surface

Q_s = solar radiation absorption through electromagnetic waves (kg/m/hr)

$$= \alpha\left[I_d \sin\theta + I_i\left(\frac{1+\cos\gamma}{2}\right)\right] \quad (25)$$

α = surface heat absorptivity of concrete (= 0.6)

I_d = direct solar radiation (kg/m/hr)

I_i = indirect solar radiation (kg/m/hr)

θ = incidence angle of solar radiation against the slab surface (degree)

γ = inclination angle of slab surface (degree)

H_v = heat of vaporization (heat removed from water on the surface of concrete slab being vaporized)

= $597.3 - 0.564T_s$ (cal/g) *(3)*

= $427(597.3 - 0.564T_s)$ (m)

J = rate of evaporation from concrete due to convective heat transfer, irradiation, and aerodynamic effects (kg/m^2/hr)

The rate of evaporation (E) consists of two components, one due to aerodynamic effects (E_a) explained as the rate of evaporation of a saturated vapor immediately above the water surface *(7)* and the other due to energy effects (E_q) as shown in Equation (3). The net radiation, which represents the energy exchange at concrete surface, consists of the elements such as solar radiation, convective heat transfer, and irradiation as:

$$Q_n = Q_s - Q_c - Q_r \tag{9}$$

where

Q_n = net radiation at concrete surface (kg/m/hr)

Q_s = solar radiation absorption (kg/m/hr)

Q_c = heat flux due to convection (kg/m/hr)

= $h_c(T_s - T_a)$ *(25)*

h_c = convective heat transfer coefficient

= $6 + 3.7v$ (W/m^2/^{o}C) *(25)*

= $367(6 + 3.7v)$ (kg/m/hr/^{o}C)

Q_r = heat energy from high to low temperature body (kg/m/hr)

= $\varepsilon\sigma(T_s^4 - T_a^4)$ *(26)*

= $\varepsilon[4.8 + 0.075(T_a - 5)](T_s - T_a)$ *(25)*

ε = surface heat emissivity of concrete (= 0.88)

σ = Stefan-Boltzmann constant (= 5.67×10^{-8} W/m^2/^{o}K^4 = 2.08×10^{-5} kg/m/hr/^{o}K^4) *(26)*

Under laboratory conditions, only convective heat transfer and irradiation are considered to have an effect on evaporation.

During bleeding, a concrete surface is covered with a continuous layer of water that is perhaps maintained for a period of time depending on the water content in the mix and the rate of evaporation. However, as evaporation continues, the water layer on the concrete surface becomes less continuous and isolated until it completely vanishes from the concrete surface. A model predicting concrete evaporation instead of water evaporation is perhaps useful when considering the drying effects on a concrete surface. The rate of evaporation at a concrete surface under laboratory curing conditions (i.e., not solar effects) in terms of the variation in moisture movement from the concrete to the atmosphere is represented by the parameter *J (22)*.

$$J = B \ln \frac{H_s}{H_a} \tag{10}$$

where *B* is surface moisture emissivity and has been found to be a function of the effective curing thickness and wind speed and is closely related to the given curing conditions. Characterization of surface moisture emissivity is very useful since it provides the means to include the moisture characteristics of the concrete as a function of curing time to be incorporated into Penman's model.

If there is no solar radiation (Q_s), such as under laboratory conditions, the evaporation rate of concrete (*E*) can be assumed to be equal to the evaporation rate of concrete due to convective heat transfer, irradiation, and aerodynamic effects (*J*). Thus, surface moisture emissivity (*B*) can be characterized by a series of laboratory tests in absence of solar radiation.

$$B = \frac{J}{\ln \frac{H_s}{H_a}} = \frac{E}{\ln \frac{H_s}{H_a}} \tag{11}$$

Test results for evaporation and curing thickness imply that the characterization of surface moisture emissivity needs to be carried out in two categories: one during bleeding and the other after bleeding. Obviously, plots of surface moisture emissivity versus effective curing

thickness in Figure A-11 showed that the data should be divided into the two categories and then analyzed separately. Effective curing thickness increases while surface moisture emissivity decreases with curing time during bleeding. Conversely, effective curing thickness decreases while surface moisture emissivity increases with curing time after bleeding. This relation between effective curing thickness and surface moisture emissivity was expected by Bazant and Najjar (*22*) even though the two categories by bleeding were not considered.

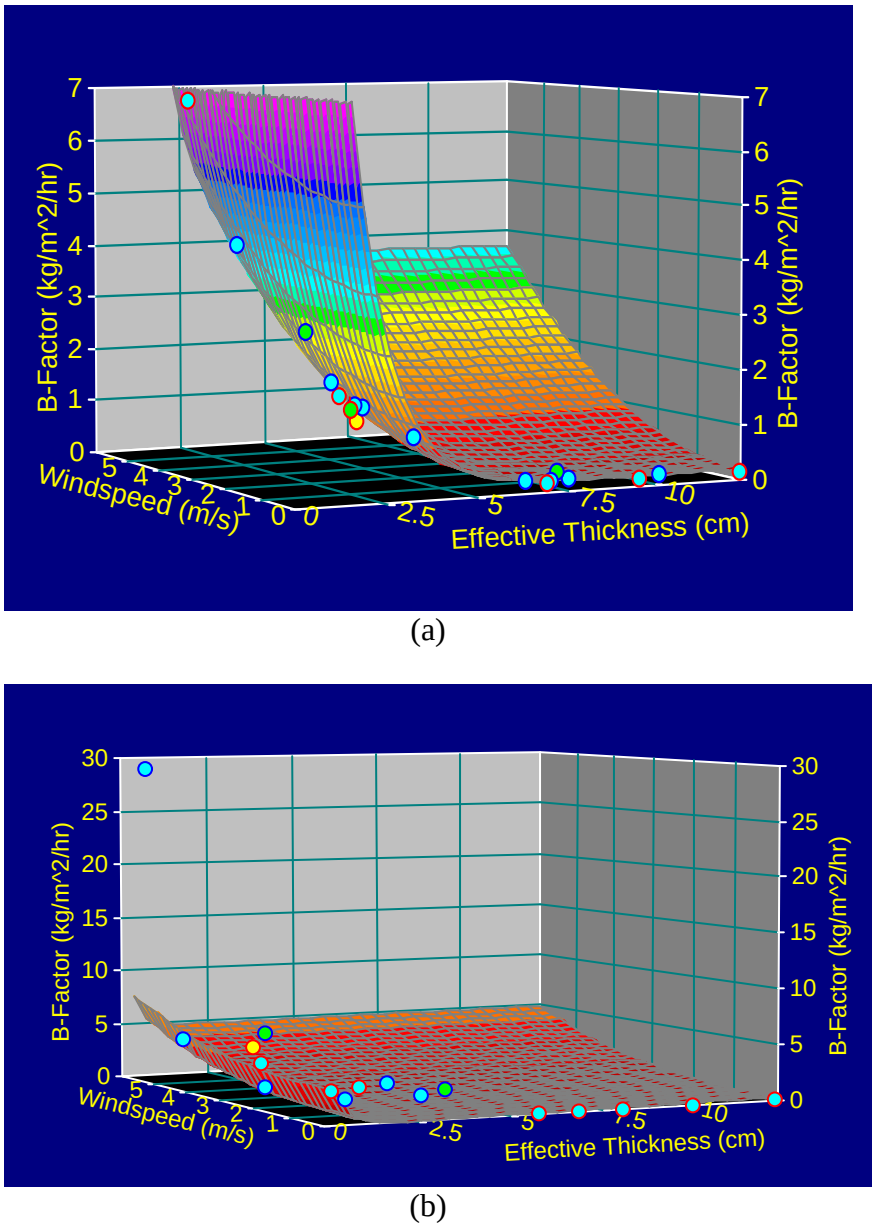

Figure A-11. Trends of Surface Moisture Emissivity: (a) During Bleeding; (b) After Bleeding.

Consequently, the surface moisture emissivity (B) can be formulized as functions of effective curing thickness (L) and wind speed (v) during and after bleeding, respectively.

During bleeding ($R^2 = 0.994$):

$$B = a + b\exp(-L) + cv^2 \quad (12)$$

After bleeding (R^2 = 0.999):

$$B = d + \frac{e \ln L}{L} + fv^{2.5} \tag{13}$$

where the unit of surface moisture emissivity is kg/m^2/hr, effective curing thickness is cm, and wind speed is m/s. The standard errors of coefficients ranged from 1.9 to 21.9 percent.

As previously mentioned, another source of evaporation is due to solar radiation at the concrete surface *(7)*. Specifically, the rate of evaporation by solar radiation is calculated from the solar radiation divided by heat of vaporization (H_v) at the slab surface *(3)*. In this regard, moisture conditions at the concrete surface with time also should be considered since during the bleeding stage, the solar radiation will cause the higher rate of evaporation. However, the evaporation by solar radiation will decrease as the concrete surface dries after bleeding. Penman's model does not consider the drying effects of concrete surface on evaporation due to solar radiation. Thus, a calibration factor considering drying effects of concrete on the evaporation by solar radiation was developed using the effective curing thickness concept to represent the moisture condition at the concrete surface.

$$\delta = 1 - \frac{L}{C} \qquad \text{when} \quad C \geq L \tag{14}$$

$$\delta = 0 \qquad \text{when} \quad C < L \tag{15}$$

Where δ is the calibration factor, and C is the ideal effective curing thickness (= 7.6 cm) determined by experimental experience of authors.

The evaporation of concrete is influenced by different curing methods as shown in Figure A-12. Both accumulative evaporation and rate of evaporation for the concrete specimen

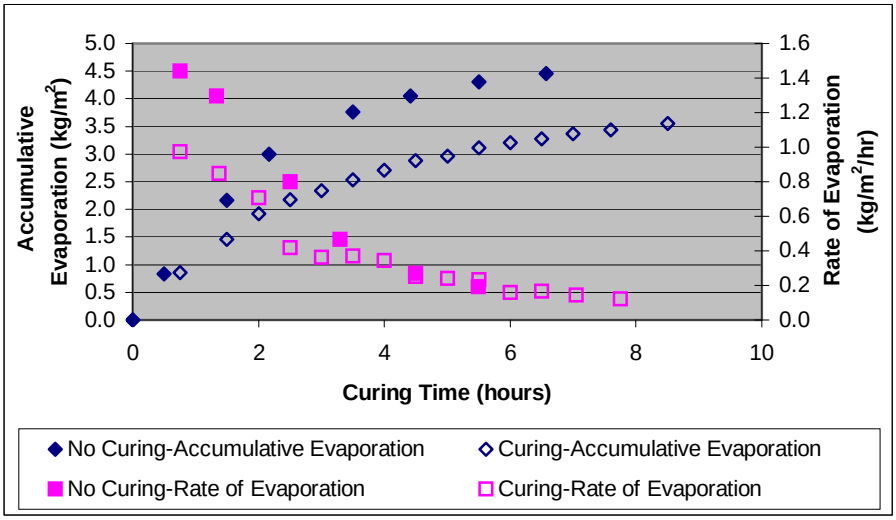

Figure A-12. Effects of Curing Methods on Evaporation (v = 5.33 m/s).

cured by 4.42 m^2/liter (180 ft^2/gallon) of Type II curing compound are much smaller than uncured concrete specimen.

A field test was conducted at the Riverside Campus of the Texas A&M University in Bryan, Texas, to demonstrate the validity of the new evaporation model shown in Figure A-13. Concrete was placed at 8:23 a.m., and the test was finished at 2:30 p.m. when the relative humidity at concrete surface had equilibrated with the ambient relative humidity. Solar radiation and wind speed were measured by a weather station placed near the concrete specimen. Ambient temperature and relative humidity, the temperature and relative humidity at the concrete surface, and inside the concrete were also measured by the ATEK curing monitoring system. The rate of evaporation calculated by the new evaporation model agrees with the measured one while the rate of evaporation from the ACI nomograph is

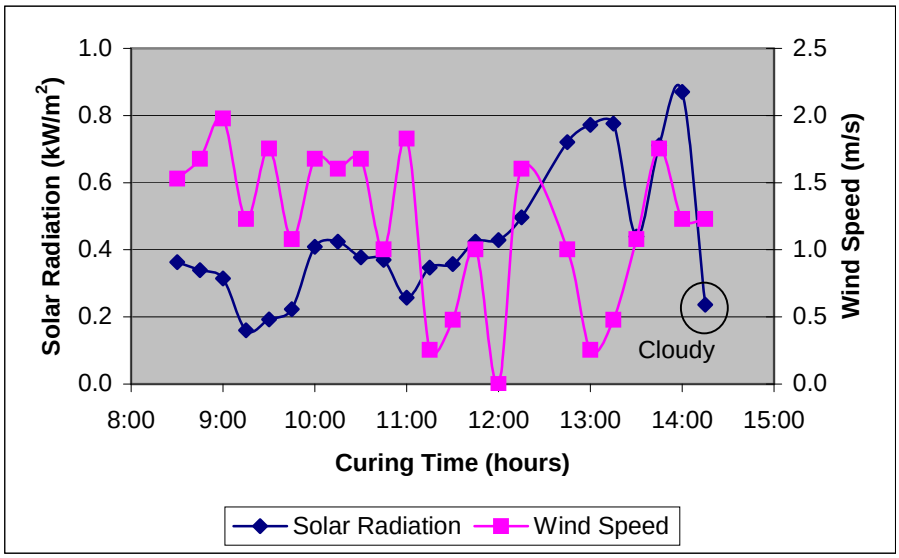

(a)

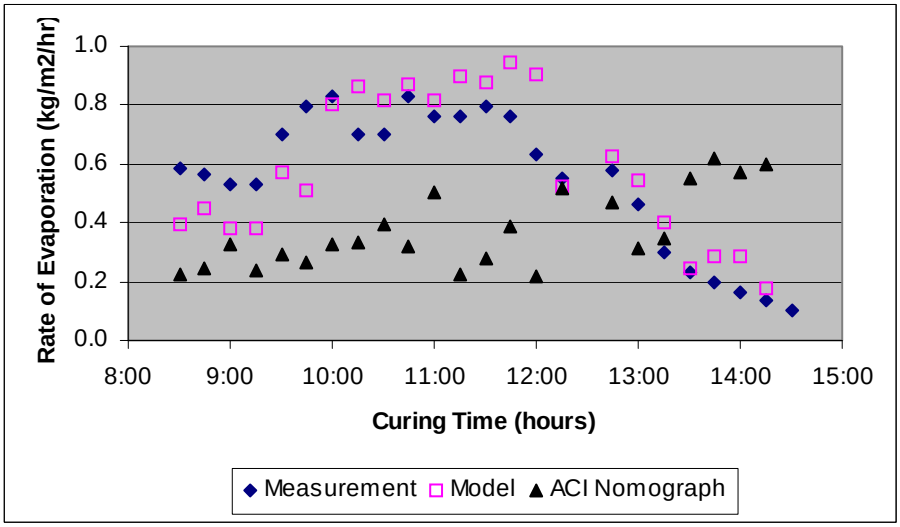

(b)

Figure A-13. Validation of New Evaporation Model at Field: (a) Solar Radiation and Wind Speed; (b) Comparison of Rate of Evaporation among Measurement, New Model, and ACI Nomograph.

underestimated during bleeding (in the morning) and overestimated after bleeding (in the afternoon). The advantages of the new evaporation model are improved prediction and sensitivity to the factors that control the amount of evaporation from hardening concrete for different curing methods.

CONCLUSIONS

A test methodology was developed to evaluate curing methods for concrete pavement. Effective curing thickness is suggested to be a parameter to evaluate or assess the quality of curing concrete. Maintaining higher levels of surface relative humidity is important for better curing quality. The curing condition was significantly influenced by wind speed, and minimization of wind effects is an important factor for high curing quality.

None of the existing evaporation models were suitable to predict the evaporation of concrete after bleeding because they were developed based on an evaporation condition that is consistent with a continuous layer of water on the concrete surface. Penman's evaporation model was modified by considering the drying characteristics of concrete after bleeding. The largest difference from the original Penman's model was considering drying characteristics of the concrete in predicting evaporation. Also, the surface moisture emissivity was characterized by a series of experiments. The surface moisture emissivity was found to be a function of effective curing thickness and wind speed. Another difference involves the adjustment of the solar radiation effect by the effective curing thickness. The modified Penman's model will allow for improved prediction of the amount of evaporation at a concrete pavement and evaluation of the method of curing.

REFERENCES

1. Mindes, S. and Young, J.F. *Concrete*. Prentice-Hall, Inc., Englewood Cliffs, New Jersey, 1981.
2. Wang, L. and Zollinger, D.G. A Mechanistic Design Framework for Spalling Distress. In *Transportation Research Record 1730*: Journal of the Transportation Research Board, TRB, National Research Council, Washington D.C., 2000, pp. 18-24.
3. Linsley, R.K., Kohler, M.A., and Paulhus, J.L. *Hydrology for Engineers.* 2nd edition, McGraw-Hill, New York, 1975.

4. Kapila, D., Falkowsky, J., and Plawsky, J.L. Thermal Effects During the Curing of Concrete Pavements. *ACI Materials Journal*, Vol. 94, No. 2, Mar.-Apr. 1997.
5. Neville, A.M. *Properties of Concrete*. 4th edition, John Wiley & Sons, Inc., New York, 1996.
6. Walker, S. and Bloem, D.L. *Studies of Flexural Strength of Concrete-Part 2: Effects of Curing and Moisture Distribution on Measured Strength of Concrete*. Proceedings, Highway Research Board, Vol. 36, Washington, D.C., 1957, pp. 334-346.
7. Penman, H.L. *Natural Evapotranspiration from Open Water, Bare Soil, and Grass*. Proceedings of the Royal Society of London, Series A, Vol. 193, 1948, pp. 120-146.
8. Thornthwaite, C.W. An Approach toward a Rational Classification of Climate. *Geographical Review*, Vol. 38, 1948, pp. 55-94.
9. Menzel, C.A. *Causes and Prevention of Crack Development in Plastic Concrete*. Portland Cement Association Annual Meeting, 1954, pp. 130-136.
10. Wilson, G.W. *Soil Evaporative Fluxes for Geotechnical Engineering Problems*. Ph.D. Thesis, University of Saskatchewan, Saskatoon, SK, Canada, 1990.
11. Wilson, G.W., Fredlund, D.G., and Barbour, S.L. Coupled Soil-Atmosphere Modeling for Soil Evaporation. *Canadian Geotechnical Journal*, Vol. 31, 1994, pp. 151-161.
12. Veihmeyer, F.J. *Evapotranspiration*. Handbook of Applied Hydrology, Ven Te Chow, editor, McGraw-Hill, New York, 1964.
13. Dalton, J. *Experimental Essays on Evaporation*. Manchester Lit. Phil. Soc. Mem. Proc., Vol. 5, 1802, pp. 536-602.
14. ACI 305R-96. *Hot Weather Concreting*. Manual of Concrete Practice, Part 2, Farmington Hills, American Concrete Institute, 1996.
15. Kohler, M.A., Nordenson, T.J., and Fox, W.E. *Evaporation from Pans and Lakes*. Research Paper, No. 38, U.S. Department of Commerce, Washington, May 1955.
16. Tetens, O. Uber Einige Meteorologische Begriffe Z. *Geophys*, Vol. 6, 1930, pp. 297-309.
17. Murray, F.W. On the Computation of Saturation Vapor Pressure. *Journal of Applied Meteorology*, Vol. 6, Feb. 1967.
18. Dilley, A.C. On the Computer Calculation of Vapor Pressure and Specific Humidity Gradients from Psychometric Data. *Journal of Applied Meteorology*, Vol. 7, Aug. 1968.

19. Mills, G.A. A Comparison of Some Formulae for the Calculation of Saturation Vapor Pressure over Water. *Meteorological Note,* No. 82, Bureau of Meteorology, Australia, Nov. 1975.
20. ASTM C 192. *Standard Practice for Making and Curing Concrete Test Specimens in the Laboratory*. Annual Book of ASTM Standards, American Society for Testing and Materials, 1994.
21. ASTM C 29. *Standard Test Method for Unit Weight and Voids Aggregates*. Annual Book of ASTM Standards, American Society for Testing and Materials, 1994.
22. Bazant, Z.P. and Najjar, L.J. Nonlinear Water Diffusion in Nonsaturated Concrete. *Materials and Structures (RILEM),* Vol. 5, No. 25, 1972.
23. Parrot, L.J. Factors Influencing Relative Humidity in Concrete. *Magazine of Concrete Research,* Vol. 43, No. 154, March 1991.
24. Xi, Y., Bazant, Z.P., Molina, L., and Jennings, H.M. Moisture Diffusion in Cementitious Materials (Moisture Capacity and Diffusivity). *Advanced Cement Based Materials,* January 1994, pp. 258-266.
25. Branco, F.A., Mendes, R.A., and Mirabell, E. Heat of Hydration Effects in Concrete Structures. *ACI Materials Journal,* Vol. 89, No. 2, 1992, pp. 139-145.
26. Incropera, F.P. and DeWitt, D.P. *Fundamentals of Heat and Mass Transfer*. 4th edition, John Wiley & Sons, New York, 1996.

APPENDIX B

DETERMINATION OF α AND β FROM CURING (ECT) DATA

The following form is used to fit the calculated ECT data with time:

$$ECT_i = \tau\left(1 - e^{-\frac{t_i}{\beta}^{\alpha}}\right)$$

The analysis process involves linearizing the above expression by taking the natural logarithm of both sides of the equation:

$$\ln ECT_i = -\ln \tau_o \left(\frac{t_i}{\beta}\right)^a \tag{1}$$

By taking the derivative of Equation (1) with respect to t_i:

$$\frac{\partial(\ln ECT_i)}{\partial(t_i)} = \frac{\partial(\ln ECT_i)}{\partial(ECT_i)} \cdot \frac{\partial(ECT_i)}{\partial(t_i)} = \frac{1}{ECT_i} \cdot \frac{\partial(ECT_i)}{\partial(t_i)} \tag{2}$$

By combining Equation (1) in Equation (2):

$$\frac{\partial(ECT_i)}{\partial(t_i)} \cdot \frac{1}{ECT_i} = \frac{\partial\left(\ln \tau_o - \left(\frac{t_i}{\beta}\right)^a\right)}{\partial t_i} \tag{3}$$

Since τ is assumed to also be a material parameter independent of time, its derivative with respect to t_i is zero. Hence, Equation (3) is converted to the following:

$$\frac{\partial(ECT_i)}{\partial(t_i)} \cdot \frac{1}{ECT_i} = \frac{\partial\left(-\left(\frac{t_i}{\beta}\right)^{\alpha}\right)}{\partial t_i} = -\frac{\alpha}{\beta} \cdot \left(\frac{t_i}{\beta}\right)^{\alpha-1} \tag{4}$$

Taking logarithm again for both sides of Equation (4), results in:

$$Ln\left(-\frac{1}{ECT_i}\left(\frac{\partial ECT}{\partial t}\right)_i\right)=Ln\left(\frac{\alpha}{\beta^{\alpha}}\right)+(\alpha-1)Ln(t_i)$$

If the above expression is compared to the form y=mx+b, then:

$$y = Ln\left(-\frac{1}{ECT_i}\left(\frac{\partial ECT}{\partial t}\right)_i\right)$$
$$x = Ln(t_i)$$
$$m = (\alpha - 1); \alpha = m + 1$$
$$b = Ln\left(\frac{\alpha}{\beta^{\alpha}}\right); \beta = \left(\frac{m+1}{e^b}\right)^{\frac{1}{m+1}}$$

Numerically, the ECT time derivative $\left(\frac{\partial ECT}{\partial t}\right)$ can be evaluated in terms of 2nd order forward, central, and backward differences, respectively as:

$$\frac{1}{\Delta x}\left(-\frac{f_2}{2}+2f_1-\frac{3}{2}f_0\right);\quad \frac{1}{2\Delta x}(f_1-f_{-1});\quad \frac{1}{\Delta x}\left(-\frac{3}{2}f_0+2f_{-1}-\frac{f_{-2}}{2}\right)$$

Finally, τ could potentially be determined via $\tau_i = \frac{ECT_i}{EI_{ECT_i}}$

APPENDIX C

LABORATORY TEST DATA

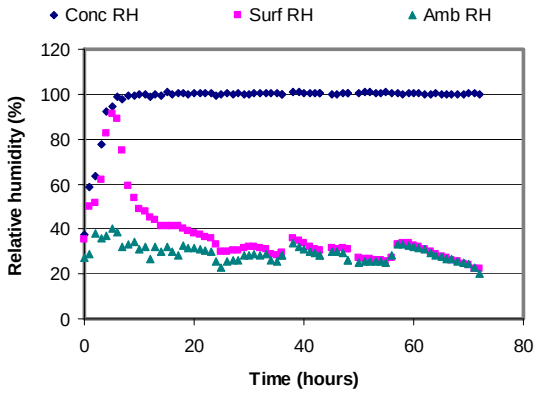

(a) Relative Humidity

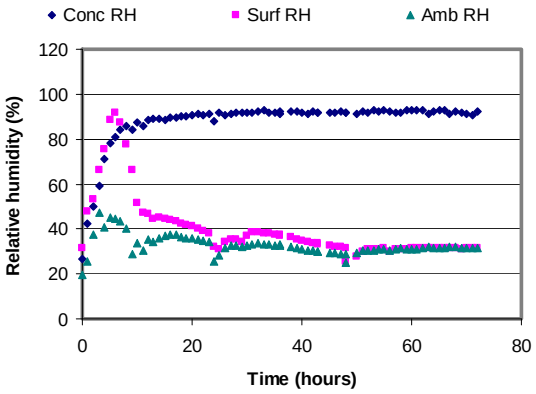

(a) Relative Humidity

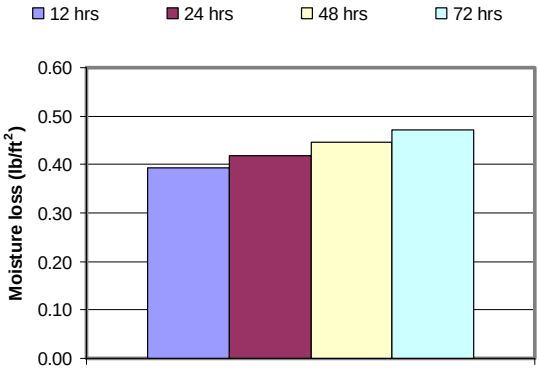

(b) Relative Humidity

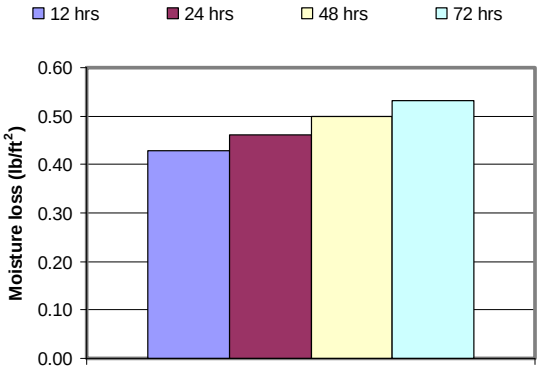

(b) Relative Humidity

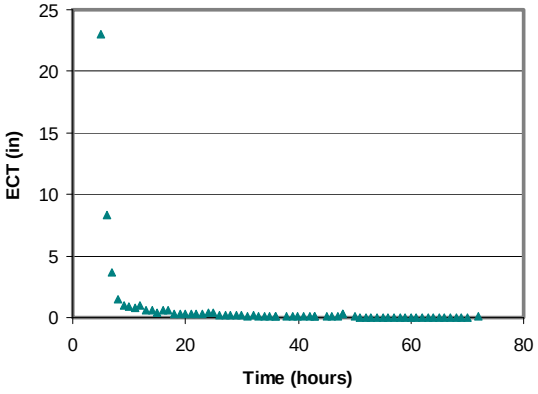

(c) ECT Data

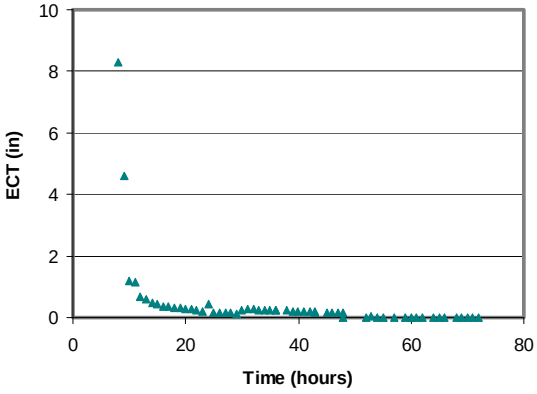

(c) ECT Data

Figure C-1. Plain: 1st Trial.

Figure C-2. Plain: 2nd Trial.

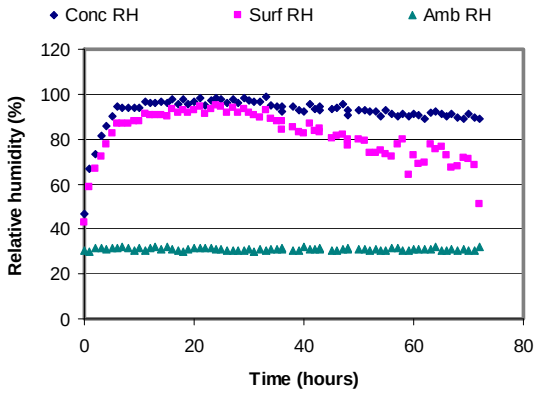

(a) Relative Humidity

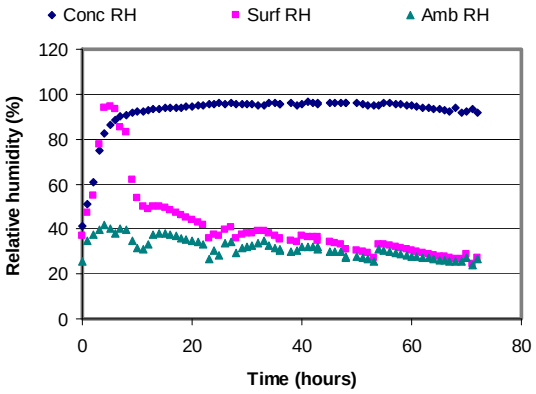

(a) Relative Humidity

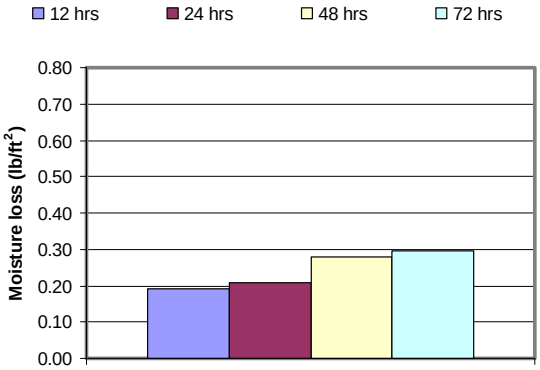

(b) Relative Humidity

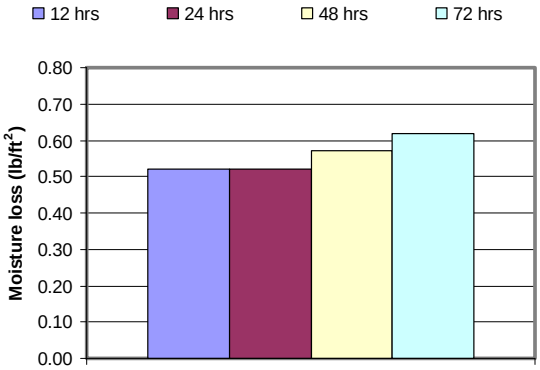

(b) Relative Humidity

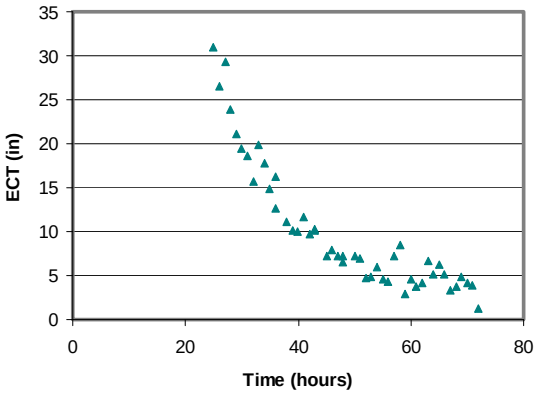

(c) ECT Data

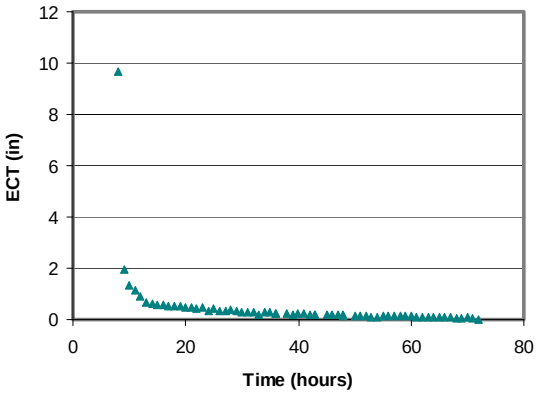

(c) ECT Data

Figure C-3. ECO II.

Figure C-4. TSC 100.

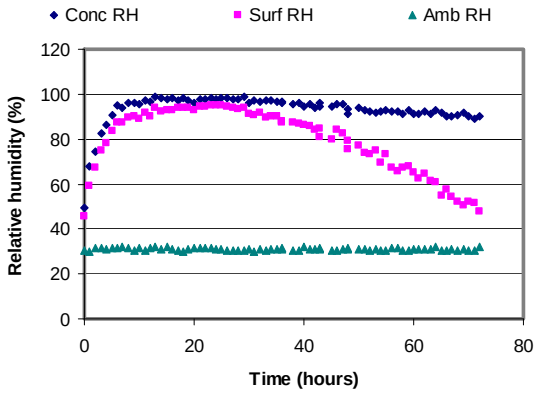

(a) Relative Humidity

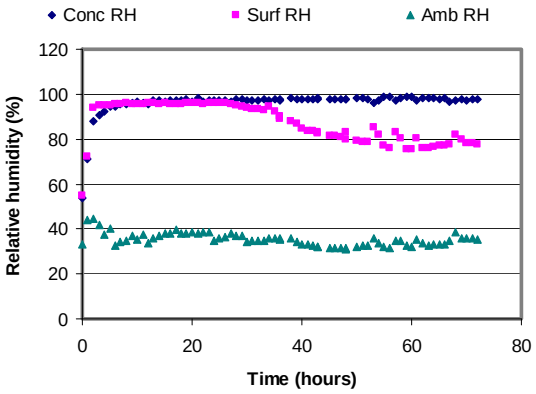

(a) Relative Humidity

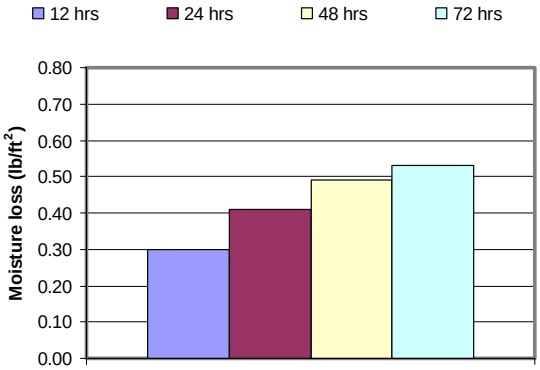

(b) Relative Humidity

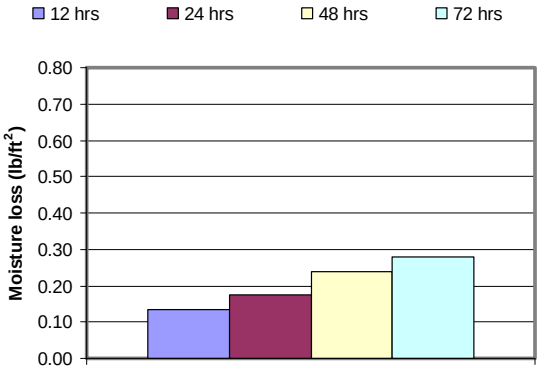

(b) Relative Humidity

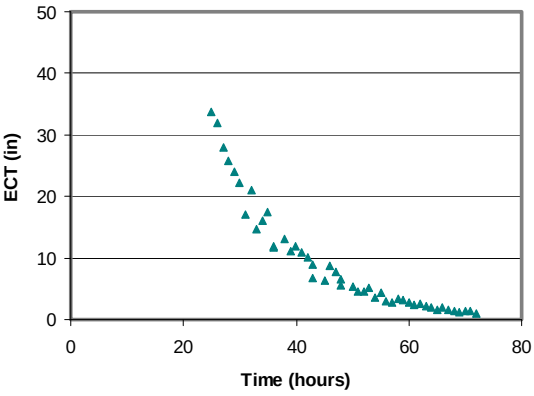

(c) ECT Data

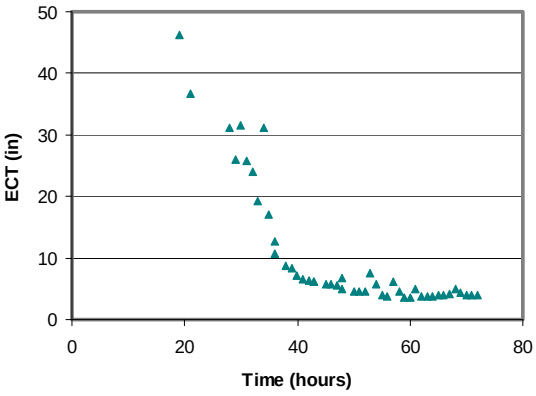

(c) ECT Data

Figure C-5. Concrete Chemical.

Figure C-6. WRM 1140.

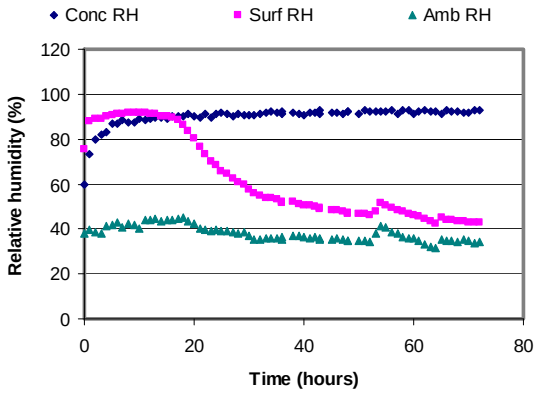

(a) Relative Humidity

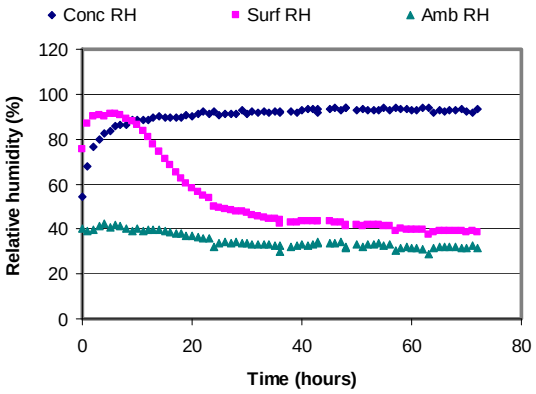

(a) Relative Humidity

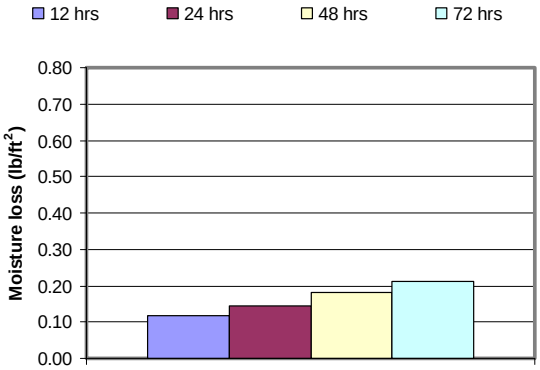

(b) Relative Humidity

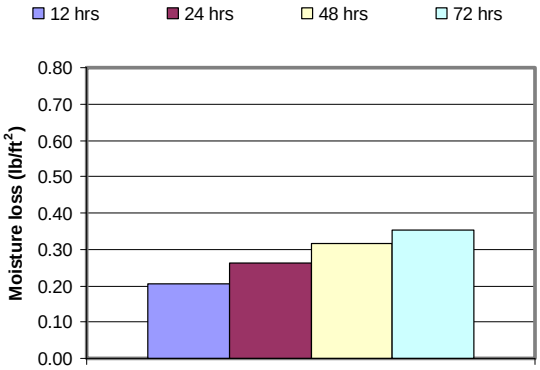

(b) Relative Humidity

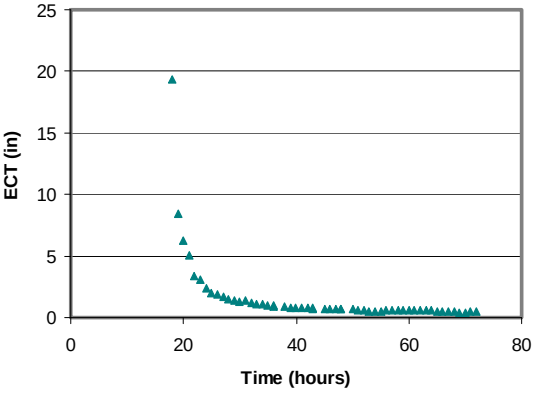

(c) ECT Data

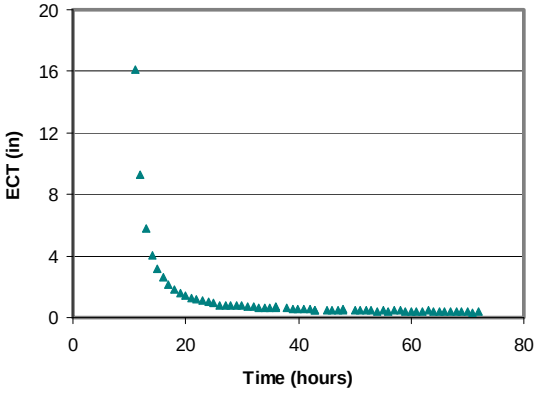

(c) ECT Data

Figure C-7. WRM 1240: 1st Trial.

Figure C-8. WRM 1240: 2nd Trial.

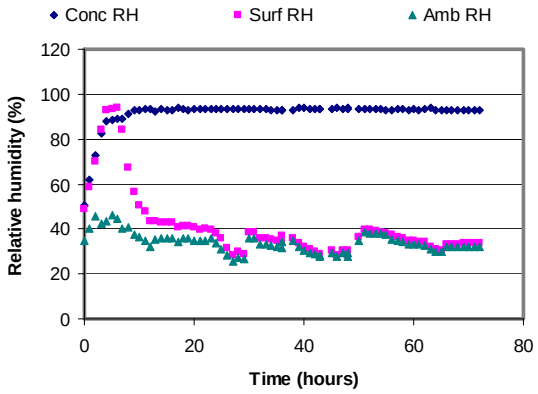

(a) Relative Humidity

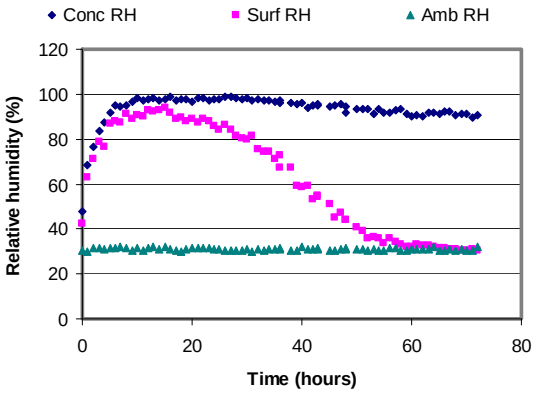

(a) Relative Humidity

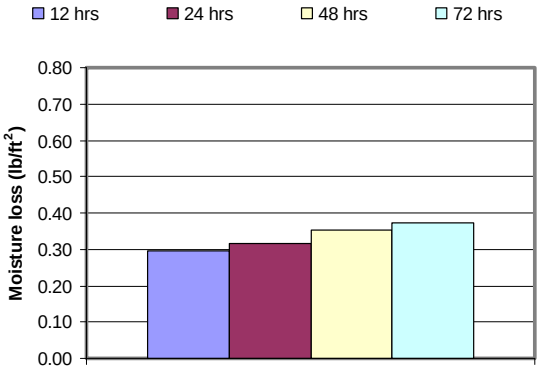

(b) Relative Humidity

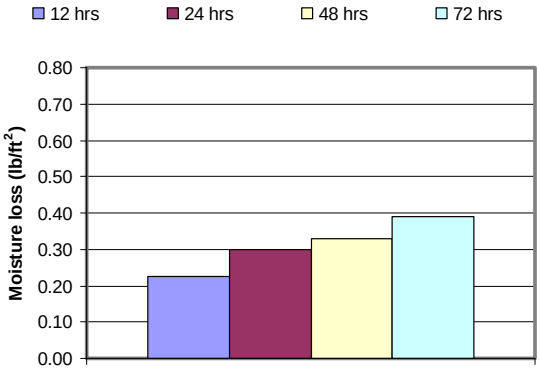

(b) Relative Humidity

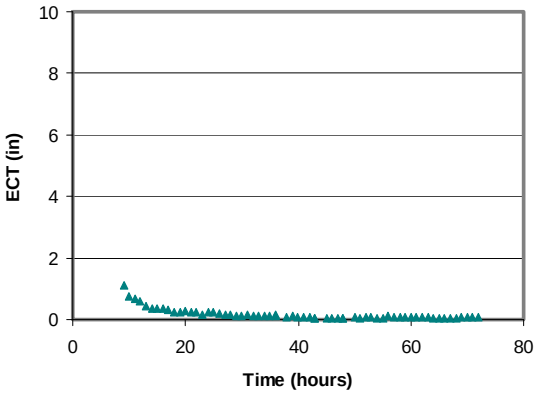

(c) ECT Data

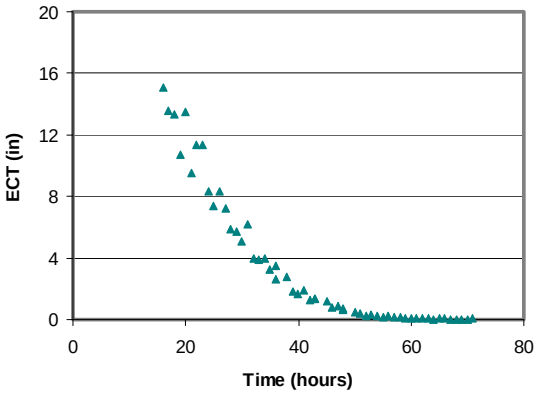

(c) ECT Data

Figure C-9. WRM 1250: 1st Trial.

Figure C-10. WRM 1250: 2nd Trial.

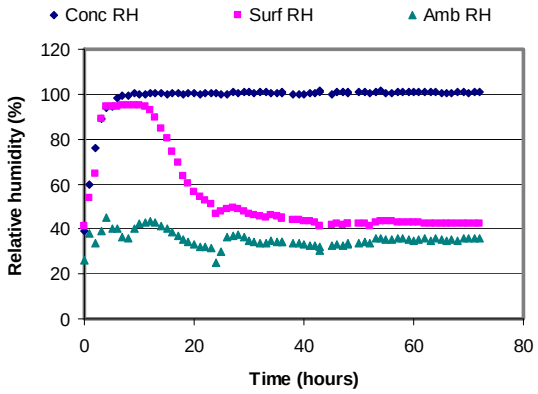

(a) Relative Humidity

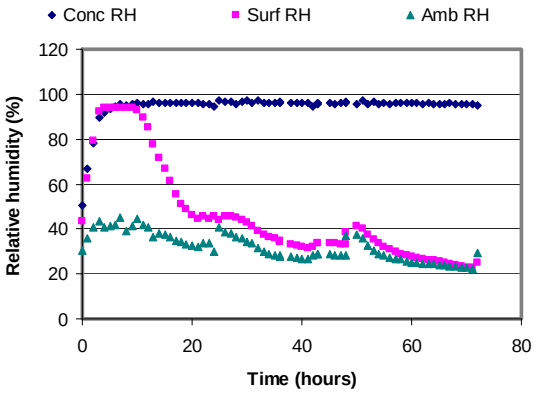

(a) Relative Humidity

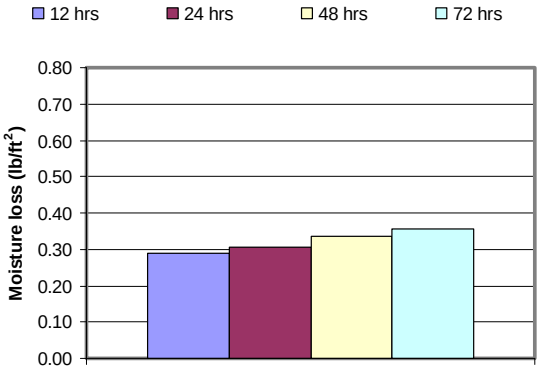

(b) Relative Humidity

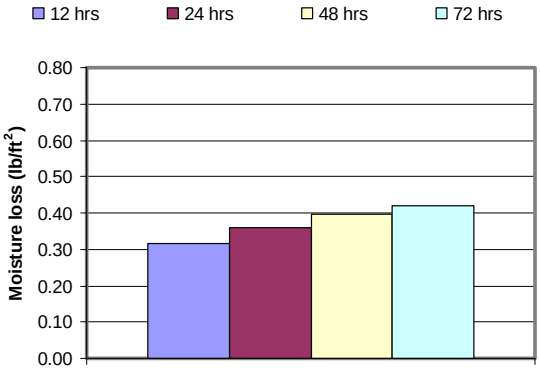

(b) Relative Humidity

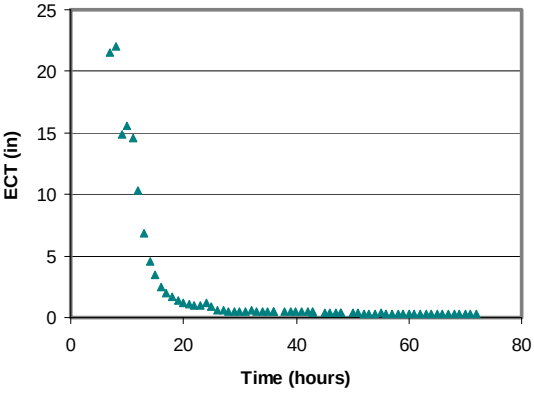

(c) ECT Data

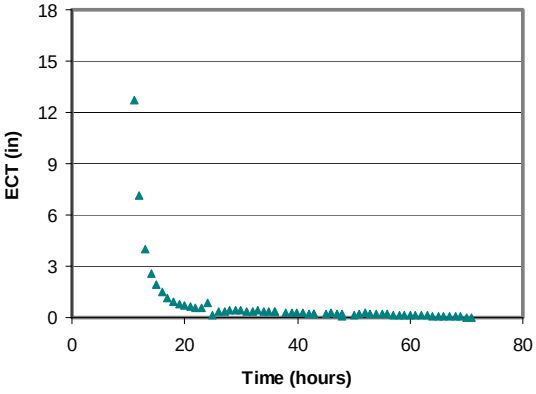

(c) ECT Data

Figure C-11. WRM 1600: 1st Trial.

Figure C-12. WRM 1600: 2nd Trial.

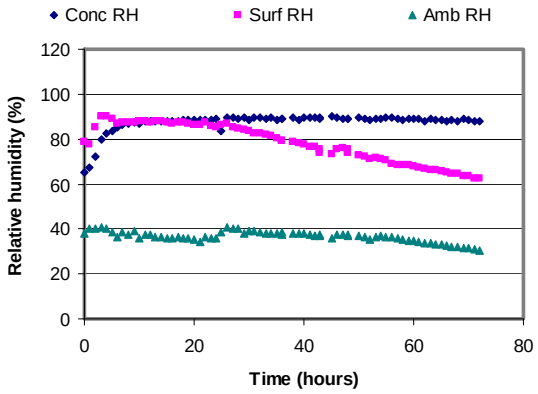

(a) Relative Humidity

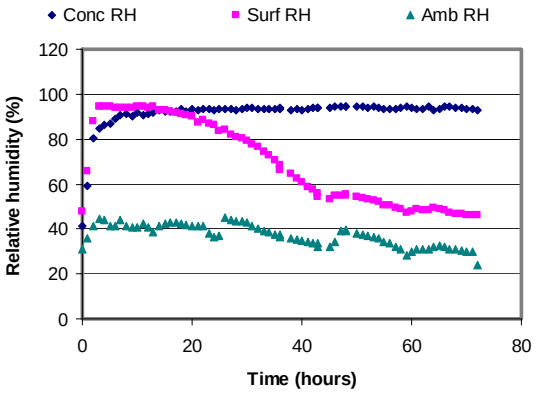

(a) Relative Humidity

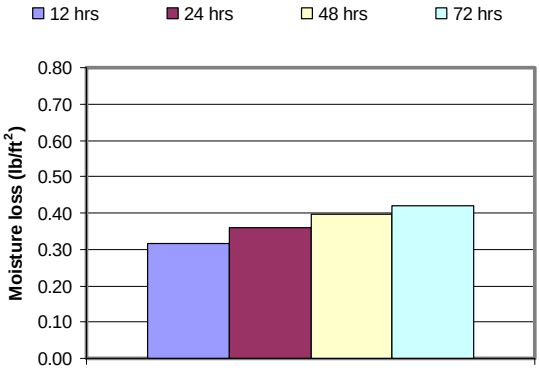

(b) Relative Humidity

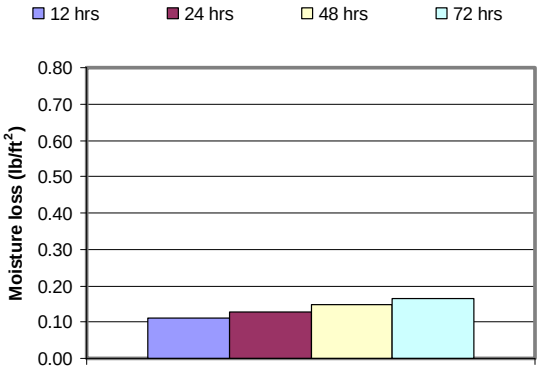

(b) Relative Humidity

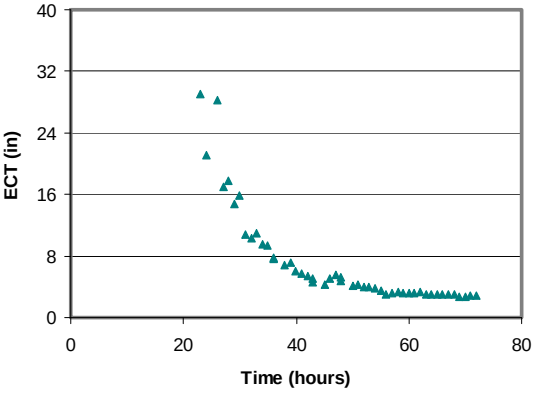

(c) ECT Data

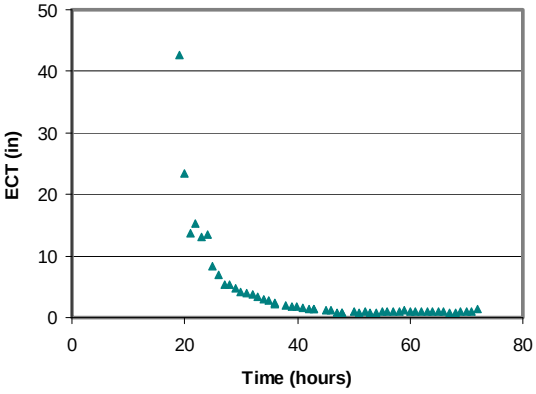

(c) ECT Data

Figure C-13. WRM 1600: 3rd Trial.

Figure C-14. WRM 1640: 1st Trial.

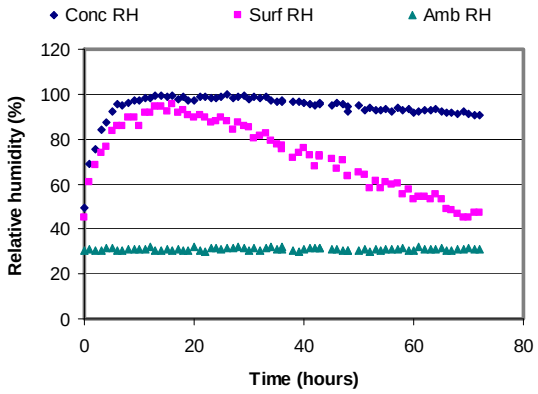

(a) Relative Humidity

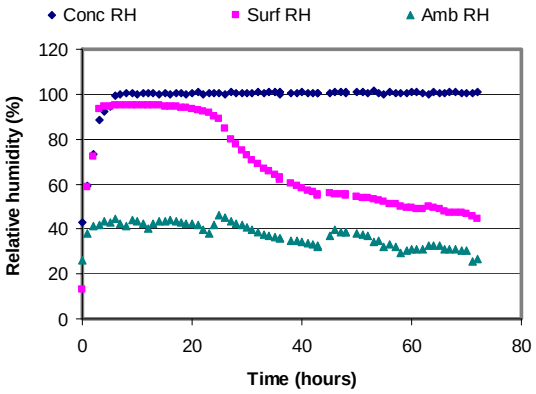

(a) Relative Humidity

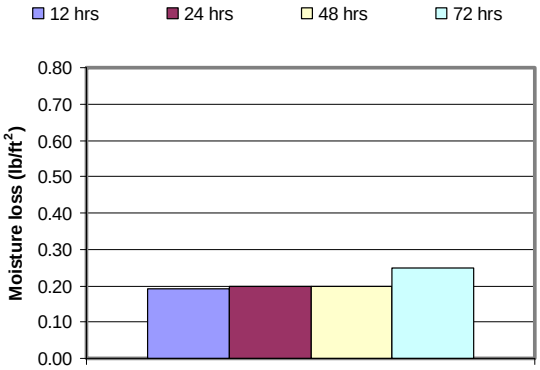

(b) Relative Humidity

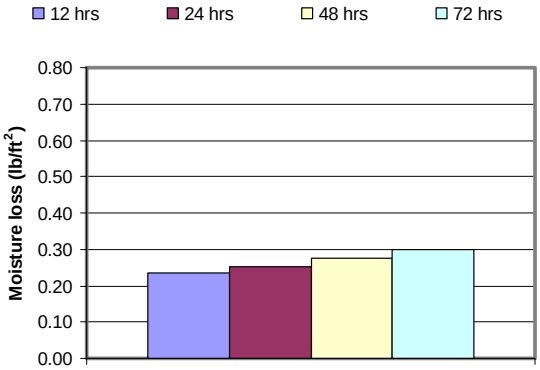

(b) Relative Humidity

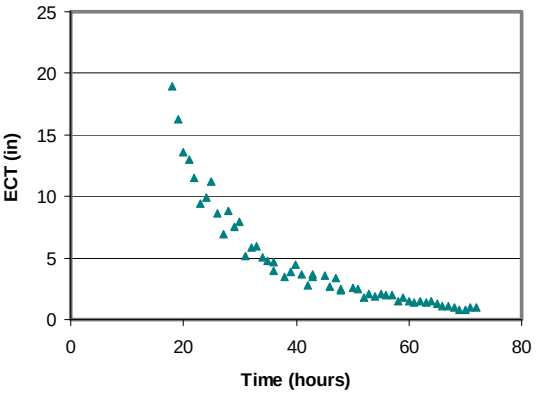

(c) ECT Data

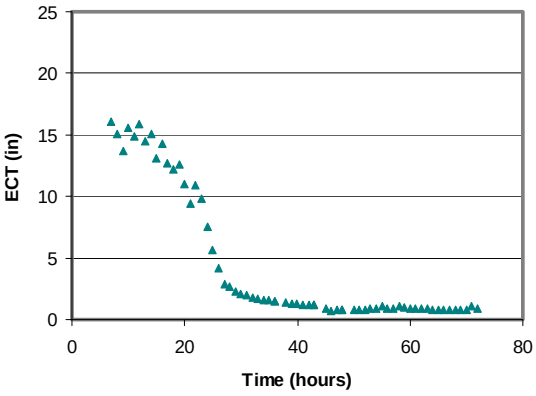

(c) ECT Data

Figure C-15. WRM 1640: 2nd Trial.

Figure C-16. WRM 2250: 1st Trial.

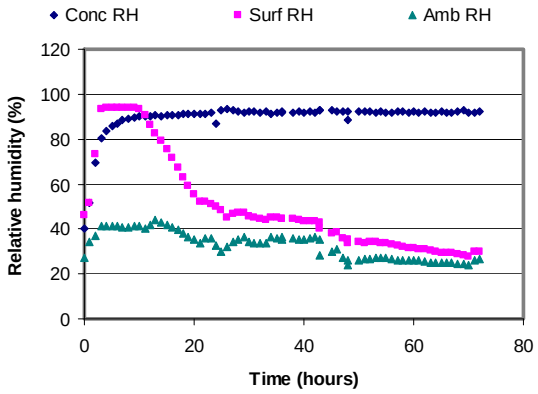

(a) Relative Humidity

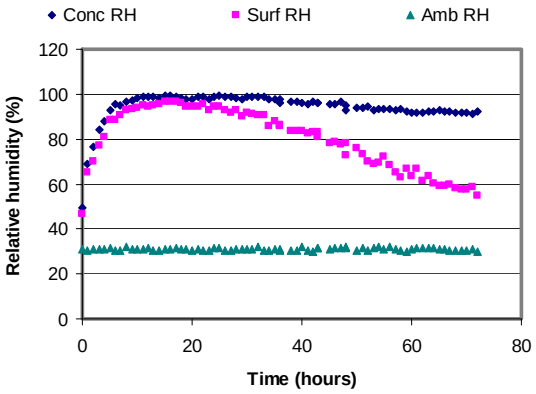

(a) Relative Humidity

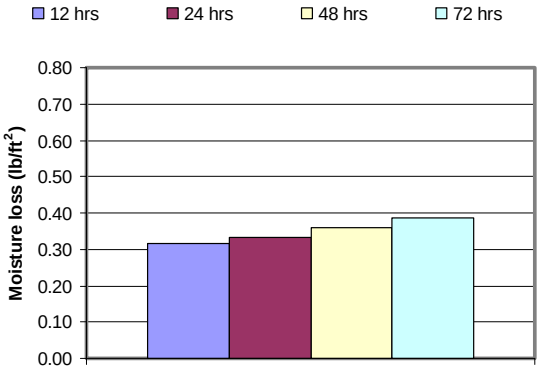

(b) Relative Humidity

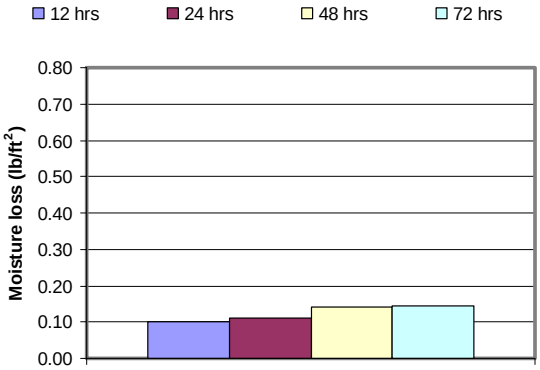

(b) Relative Humidity

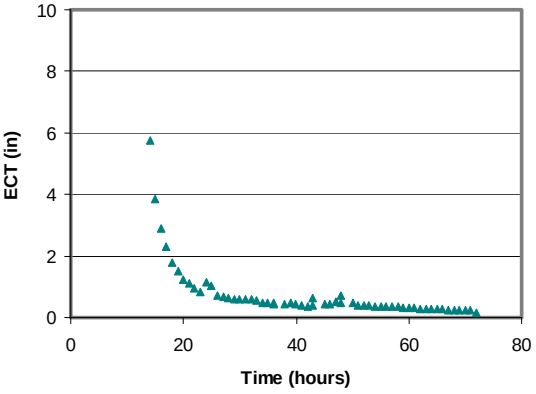

(c) ECT Data

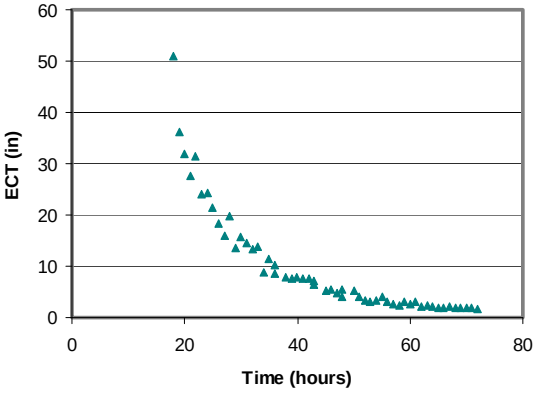

(c) ECT Data

Figure C-17. WRM 2250: 2nd Trial.

Figure C-18. WRM 2250: 3rd Trial.

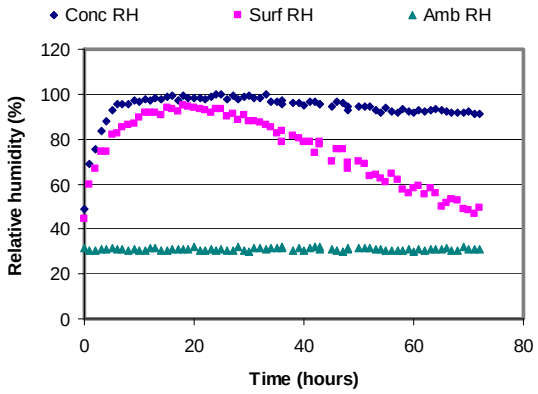

(a) Relative Humidity

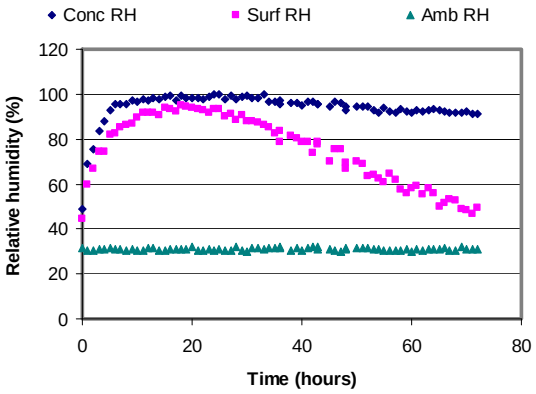

(a) Relative Humidity

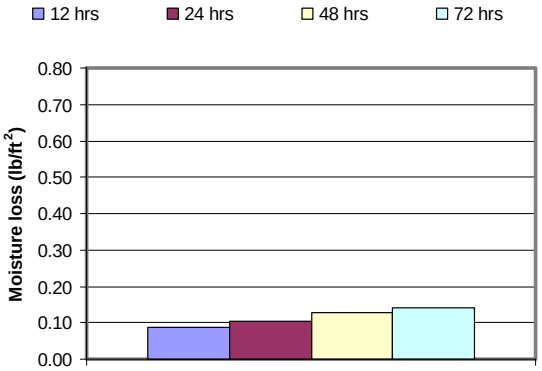

(b) Relative Humidity

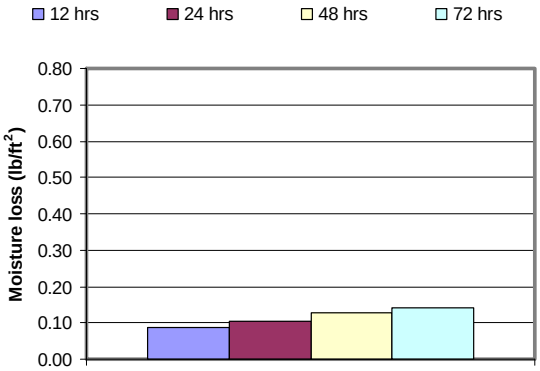

(b) Relative Humidity

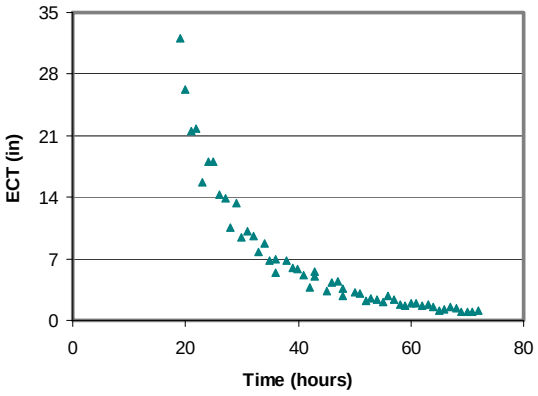

(c) ECT Data

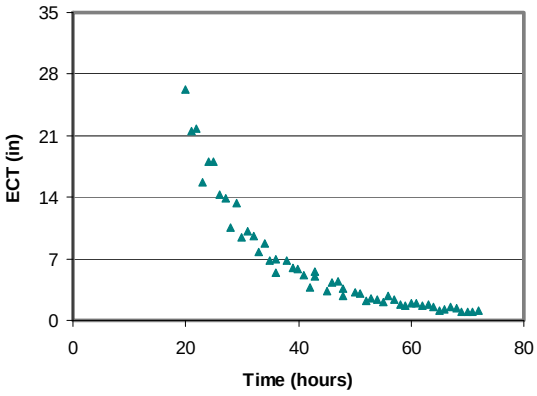

(c) ECT Data

Figure C-19. WRM 2255: 1st Trial.

Figure C-20. WRM 2255: 2nd Trial.

APPENDIX D
LAB TEST PROTOCOL

1. SCOPE

1.1 Curing is an important activity that involves two factors that affect curing quality. One is related to the quality of the curing compound, and the other is related to the quality of the concrete. The aim of the laboratory protocol is to rank curing effectiveness based on the quality of the curing compound.

1.2 Lab test protocol consists of test procedures, analysis, and curing compound effectiveness evaluation as shown in Figure D-1. A curing monitor system and a high accuracy weighing scale are used to monitor mortar specimen with a height of 2 in. and a diameter of 12 in. Weight loss, relative humidity (RH) at three locations (ambient, surface, and concrete), and temperatures at the same three locations are recorded.

1.3 The evaporation rate and the effective curing thickness (ECT) are described in the "Development of Evaluation Index to Assess Curing Compound" section in Chapter 3. Based on calculated results, curing compound performance under lab conditions is ranked as well related to its ingredients; furthermore the regressed evaporation model can be used for field evaluation of a curing compound.

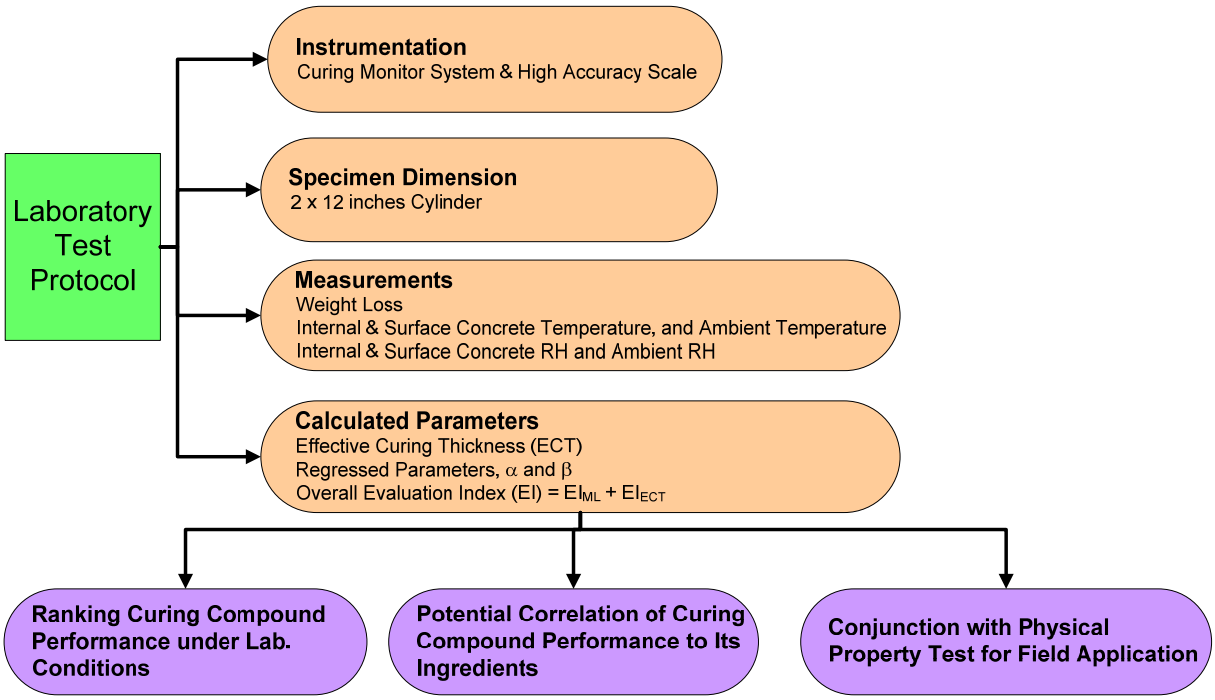

Figure D-1. Lab Test Protocol.

2. APPARATUS

2.1 Weight loss data and relative humidity data are two primary test measurements. A weighing scale, shown in Figure D-2 (a) High Accuracy Scale and (b) Cylindrical Mold with 0.1 g accuracy was used.

2.2 The moisture loss specimen consists of a mortar cast in a cylindrical mold with an inside diameter of 12 in. and a height of 2 in. shown in Figure D-2 (b). The mold also consists of 0.5-in. thick PVC wall and an end plate with a thickness of 0.25 in.

(a) High Accuracy Scale (b) Cylindrical Mold

Figure D-2. Weighing Scale and Specimen Mold.

2.3 Relative humidity measurements at a concrete surface and 1 in. below require sampling chambers in order for the chamber pressure to equilibrate with the pore pressure inside the concrete. Sampling chambers are shown in Figure D-3. The chamber for the chilled mirror sensor is inserted 1 in. into the concrete. The chamber for concrete surface humidity rests on the surface of the fresh concrete and consists of a filter paper on which a layer of curing compound is sprayed. The relative humidity in the surface humidity chamber represents the humidity of concrete surface immediately below the curing membrane.

2.4 The relative humidity data were measured using the CMS device (manufactured by ATEK Co. in Dallas, Texas). The detailed view of this device is shown in Figure D-4. The unit consists of three relative humidity sensors arranged to measure the relative humidity above, at, and below the concrete surface. Concrete RH sensor, a chilled mirror

hydrometer type sometimes called an optical condensation hygrometer, is the most accurate, reliable, and fundamental hygrometer commercially available. As a result, it is widely used as a calibration standard. Since the moisture state inside early-aged concrete is mostly saturated, the chilled mirror hygrometer is the most suitable sensor to measure the RH inside concrete. Recent modifications of the CMS unit added the capacity to monitor wind speed and solar radiation, which are two other important factors to affect evaporation and curing quality under field conditions. Those two sensors are also shown in Figure D-4.

(a) Filter Paper Cover (b) Surface Chamber (c) Chilled Mirror Chamber

Figure D-3. Surface Chamber Setup.

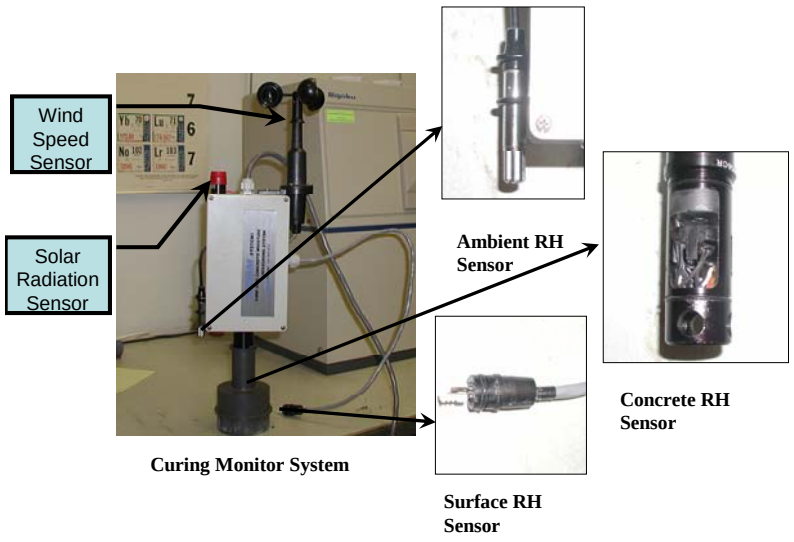

Figure D-4. CMS Sensors.

3. TEST SPECIMEN PREPARATION

3.1 The protocol can be demonstrated by first preparing the moisture loss mortar specimens. Mortar specimen preparation and mixing can be carried out using an electrically driven mechanical mixer according to ASTM C 305, *Standard Practice for Mechanical Mixing of Hydraulic Cement Pastes and Mortars of Plastic Consistency,* using the following sequence.

3.2 As shown in Figure D-5, the schematic mixing procedure is as follows.

3.2.1 The total amount of water is first placed in the mixing bowl.

3.2.2 The cement is introduced and mixed at a slow speed for 30 s.

3.2.3 The required amount of aggregate is added to the mixer over a period of 30 s while the mixer continues to operate.

3.2.4 The resulting mortar is allowed to mix for an additional 30 s at a medium speed.

3.2.5 After a minute rest period, the mixing is continued for an additional minute until a homogeneous mortar with no lumps is obtained.

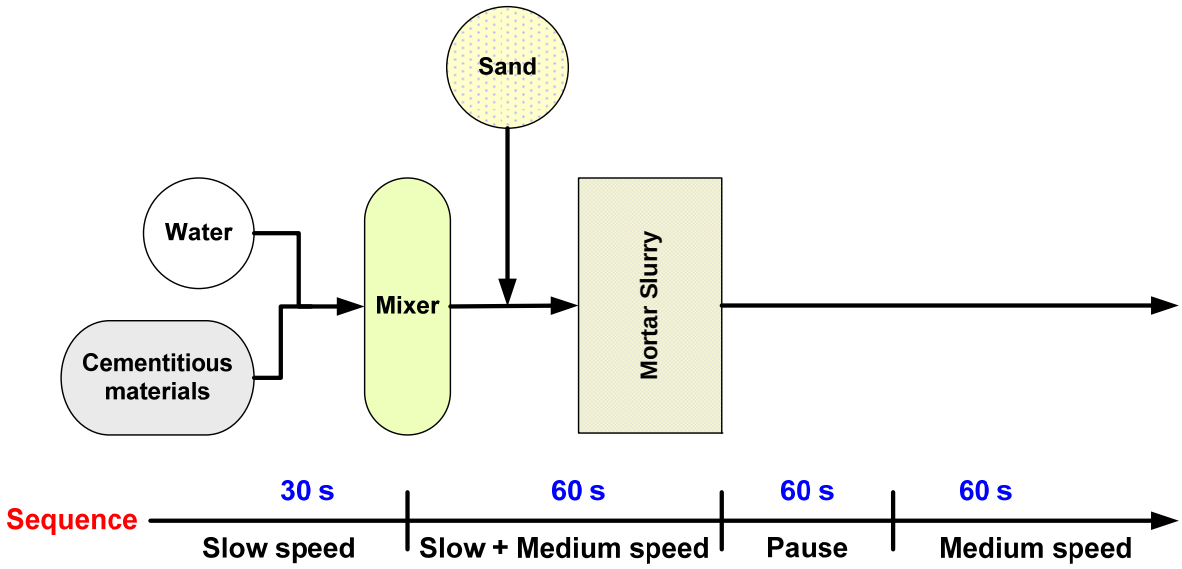

Figure D-5. Mixing Procedure.

4. TEST CONDITION

4.1 The occurrence of evaporation is mainly due to the vapor pressure difference between air and concrete surface; the bigger the difference, the faster the evaporation rate. Air flow over the mortar specimen continuously replaces the saturated air near the

evaporating surface with less saturated air, which maintains the vapor pressure difference and evaporation rate. Ambient relative humidity is a direct indicator of the ambient water vapor pressure; the lower the ambient relative humidity, the lower the ambient water vapor pressure and the larger the vapor pressure difference across the membrane leading to a higher evaporation rate. Temperature increases the saturated vapor pressure level and the relative differences in vapor pressure. If the water vapor pressure in the air remains the same, the increased concrete temperature would decrease the vapor pressure difference, which decreases the evaporation rate.

4.2 For consistency purposes, the test is carried out under laboratory testing conditions. The ambient RH and the wind speed are fixed at 30 percent and 10 mph, respectively. A curing compound is used at an application rate of 180 ft^2/gallon.

5. TEST PROCEDURE FOR CURING COMPOUND TEST SETUP

5.1 Prepare mortar mixture according to the procedure described in Section 3 of Appendix D.

5.2 Fill the mold with mortar mixture, and then make surface of mortar smooth and flat by strikeoff and darbying. Figure D-6 shows the flat surface of mortar specimen.

5.3 Make a hole of 1 in. depth into the specimen with a cylindrical PVC block in order to set up the chamber for the chilled mirror sensor (Figure D-6).

5.4 Place a filter paper cover on the surface of the fresh mortar specimen before the curing compound is sprayed. The chamber for mortar surface humidity is located on this area (Figure D-7 (a)). The RH in the surface humidity chamber represents the humidity of concrete surface immediately below the curing membrane.

5.5 Spray curing compound on the mortar specimen. Figure D-7 (b) shows the specimen after spraying curing membrane.

5.6 Place the mortar specimen on the weighing scale for moisture loss measurement.

5.7 Insert a special chamber (casing) to install a chiller mirror type moisture sensor, and then apply Vaseline® on the boundary between chamber and the mortar specimen to ensure better equilibration with the mortar vapor pressure.

5.8 Install a surface chamber covered by a filter paper on which a layer of curing compound is sprayed. Figure D-8 shows the entire test setup for the proposed protocol.

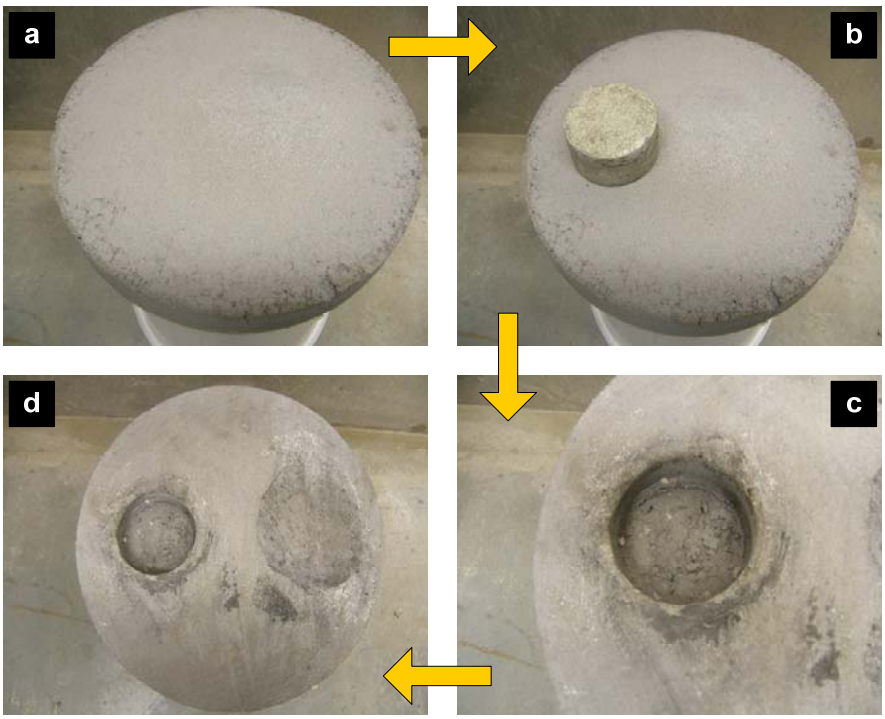

Figure D-6. Preparation of Specimen for CMS Setup.

(a) Before Spraying Curing Compound (b) After Spraying Curing Compound

Figure D-7. Mortar Specimen Before and After Spraying Curing Compound.

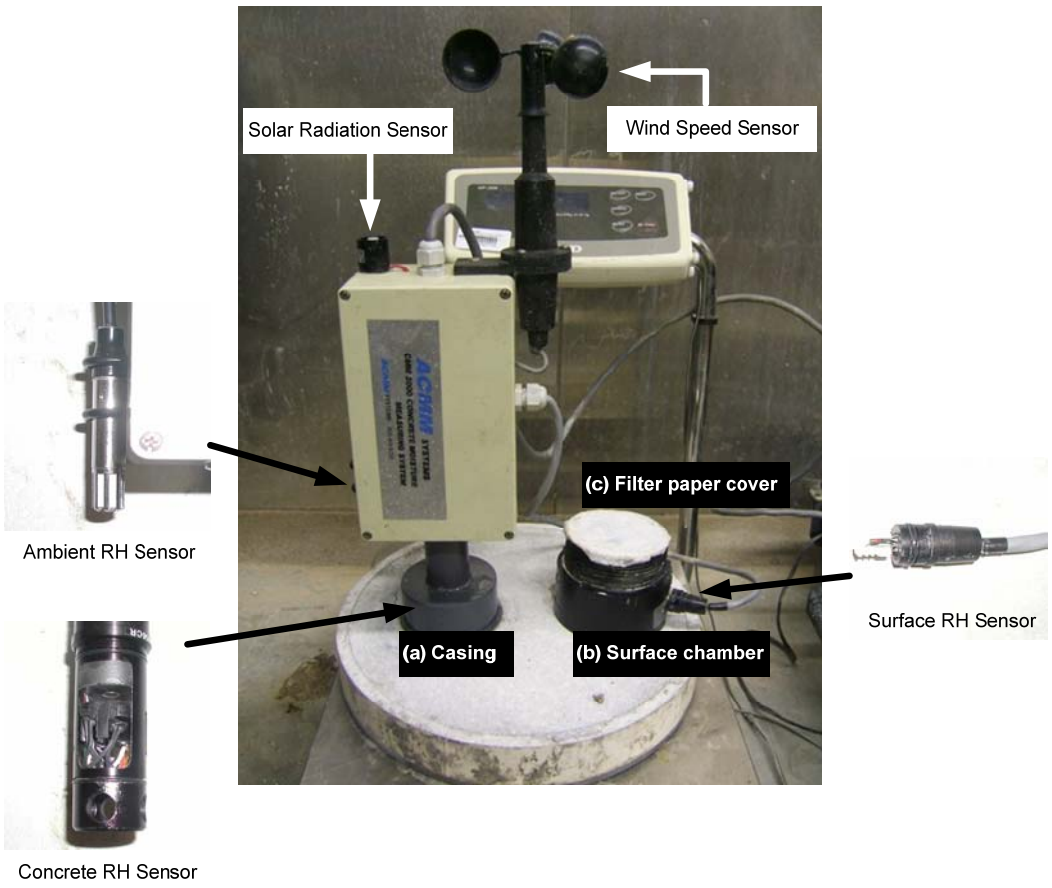

Figure D-8. Test Setup for Laboratory Protocol.

6. DETERMINATION OF EVALUATION INDEX

6.1 An evaluation index (EI) to ascertain performance differences between different curing compounds is obtained from a combination of moisture loss and curing compound effectiveness elaborated below.

6.2 Moisture loss-based evaluation index (EI_{ML})

6.2.1 The moisture loss-based EI can be formulated (based on the accumulated 24-hour moisture loss) as:

$$EI_{ML} = 1 - \frac{Wt\ loss_{24}}{Wt\ loss_{24-uc}} \qquad (1)$$

where:

$Wt\ loss_{24}$ = 24-hour weight loss of the cured sample, and
$Wt\ loss_{24-uc}$ = 24-hour weight loss of the uncured sample

6.3 Effective curing thickness-based evaluation index (EI_{ECT})

6.3.1 The effective curing thickness-based EI is determined to model a variety of characteristics relative to either the moisture loss or curing compound behavior by using by a Weibull accumulative distribution as:

$$EI_{ECT} = \frac{ECT}{\tau} = \left[1 - e^{-\left(t/\beta\right)^{\alpha}}\right] \quad (2)$$

where:

τ = maximum ECT,
β = residence time factor, and
α = degradation factor

6.3.2 The Weibull function relates well to the degradation of the curing compound as it ages (as governed by the α parameter) and the duration or the residence time of the curing (as governed by the β parameter) but at 24 hours after placement the 24-hour EI_{ECT} can be determined.

6.3.3 EI_{ECT} ranges between 1 and 0 where quality curing would be reflected by a value closer to 1. Equation (2) has obvious similarities to Equation (1) but does involve two unknowns that require definitions based on the calculated ECT data. The determination of EI_{ECT} will be subsequently elaborated following a description of the equipment and procedures to carry out the data collection.

6.4 The averaging of EI_{ML} and EI_{ECT} integrate the coupled effects of temperature, relative humidity, and time relative to a cured concrete specimen into the EI parameter. EI_{ML} representing the moisture loss at 24 hours is largely independent of the effects of hydration on reduction of moisture loss and consequently represents the moisture retentivity of the curing compound. After bleeding, the EI_{ECT} decreases gradually, as a sign of the deterioration of curing compound with time since: (a) the difference between the concrete and surface humidity is increasing and (b) the difference between the surface

and ambient humidity is decreasing. It is evident that the EI is an overall indicator of curing compound effectiveness and the quality of the curing membrane.

$$EI_{Overall} = EI_{ML} + EI_{ECT}$$

7. EXAMPLE OF CALCULATING OVERALL EVALUATION INDEX

7.1 An example of the data collected during an evaporation test of a given compound is shown in Figure D-9. The ambient RH and the wind speed are fixed at 30 percent and 10 mph, respectively.

7.2 Using the data in Figure D-9, calculation of instantaneous ECT using Equation (2) is shown in Figure 3-3. It is noted that relative humidity gradient (grad(RH)) in Equation (3-4) can be approximated by taking the difference between the surface and concrete RH divided by the distance between their monitoring points. The peak of the ECT curve actually coincided with the end of the bleeding period for hardening concrete in accordance with vapor pressure trends.

7.3 Using Equations (1) and (2), EI_{ML}, EI_{ECT}, and overall EI are calculated and summarized in Table D-1. The Table D-9 parameters are used to rank the compound effectiveness.

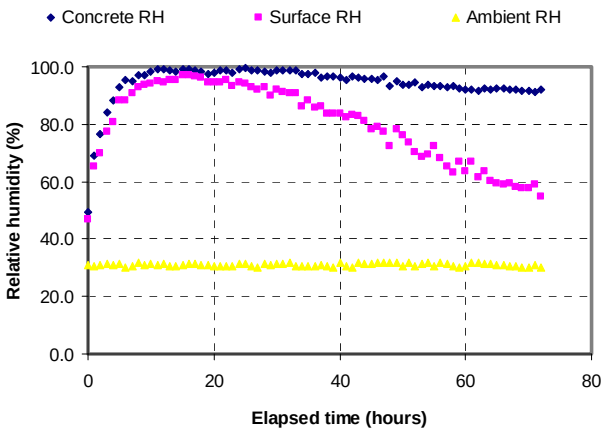

(a) Relative humidity

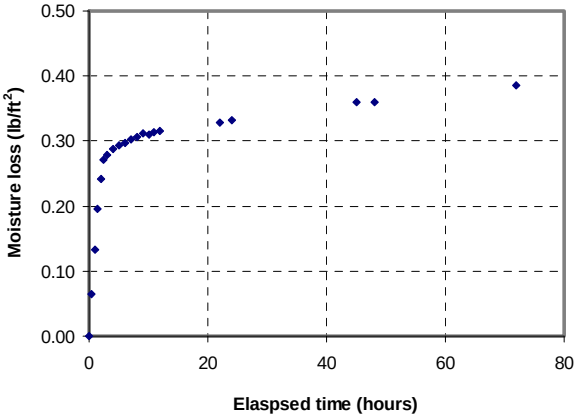

(b) Moisture loss

Figure D-9. Typical Relative Humidity and Moisture Weight Loss Curves (WRM 2250).

Table D-1. Curing Compound Ranking Parameters.

Sample ID	24 hr EI_{ML}	α	β	24 hr EI_{ECT}	COV	* $EI_{Overall}$
WRM 2250	0.47	2.87	30.59	0.59	0.36	0.53

*The $EI_{Overall}$ is the average of EI_{ML} and EI_{ECT}

APPENDIX E
CURING COMPOUND RANKING

According to ASTM C 309-03, the following types of liquid membrane-forming compounds are delineated:

- Type 1 – Clear or translucent without dye,
- Type 1-D – Clear or translucent with fugitive dye, and
- Type 2 – White pigmented.

The solids dissolved in the vehicle shall be one of the following classes:

- Class A – No restrictions,
- Class B – Must be a resin as defined in Terminology D 883.

TxDOT uses only Type 1-D and 2 curing compounds. However, in the test program, five different curing compounds, three of which were resin-based and the other two were wax-based, were tested. The classification of the tested curing compound samples is presented in Table E-1.

Table E-1. Classification of Curing Compounds.

Designation	Type	Comments/Cost Data
WR Meadows 2255	Type 2, Class B	*High Reflective/ $7.25-8.75/gal
WR Meadows 2250	Type 2, Class B	*High Reflective/ $7.25-8.75/gal
WR Meadows 1640	Type 2, Class A	*Wax-based/ $4.00-5.00/gal
WR Meadows 1600	Type 2, Class A	*Wax-based/ $2.80-3.50/gal
WR Meadows 1240	Type 2, Class B	*Normal Resin-based/ $4.15-$5.15/gal
WR Meadows 1250	Type 2, Class B	*Normal Resin-based/ $3.50-$4.50/gal
WR Meadows 1140	Type 1-D, Class B	*Clear/ $4.50-$5.50/gal
ECO	Type 2, Class A	Clay-based/$3.30 gal FOB Wharton, Texas
Concrete Chemical	Type 2, Class A	Normal Resin-based

* FOB Ft. Worth, Texas: All prices based on 55-gal drum packaging.

Table E-2 lists the ranking of the tested compounds by the high reflective curing compounds, and wax-based curing compounds showed the best EIs. Concrete Chemical and ECO curing compounds showed similar performance, while TSC 100 had the lowest EI.

Table E-2. Ranking of Curing Compounds.

Type of Curing Compound	EI_{ML}	α	β	EI_{ECT}	COV	*Overall EI	Ranking
Plain	0.00	2.66	11.42	0.00	1.36	0.00	10
ECO II	0.12	2.77	10.59	0.00	-	0.06	8
TSC 100	0.00	2.57	13.36	0.01	-	0.00	10
Concrete Chemical	0.07	-	-	0.00	-	0.03	9
WRM 1140	0.50	3.25	27.37	0.80	-	0.65	4
WRM 1240	0.54	2.67	18.37	0.14	0.82	0.34	6
WRM 1250	0.30	3.98	26.30	0.53	0.66	0.41	5
WRM 1600	0.22	3.13	20.74	0.22	0.95	0.22	7
WRM 1640	0.63	3.34	33.30	0.69	0.21	0.66	2
WRM 2250	0.47	2.87	30.59	0.59	0.36	0.53	3
WRM 2255	0.71	3.52	37.81	0.82	0.00	0.77	1

*The overall EI is the average of EI_{ML} and EI_{ECT}.

APPENDIX F

FIELD TEST AT THE FRONTAGE ROAD AT LOOP 610

Field tests were carried out on a Loop 610 frontage road construction site near Stella Link Road, in the Houston District during the month of September 2005 to investigate the performance of ECO and American Highways Technology (AHT) curing compounds under field conditions.

Two 150-ft sections were placed with the first section cured by AHT cure and the second section cured by ECO cure. Three coats were applied for both the AHT and ECO cure sections. The first coat was applied immediately after the bleeding was over, and the second coat was applied right after the first coat with the time delayed less than 30 min. The third coat for AHT cured section was applied 5 hr later after the second coat, and the ECO cured section was applied 12 hr after the second coat. All of the applications were conducted manually.

Two CMSs were used to monitor the ambient relative humidity, surface relative humidity, and concrete relative humidity at 1 in. below the concrete surface to help characterize the behaviors of the curing membrane. Temperature information at these positions could be acquired as well, including solar radiation and wind speed, which were useful to assess the rate of evaporation.

AMBIENT CONDITIONS

The ambient weather conditions were characterized in Figure 2-7 (ACI 308 R-01: 2008). The PE is shown in Figure F-1, which normally reaches its peak values during the noon hours when the ambient relative humidity is low, and the air temperature, solar radiation, and the wind speed are high. In this field test, the highest PE was about 0.20 lb/ft^2/hr.

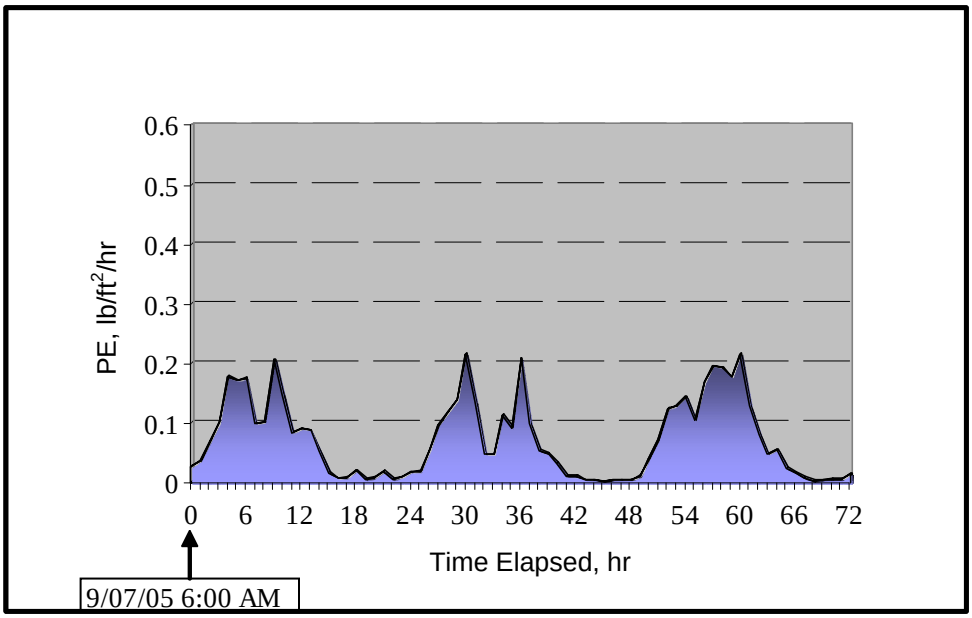

Figure F-1. Potential of Evaporation at Loop 610.

DATA PRESENTATION

Relative humidity data for the AHT cured section are presented in Figure F-2. From Figure F-2, it is observed that the surface relative humidity stayed at a high level during the night hours, but it began to fluctuate when daytime arrived the second day. During the first day the membrane curing surface relative humidity fluctuated without dropping too much. During the second day however, it, dropped dramatically.

Relative humidity data for the ECO cured section are presented in Figure F-3. The surface relative humidity followed the same pattern as that of the AHT cured section. Thus, it is evident the effectiveness for these two curing compounds is about the same in this field test.

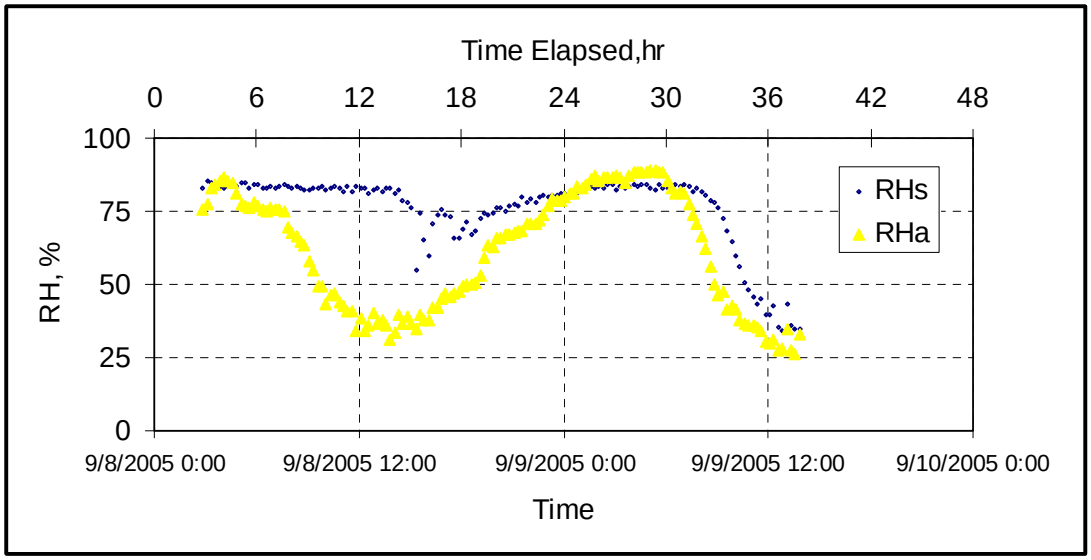

Figure F-2. Relative Humidity Trend for the Section Cured with AHT.

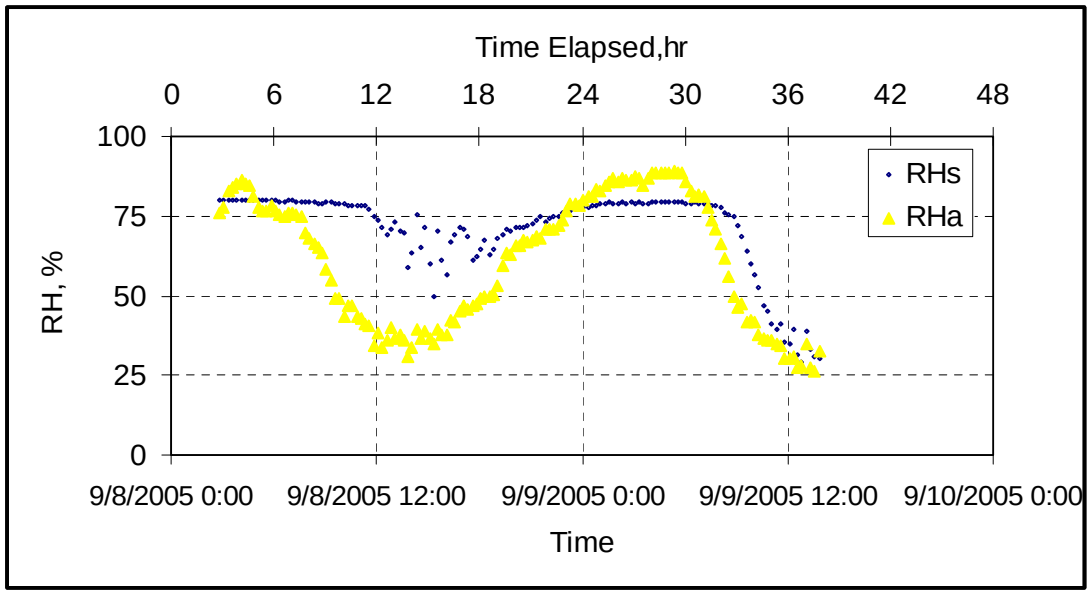

Figure F-3. Relative Humidity Trend for the Section Cured with ECO.

APPENDIX G
FIELD TEST AT SH 130 ROUND ROCK

A field test was carried out on SH 130 at a construction site near FM 685 in Round Rock, Texas, during the month of September 2005 to compare the performance of high reflective curing compound (Sealtight® 2255) and a normal resin-based curing compound (Sealtight® 1240) under field conditions. Two sections were placed with the first section being cured with Sealtight® 1240 and the second section cured with Sealtight® 2255. Two coats were applied for both sections according to TxDOT practice. The third coat was applied manually when a drop in the surface humidity took place.

AMBIENT CONDITIONS

The ambient weather conditions were again characterized using ACI 308 nomograph shown in Figure 2-7. The resulting PE is shown in Figure G-1. In this field test, the highest PE was about 0.33 lb/ft^2/hr. It was about 0.1 lb/ft^2/hr higher than that of the ambient conditions at Loop 610.

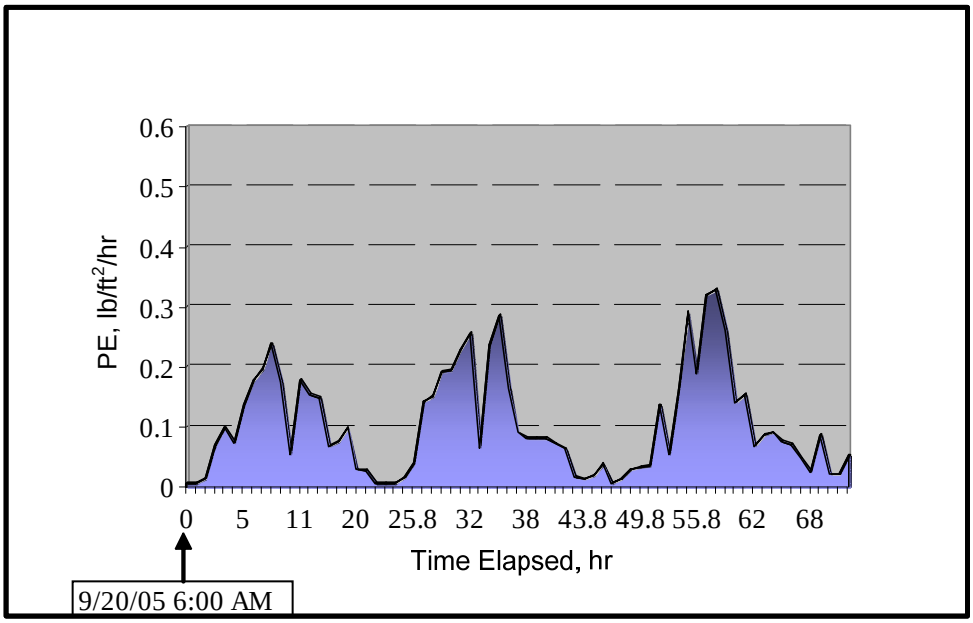

Figure G-1. Potential of Evaporation at SH 130.

DATA PRESENTATION

Relative humidity data for the normal curing compound cured sections are presented in Figure G-2. It is observed that the surface relative humidity was beginning

to break during the second day; although it began to recover after sundown, it began to break again after sun up the next day.

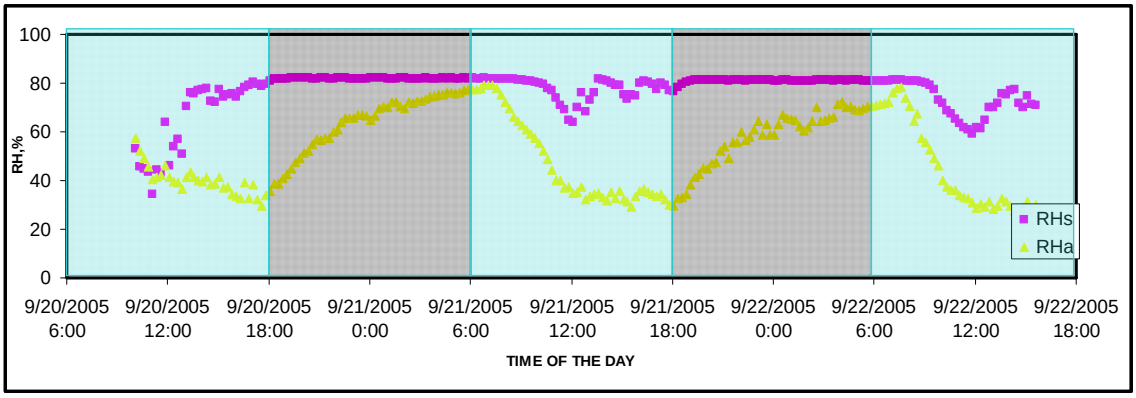

Figure G-2. Relative Humidity Trend for Normal Curing Compound.

Relative humidity data for the high reflective curing compound cured sections are presented in Figure G-3. It was expected to have better performance. But it is observed that the surface relative humidity was beginning to break during the second day. After a third coat was applied, there was an increase in the surface relative humidity. However, it was maintained for only a couple of hours before breaking again.

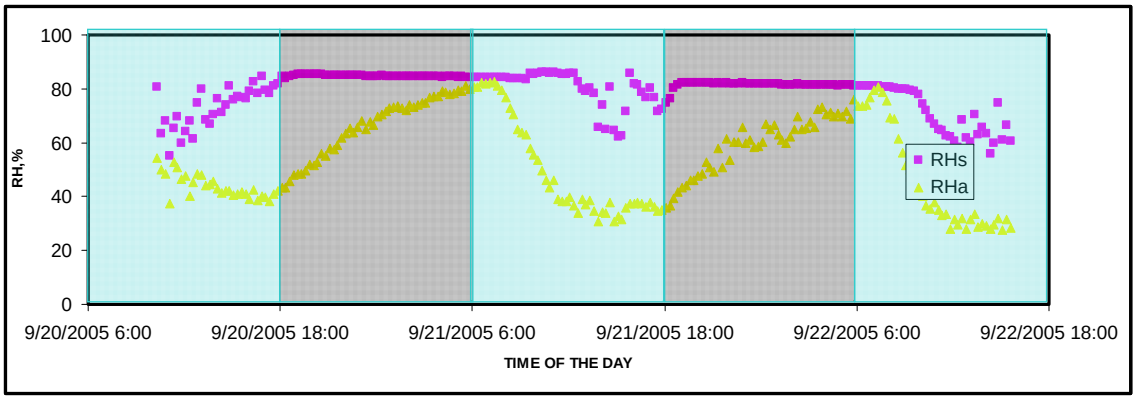

Figure G-3. Relative Humidity Trend for High Reflective Curing Compound.

For this field test and the field tests thereafter, the DC measurements were conducted to assess the curing effectiveness (Figure G-4). Based on the DC slope, the high relative curing compound (HRC) showed, as expected, better performance than the

normal curing compound (NC). The DC slope represents a rate of moisture loss over time.

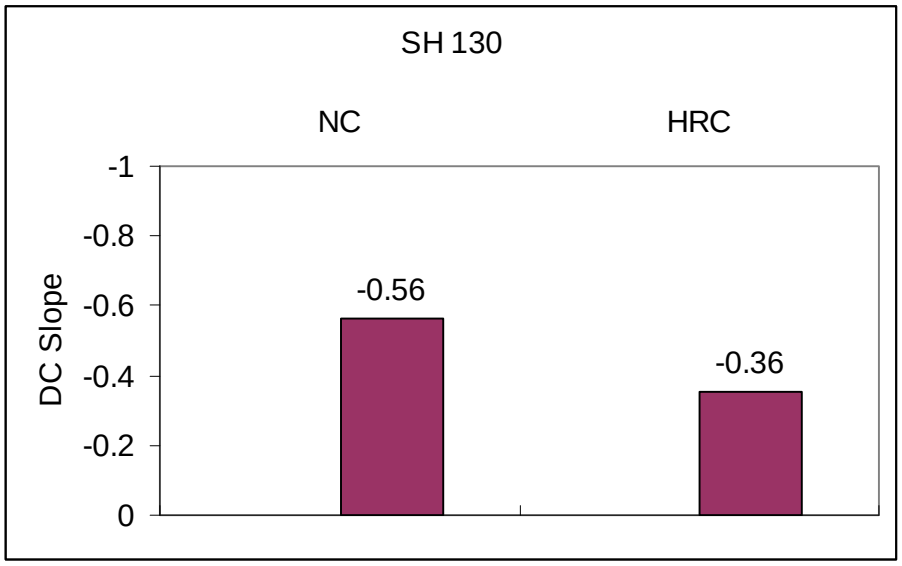

Figure G-4. DC Slopes for SH 130 Field Test.

APPENDIX H
FIELD TEST AT SH 288 PEARLAND

Field testing was carried out on SH 288, a construction site near Pearland, Texas, during the month of November 2005 to collect data on the performance of the high reflective curing compound (Sealtight® 2255) and normal resin-based curing compound (Sealtight® 1240) under field conditions.

This site consisted of four test sections for the purpose of evaluating the curing effectiveness of the subject curing compounds. The curing compound in HRC was applied manually, but only in section 2. All other sections were placed using the spray machine to apply the curing compound to the pavement surface. The basic information about each section is listed in Table H-1.

Table H-1. Curing Facts in SH 288.

	Curing Compound	**Spray Method**
Section 1	NC - Sealtight® 1240	Machine Spray
Section 2	HRC - Sealtight® 2255	Manual Spray
Section 3	NC - Sealtight® 1240	Machine Spray
Section 4	NC - Sealtight® 1240	Machine Spray

AMBIENT CONDITIONS

The PE trends for the ambient weather conditions using Figure 2-7 are shown in Figure H-1. Since it was conducted in November, the highest PE was only about 0.15 lb/ft^2/hr, which was relatively mild.

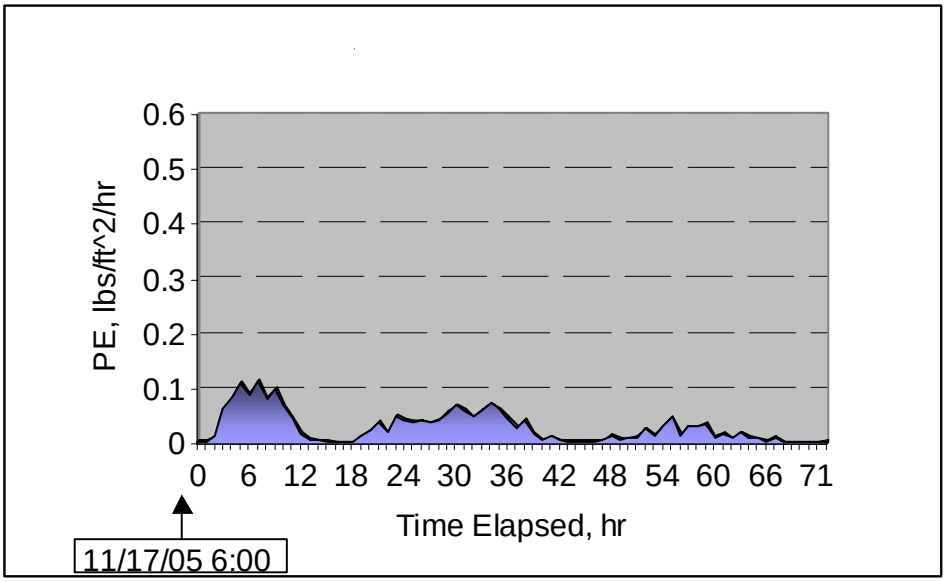

Figure H-1. Potential of Evaporation at SH 288.

Data Presentation

Relative humidity data are presented in Figures H-2 through H-5. WS/RH is the ratio between the wind speed and the air relative humidity and is referred to as the effective wind speed that provides, relative to the severity of the curing environment, an indicator of ambient weather condition.

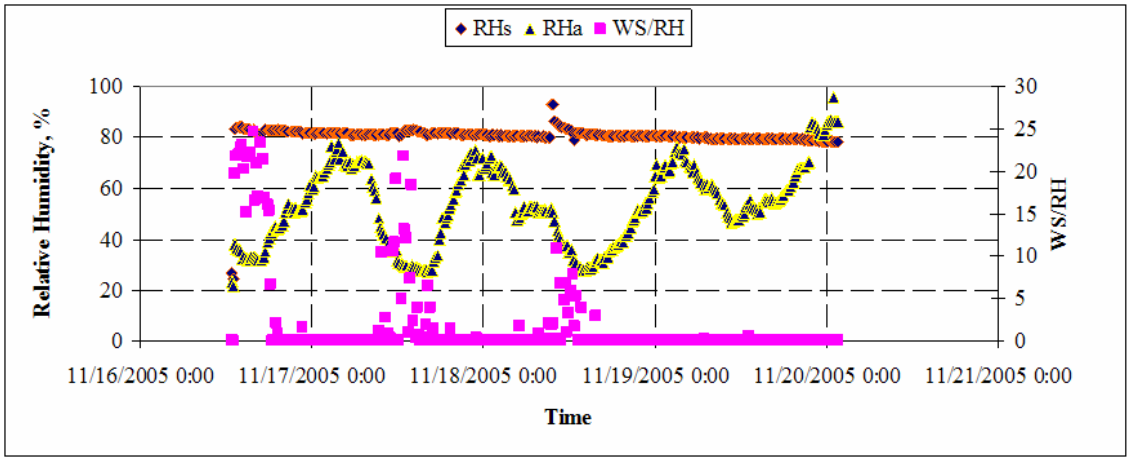

Figure H-2. Relative Humidity Trend for Section 1 (SH 288, Nov 2005).

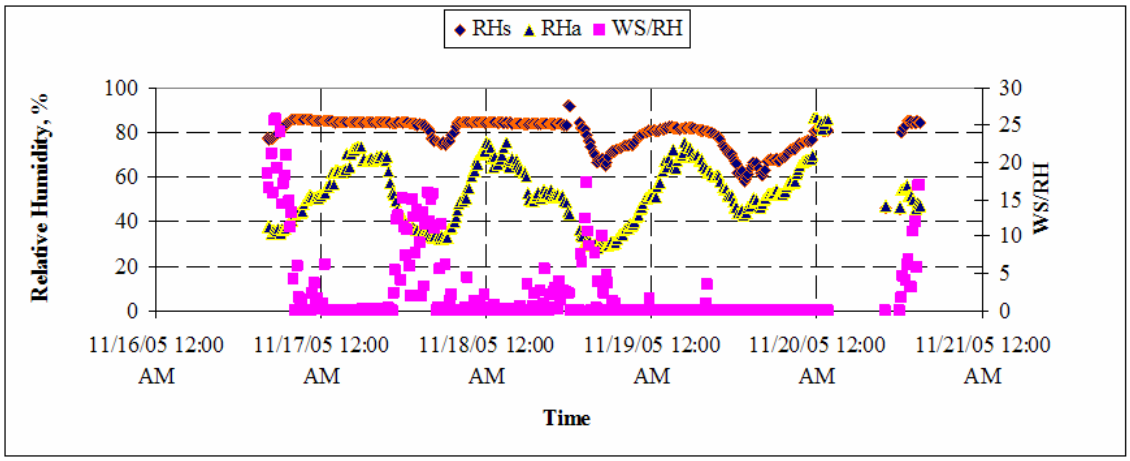

Figure H-3. Relative Humidity Trend for Section 2 (SH 288, Nov 2005).

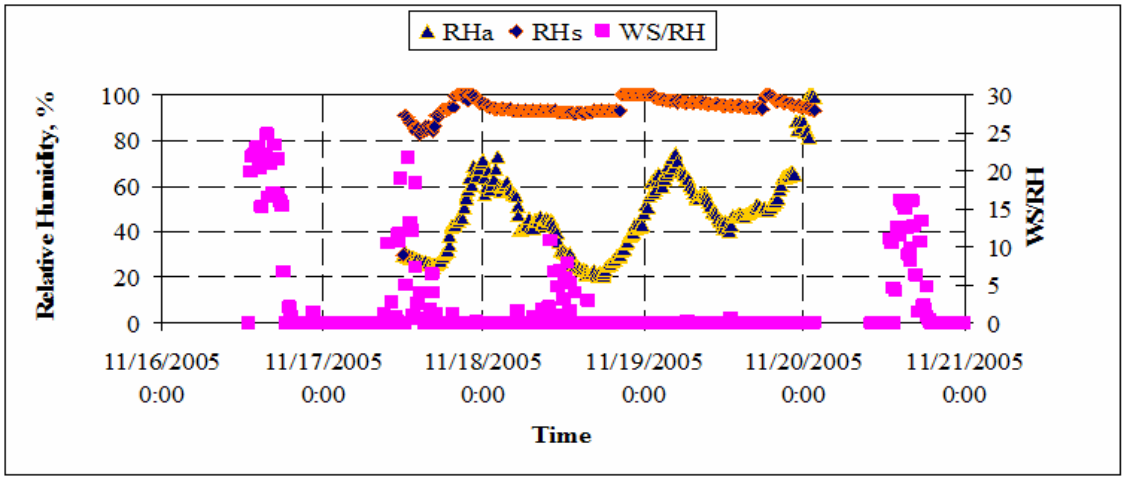

Figure H-4. Relative Humidity Trend for Section 3 (SH 288, Nov 2005).

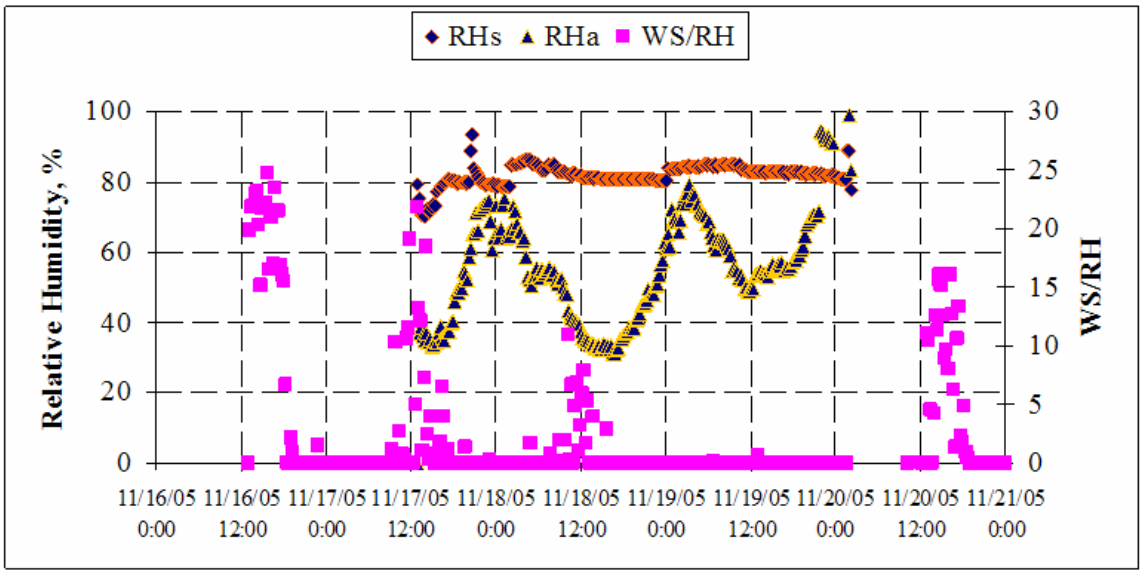

Figure H-5. Relative Humidity Trend for Section 4 (SH 288, Nov 2005).

Surface relative humidity data for the normal curing compound cured sections were all above 80 percent, which is an indicator of good curing as noted in the literature review. On the contrary, relative humidity levels for the high reflective curing compound cured section (Figure H-3) were beginning to break down the second day, and the drop increased the second and third days. According to the laboratory-based rankings, the high reflective curing compound rank higher than the normal resin-based curing compound. However, manual spraying of high reflective curing compound may account for the relatively poor performance (i.e., surface relative humidity breakdown) in the field. It is difficult to achieve uniformity manually applying the curing membrane.

Measured DC data are shown in Figure H-6. The DC slopes for normal curing compound cured sections range from -0.2 to -0.3, while the slope for high reflective curing compound cured section is the lowest. These trends may be due to the fact that the spot, where the DC measurements were taken, had excessive curing compound sprayed due to the manual spraying operation.

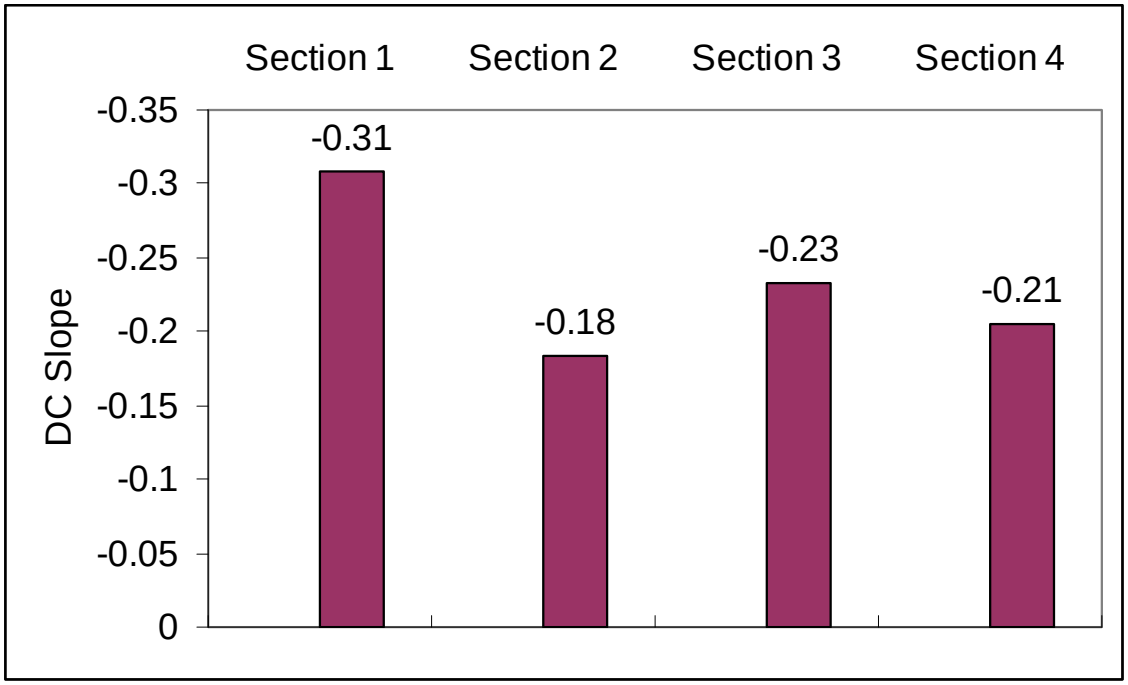

Figure H-6. DC Slopes for SH 288 Field Test.

APPENDIX I
FIELD TEST ON SH 35

Field testing was carried out on SH 35, a construction site in West Columbia, Texas, during the month of April 2006 to collect data on the performance of high reflective curing compound (Sealtight® 2255) and normal resin-based curing compound (Sealtight® 1240) under field conditions. There were four test sections for curing effectiveness evaluation. Manual spray was used for all sections (as listed in Table I-1). Sections 1, 3, and 4 are replicates.

Table I-1. Curing Facts in SH 35 (April 2006).

	Curing Compound	**Spray Method**
Section 1	NC	Manual Spray
Section 2	HRC	
Section 3	NC	
Section 4	NC	

AMBIENT CONDITIONS

The ambient weather PE Figure 2-7 is shown in Figure I-1. The highest PE was about 0.20 lb/ft^2/hr. During the first two days, the PE was mild and became more severe during the third day.

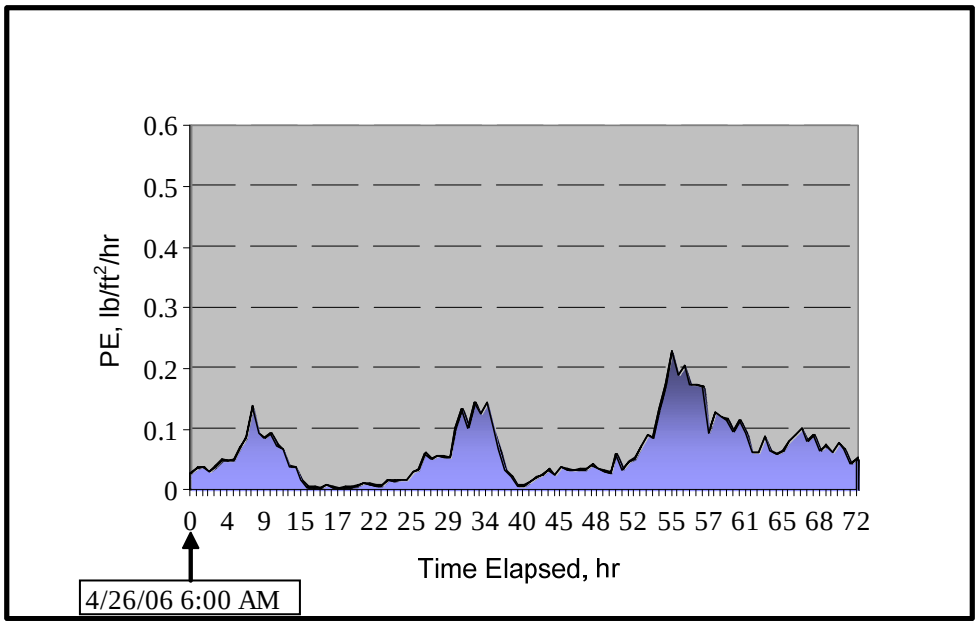

Figure I-1. Potential of Evaporation at SH 35 (April 2006).

DATA PRESENTATION

Relative humidity data are presented in Figures I-2 through I-5.

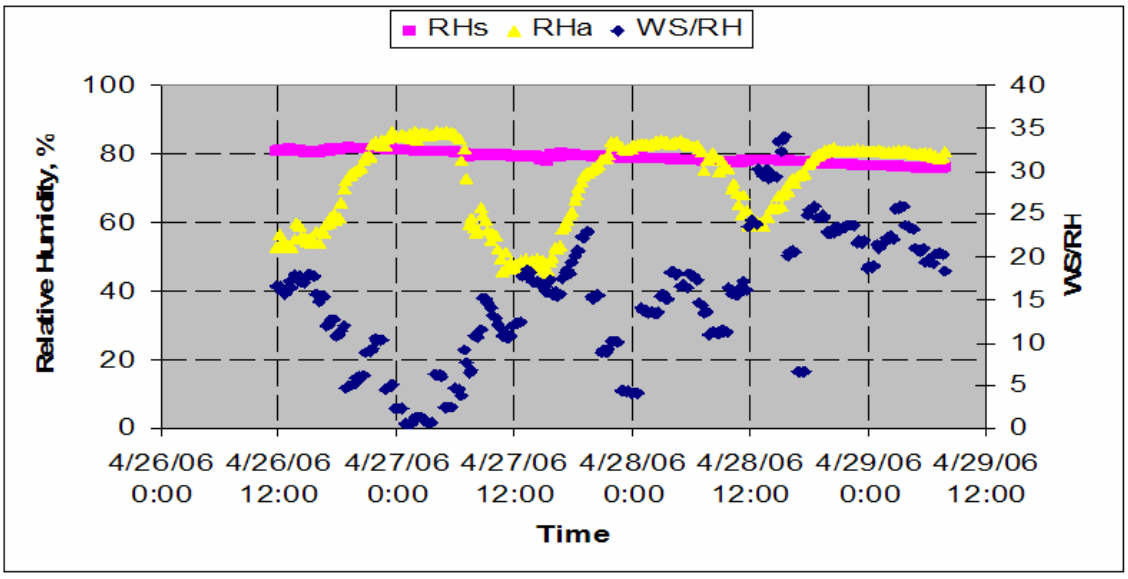

Figure I-2. Relative Humidity Trend for Section 1 (SH 35, April 2006).

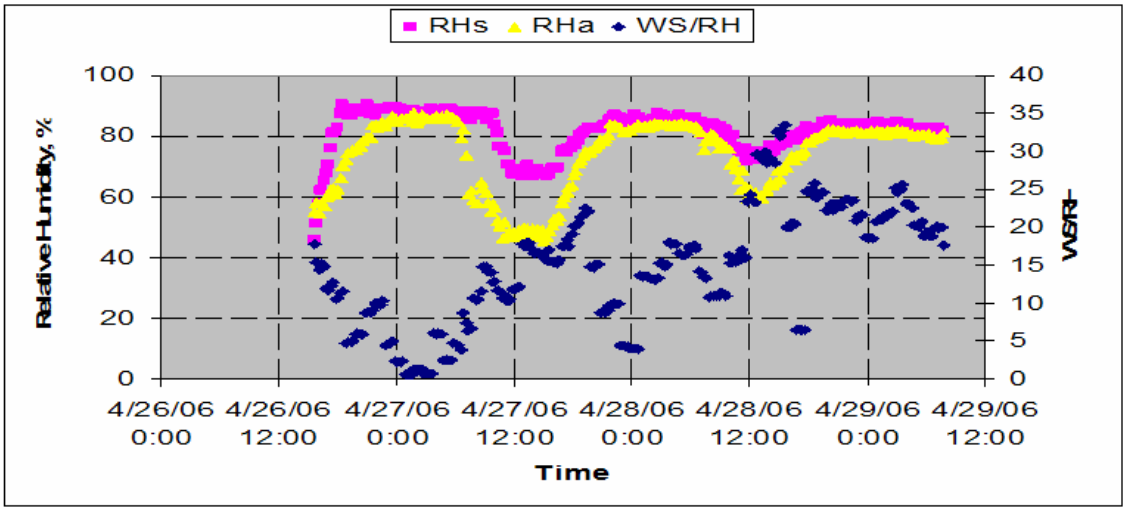

Figure I-3. Relative Humidity Trend for Section 2 (SH 35, April 2006).

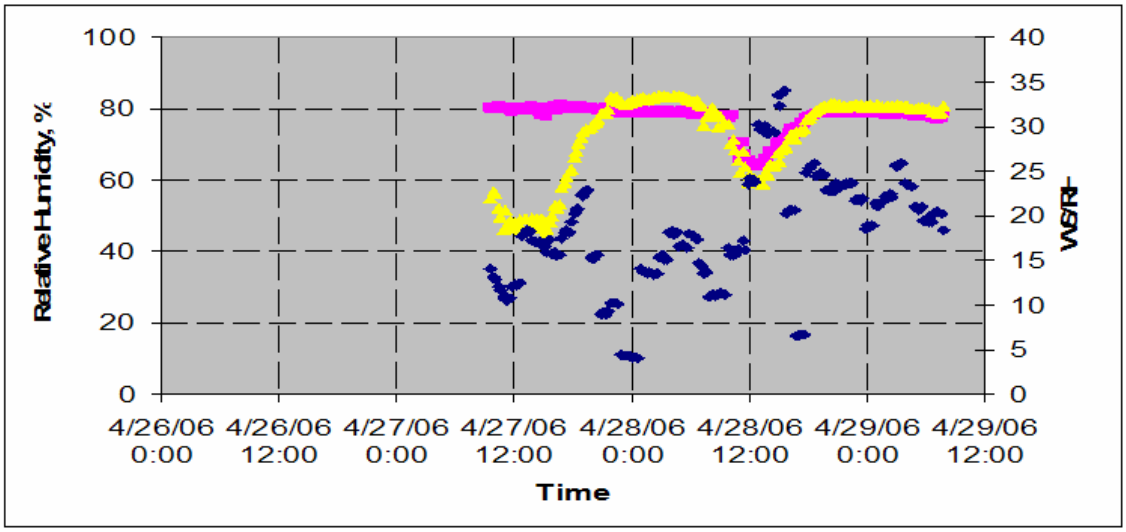

Figure I-4. Relative Humidity Trend for Section 3 (SH 35, April 2006).

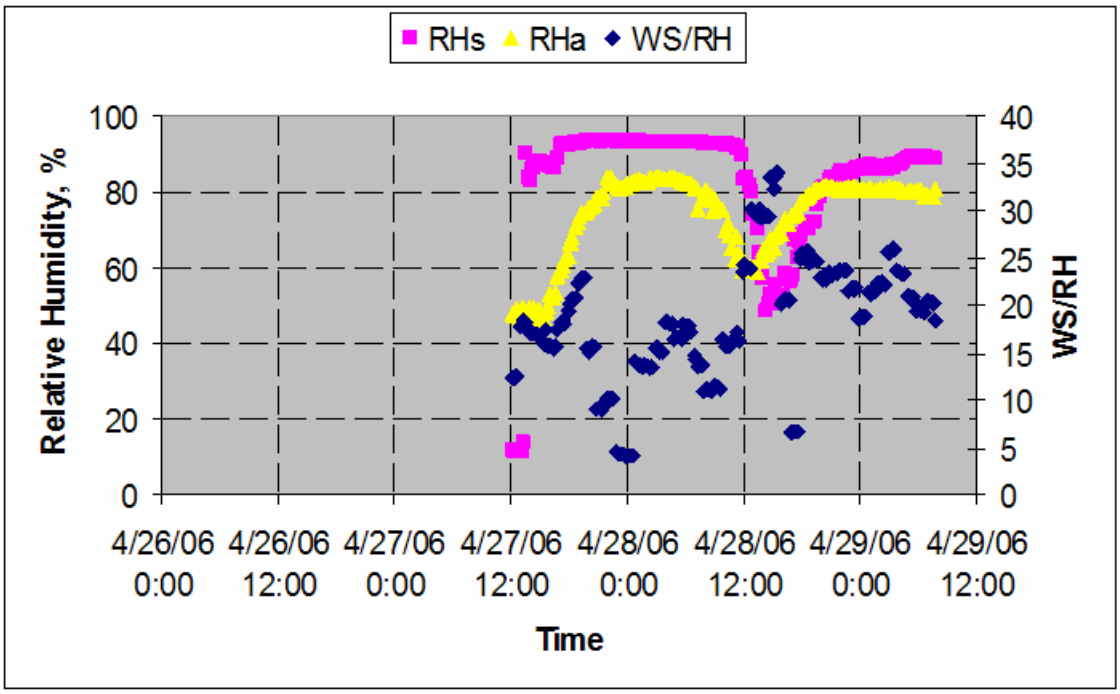

Figure I-5. Relative Humidity Trend for Section 4 (SH 35, April 2006).

Based on surface relative humidity, it is observed that only section 1 had good curing as indicated by the surface relative humidity. In all other sections, the surface relative humidities broke down the second day after concrete placement.

DC measurements are available only in sections 1 and 2. The DC slopes are shown in Figure I-6. These slopes match well with measured moisture data. The slope of the unbroken surface relative humidity section was smaller than that of the broken surface humidity section.

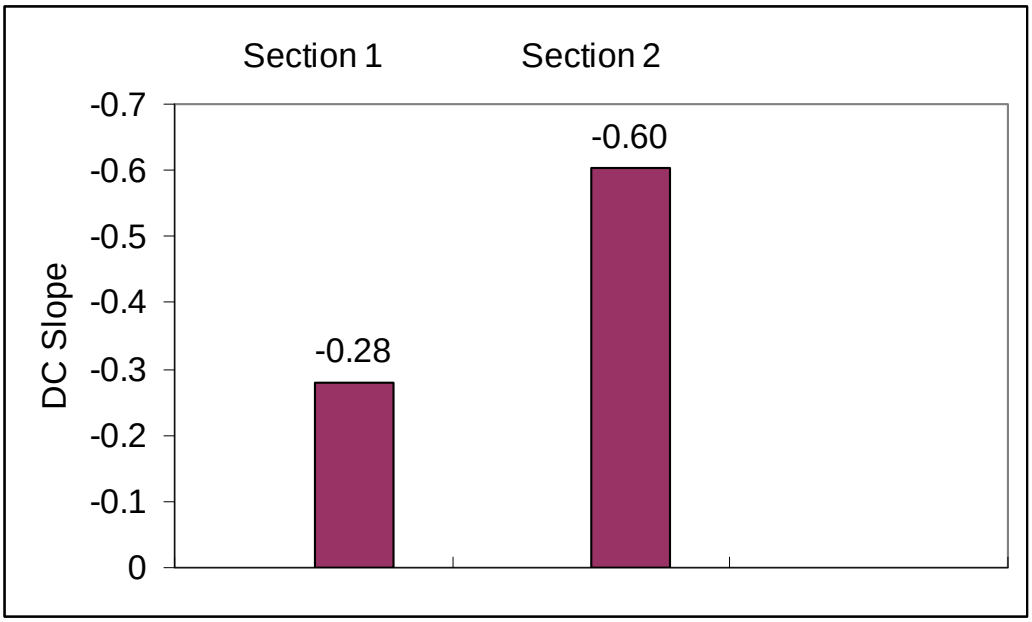

Figure I-6. DC Slopes for SH 35 Field Test (April 2006).

APPENDIX J
FIELD TEST AT SH 35

Field testing was carried out on a construction site on SH 35 in West Columbia, Texas, during the month of May 2006 to reexamine the effects of delayed application and reapplication of the curing on the second day after placement on curing effectiveness.

The application scheme for this test site is shown in Table J-1. The application schemes for sections 1 and 2 were the same, except that section 1 was placed in the morning and section 3 was placed in the afternoon. Consequently, the PEs for these placement conditions were less than 0.2 lb/ft^2/hr for the morning placement and greater than 0.3 lb/ft^2/hr for the afternoon placement. Normal curing compound MRW 1240 and manual spraying were used on this field test.

Table J-1. Application Scheme for SH 35 (May 2006).

	First Coat	Second Coat	Third Coat
Section 1	1 hr after concrete placement (morning)	Second day–10 am	
Section 2	1 hr after concrete placement	5 hr after concrete placement	Second day–10 am
Section 3	1 hr after concrete placement (afternoon)	Second day–10 am	

<0.2 lb/ft^2/hr for the morning placement; >0.3 lb/ft^2/hr for the afternoon placement.

AMBIENT CONDITIONS

The PE of the ambient weather conditions using Figure 2-7 is shown in Figure J-1. The highest PE was about 0.35 lb/ft^2/hr.

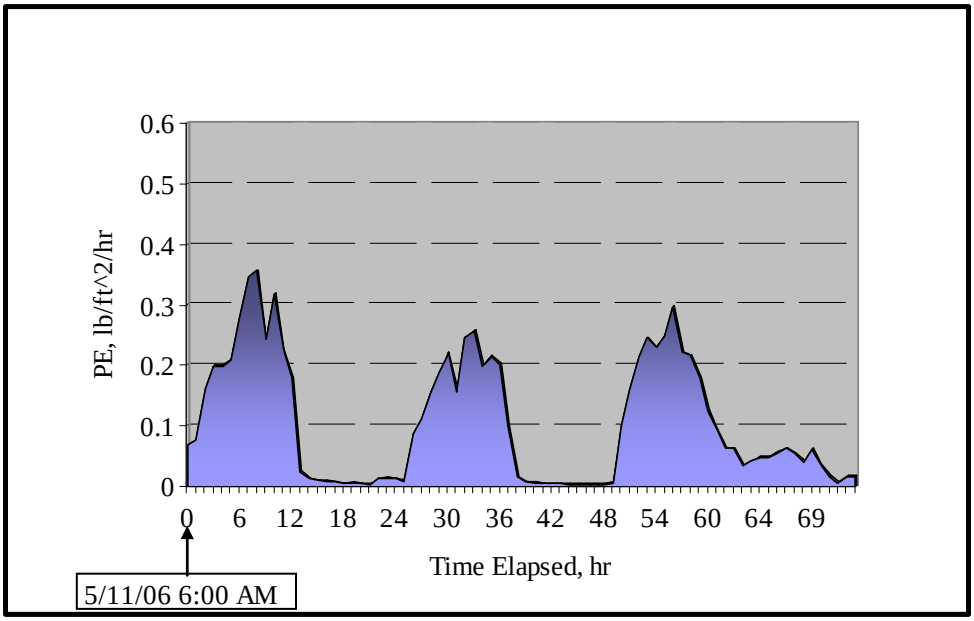

Figure J-1. Potential of Evaporation at SH 35 (May 2006).

DATA PRESENTATION

Relative humidity data are presented in Figures J-2 through J-4. The pink curves are surface relative humidity, and the yellow curves are ambient relative humidity.

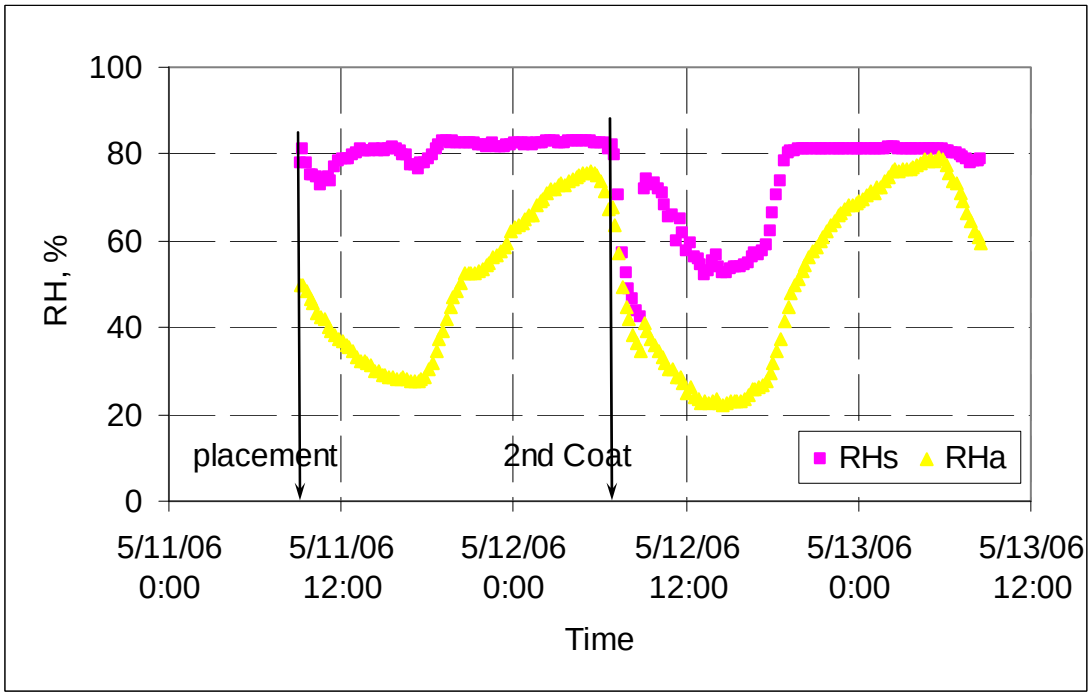

Figure J-2. Relative Humidity Trend for Section 1 (SH 35, May 2006).

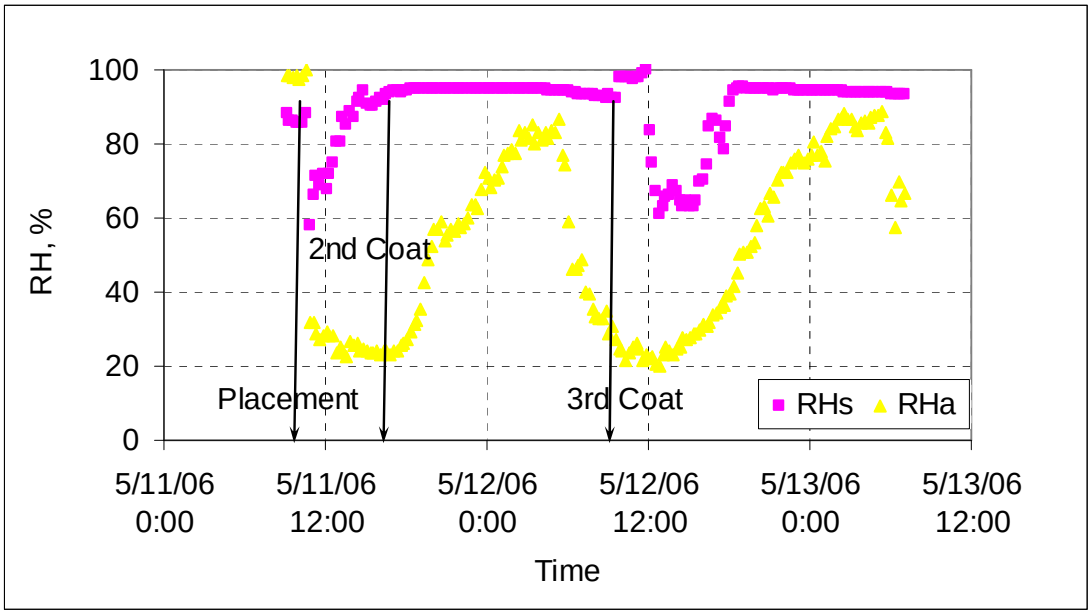

Figure J-3. Relative Humidity Trend for Section 2 (SH 35, May 2006).

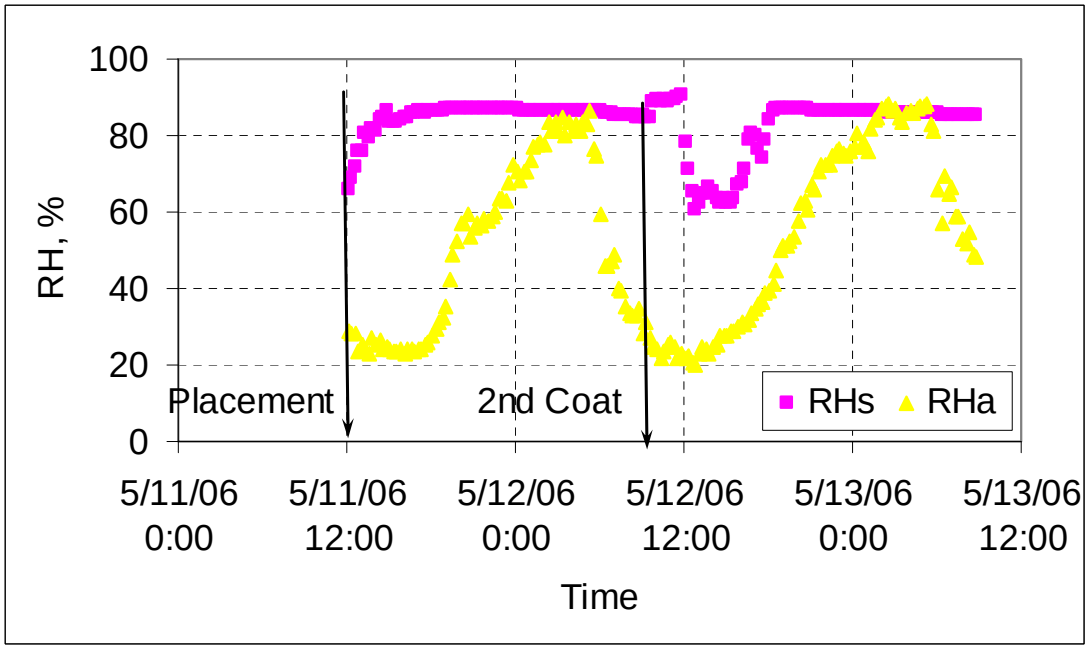

Figure J-4. Relative Humidity Trend for Section 3 (SH 35, May 2006).

From the surface humidity data, it is found that neither of the sections had demonstrated good curing on the second day, which was probably due to poor coverage due to manual spraying; the second day application could not improve the curing quality. The application scheme in section 2 showed the best curing quality among the three test sections. DC slopes are shown in Figure J-5. Due to non-uniformity by manual spraying, the data were less representative.

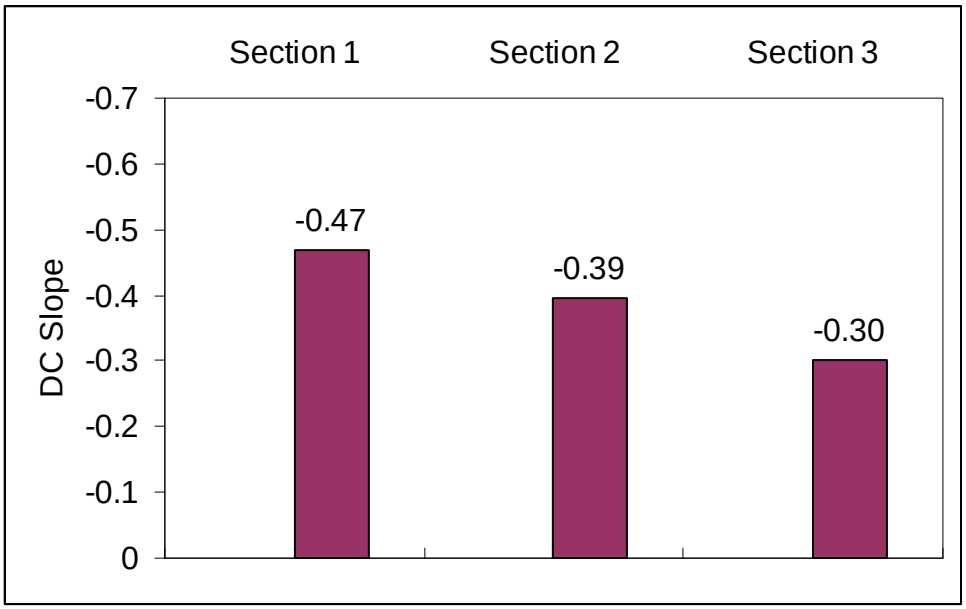

Figure J-5. DC Slopes for SH 35 Field Test (May 2006).

APPENDIX K
FIELD TEST AT SH 35

A field test was carried out on a construction site on SH 35 in West Columbia, Texas, during the month of June 2006 to examine the effects of retardant and reapplication of high reflective curing compound on the second day of curing relative to its effectiveness.

Three sections were established for investigation. The application scheme is shown in Figure K-1. The application schemes for sections 1, 2, and 3 were the same, except that sections 1 and 3 included a second coat placed on the same day, and section 1 was placed in the morning and section 3 was placed in the afternoon. Manual spray application was used on this test site. An evaporation retardant was applied immediately after surface finishing to prevent plastic shrinkage.

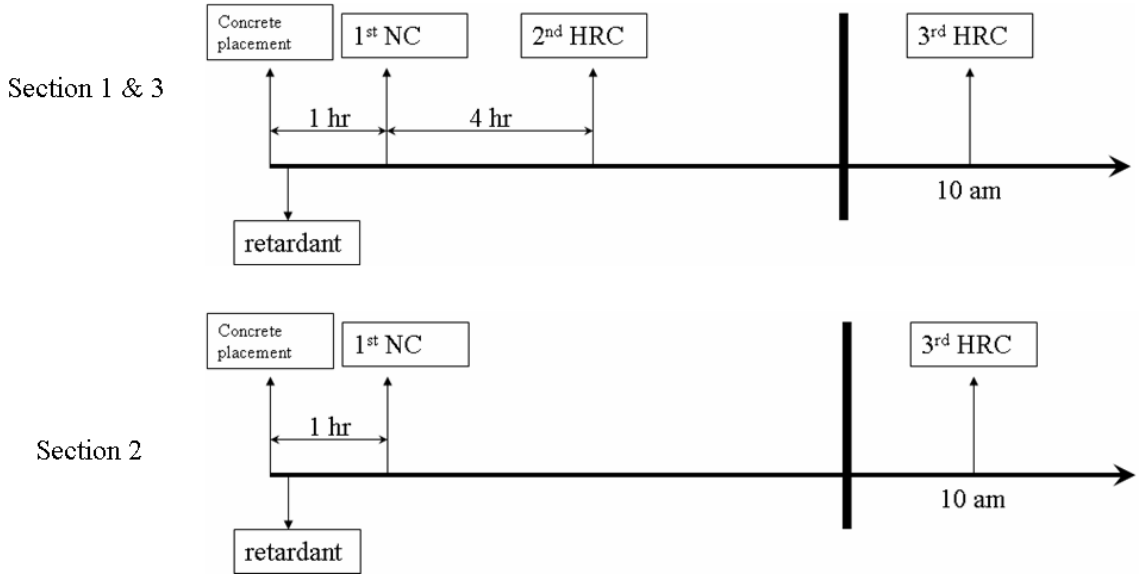

Figure K-1. Application Scheme for SH 35 (June 2006).

AMBIENT CONDITIONS

The PE for the ambient weather conditions according to Figure 2-7 is shown in Figure K-2. The highest PE was about 0.20 lb/ft^2/hr.

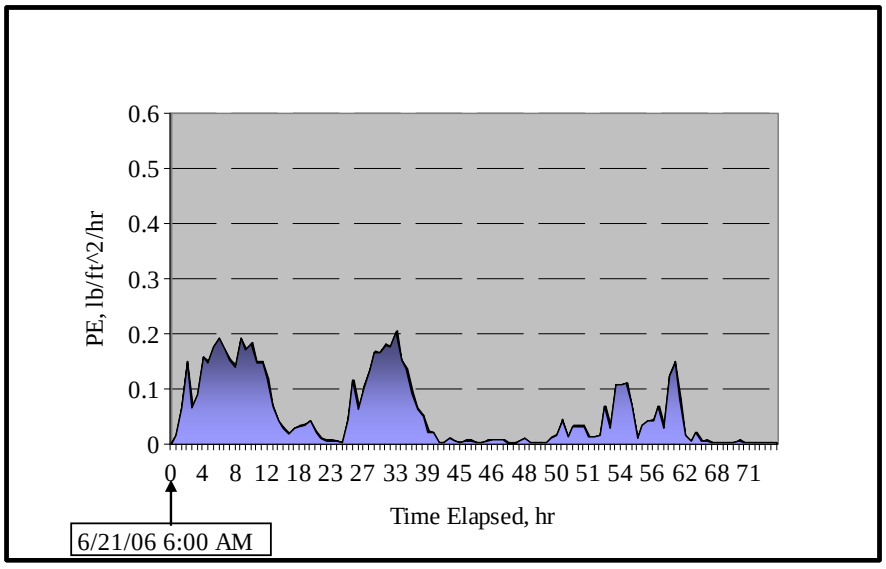

Figure K-2. Potential of Evaporation at SH 130.

DATA PRESENTATION

Relative humidity data are presented in Figures K-3 through K-5. The pink curves are surface relative humidity, and the yellow curves are ambient relative humidity.

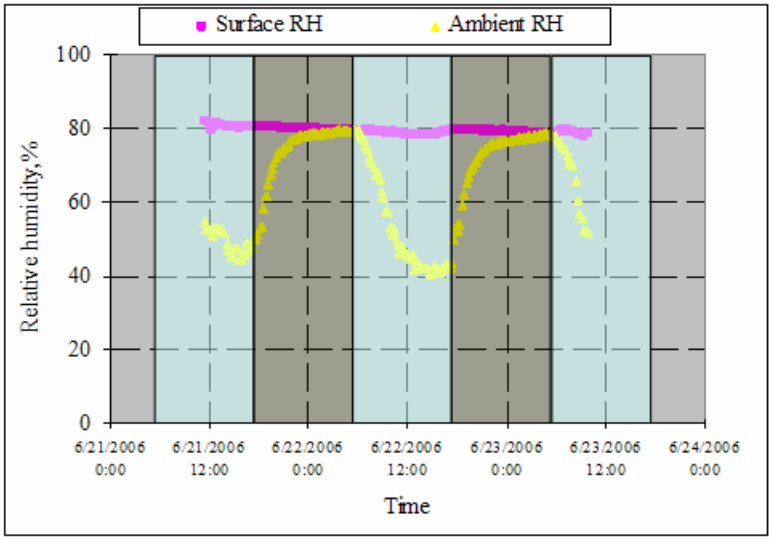

Figure K-3. Relative Humidity Trend for Section 1 (SH 35, June 2006).

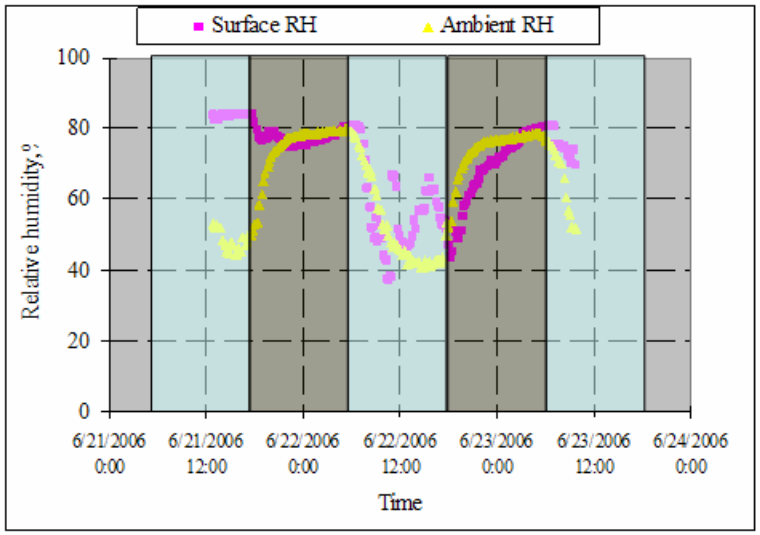

Figure K-4. Relative Humidity Trend for Section 2 (SH 35, June 2006).

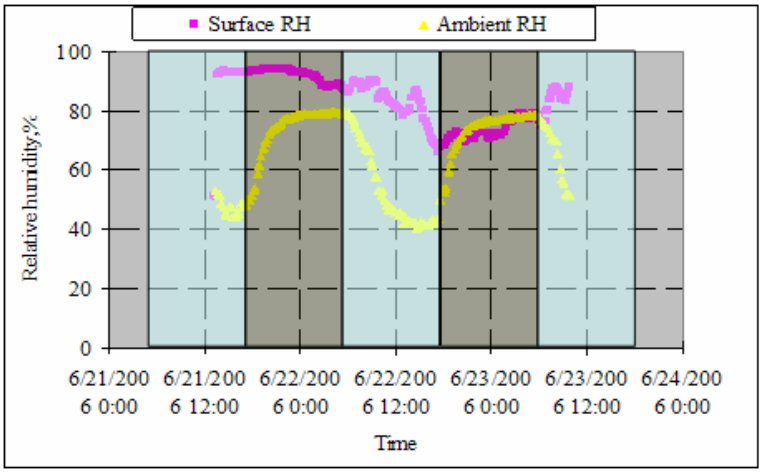

Figure K-5. Relative Humidity Trend for Section 3 (SH 35, June 2006).

Sections 1 and 3 showed good curing quality, since a higher quality of curing was achieved by using a rate of application of 60 gallon/ft^2. The double-delayed application made a difference in curing quality particularly during the second day after placement when vapor pressures have sufficiently diminished before placement of the second application.

DC slopes are shown in Figure K-6. From DC slopes, there was a difference between section 1 and sections 2 and 3.

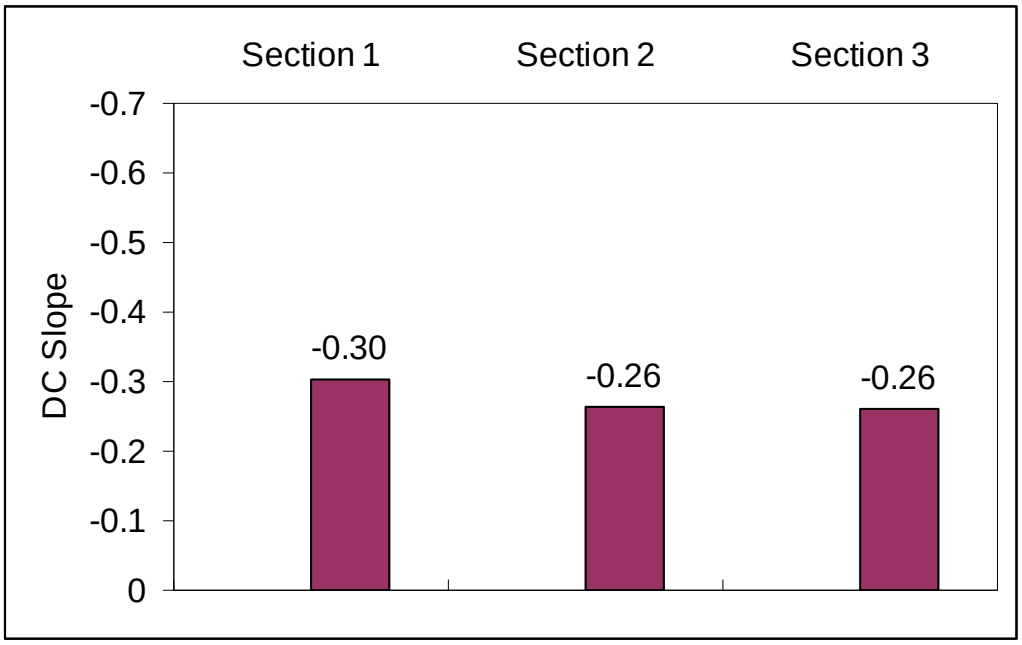

Figure K-6. DC Slopes for SH 35 Field Test (June 2006).

APPENDIX L
FIELD TEST AT I 40 AMARILLO

An extensive field test was carried out on an I 40 construction site near Amarillo, Texas, during the month of August 2006 to collect data on the effectiveness of high reflective curing compound, wax-based curing compound, and normal resin-based curing compound. Besides relative humidity and DC measurements, mortar cubes strength was obtained to justify the curing effectiveness from a physical properties standpoint of view.

Six sections were established for investigation. The information for each section is presented in Table L-1. The effectiveness of a single coat of curing compound versus a double coat was investigated. For this job site, normal resin-based curing compound was used by the contractor, so machine spray was used to apply this type of compound. It was not convenient to switch tanks on the spray machine to the wax-based or the reflective curing compound. As a result, hand spray was used for these two types of curing compounds.

Table L-1. Facts in Each Section.

	No. of Coats	**Type of Curing Compound**	**Application**
Section 1	Single	Normal Resin-based	Machine
Section 2	Double	Normal Resin-based	Machine
Section 3	Single	Wax-based	Manual
Section 4	Double	Wax-based	Manual
Section 5	Single	High Reflective	Manual
Section 6	Double	High Reflective	Manual

AMBIENT CONDITIONS

The ambient weather conditions were characterized by the ACI 308 nomograph shown in Figure 2-7, and the PE is shown in Figure L-1. The highest PE was about 0.40 lb/ft^2/hr. It dropped dramatically due to the rain in the afternoon of August 25, 2006.

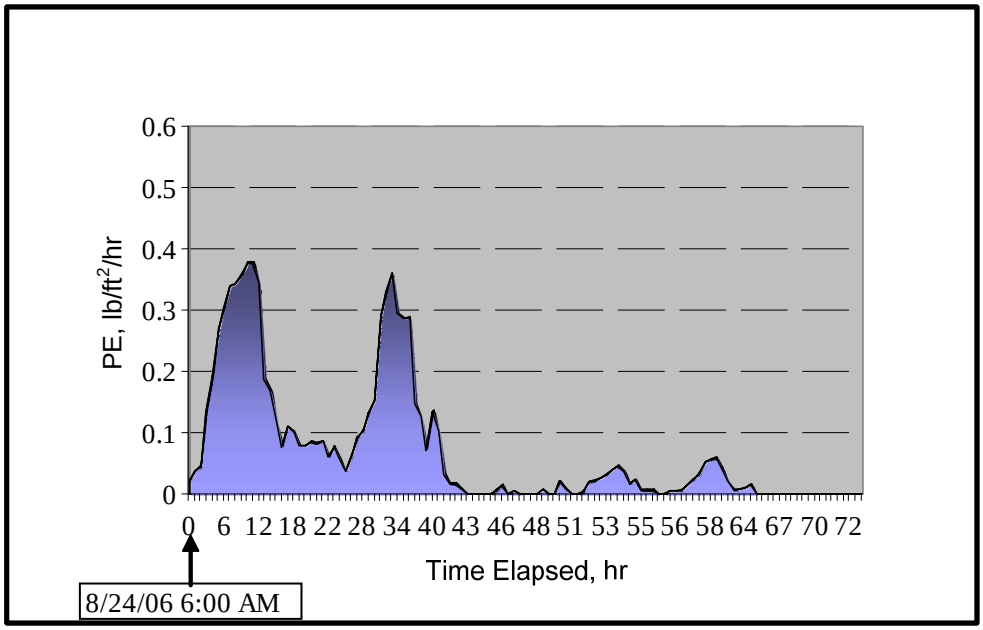

Figure L-1. Potential of Evaporation at I 40.

DATA PRESENTATION

Relative humidity data are presented in Figures L-2 through L-7. The pink curves are surface relative humidity, and the yellow curves are ambient relative humidity.

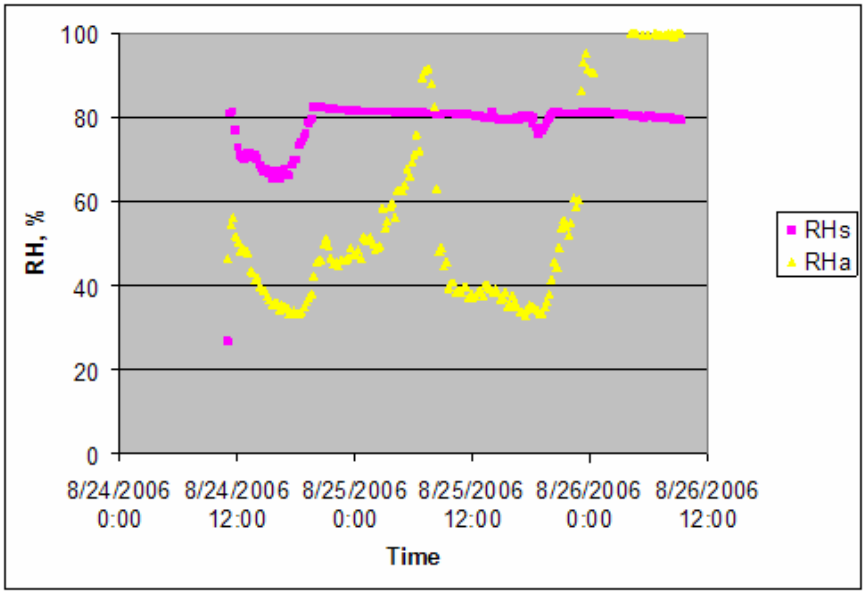

Figure L-2. Relative Humidity Trend for Section 1 (I 40, Aug 2006).

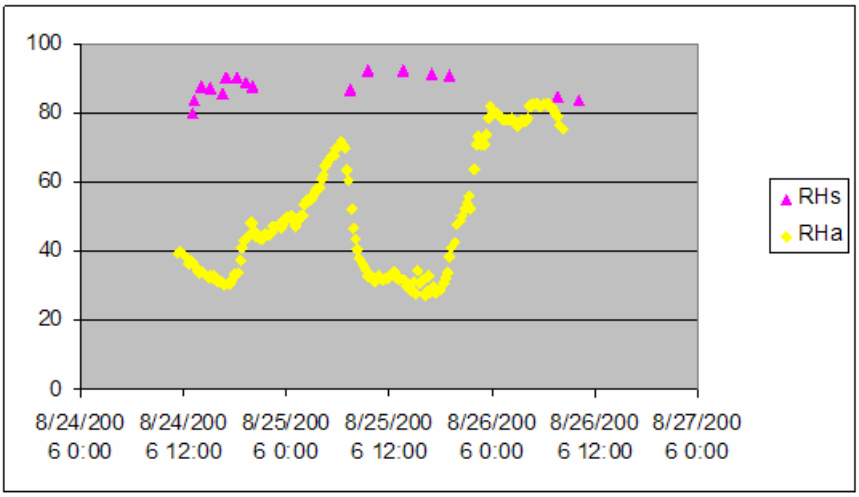

Figure L-3. Relative Humidity Trend for Section 2 (I 40, Aug 2006).

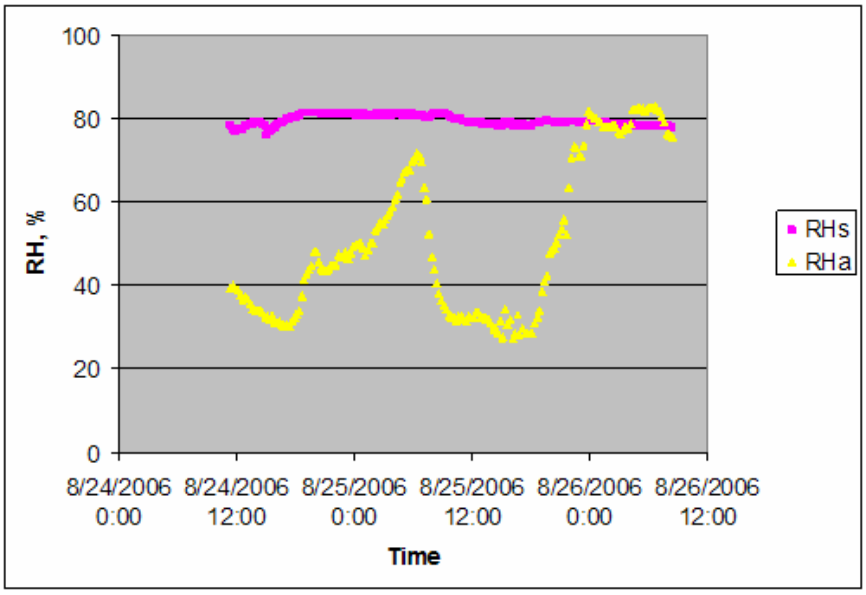

Figure L-4. Relative Humidity Trend for Section 3 (I 40, Aug 2006).

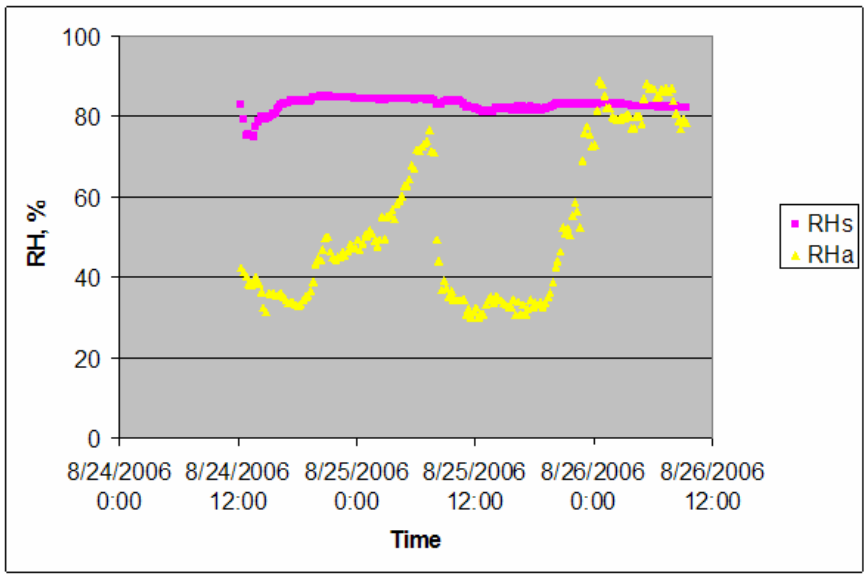

Figure L-5. Relative Humidity Trend for Section 4 (I 40, Aug 2006).

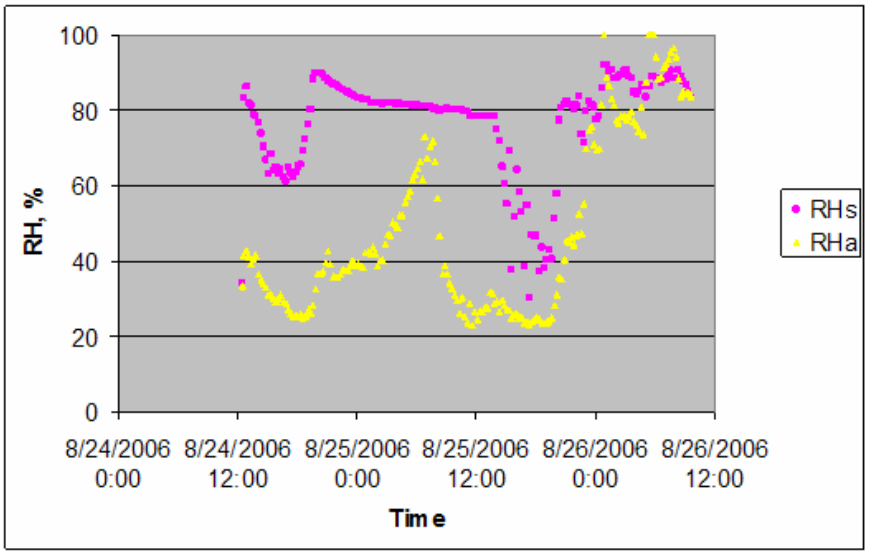

Figure L-6. Relative Humidity Trend for Section 5 (I 40, Aug 2006).

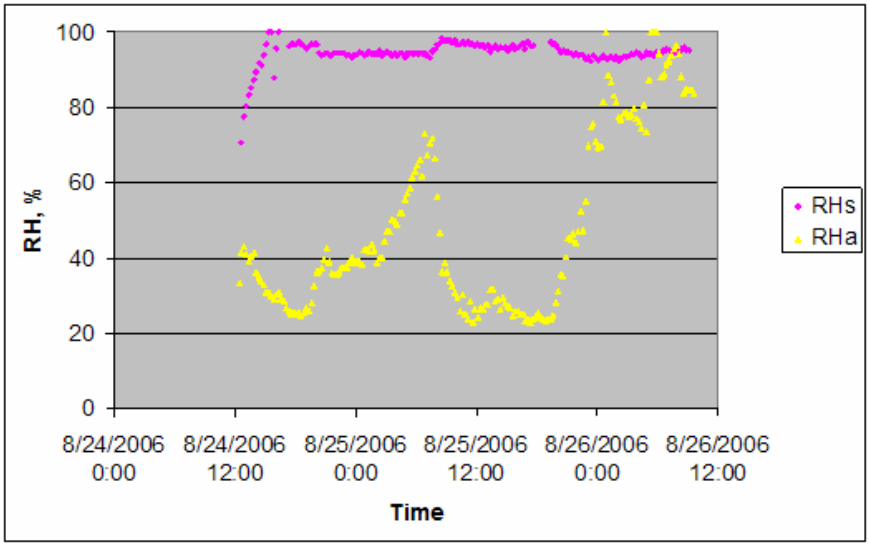

Figure L-7. Relative Humidity Trend for Section 6 (I 40, Aug 2006).

Surface relative humidity showed that the curing performance for section 5 was poor. All other sections showed the surface humidities were above 80 percent, even the single coat of normal resin-based curing compound in section 1. This should be accredited to the machine spray, which is capable of applying a uniform coat of curing membrane.

DC slopes were obtained for sections 1, 3, 4, 5, and 6 shown in Figure L-8. It is evident that double coats increased the curing quality, as noted in the relative humidity data.

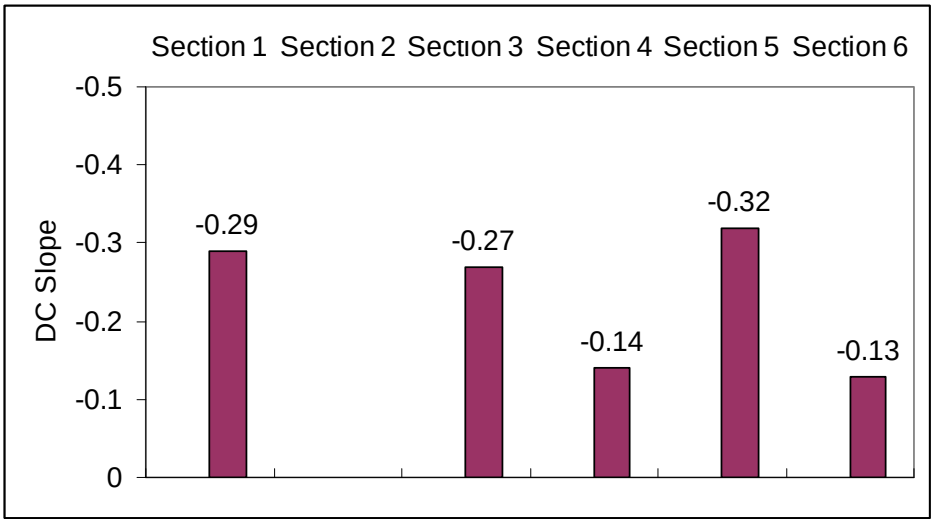

Figure L-8. DC Slopes for I 40 Field Test.

Six sets of mortar cubes were prepared for each section. In each set, three types of cubes were prepared, shown in Figure L-9. Sealed specimens were used to determine strength under perfect curing conditions (without any moisture loss); curing compound cured specimens were used to determine strength achieved with the curing compound; and the exposed specimens were used to determine strength under the worst conditions. The curing effectiveness can be obtained from a relative scale (Figure L-10).

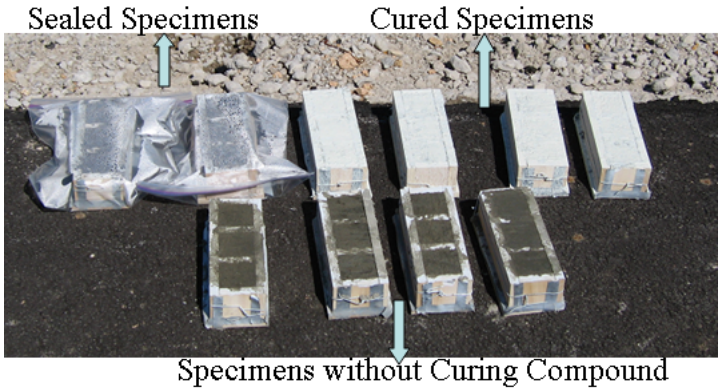

Figure L-9. Mortar Cubes.

$$CE = \frac{S_C - S_E}{S_S - S_E}$$

Where,

S_C- strength of cured sample

S_E- strength of exposed sample

S_S- strength of sealed sample

Figure L-10. I 40 Field Test.

The mortar cubes were tested after curing in the field for three days. The results are presented in Figure L-11. As expected, the sealed specimens gave the highest strength while the exposed specimens gave the lowest strength.

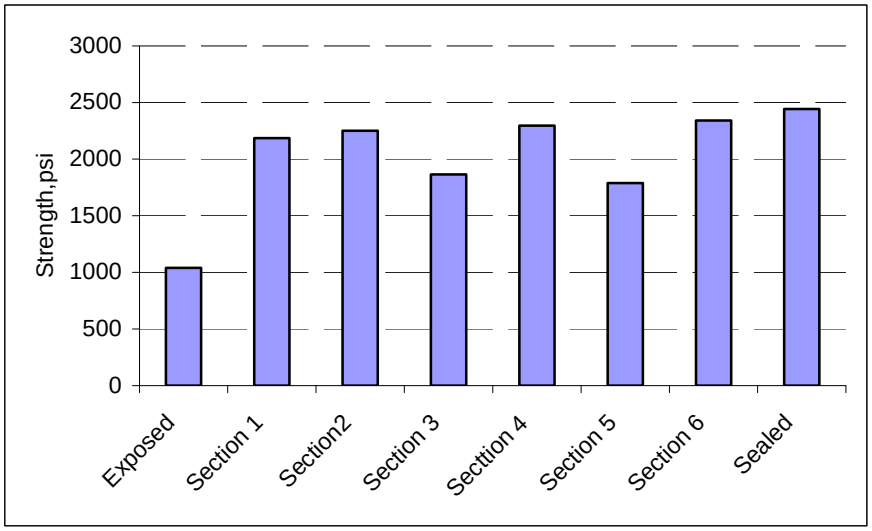

Figure L-11. Mortar Cube Strength (I 40, Aug 2006).

The CE was thus calculated. The CEs are presented in Figure L-12. The CEs for sections 4 and 6 were the best. However, the CEs for sections 3 and 5 were the worst. It is noted that manual spray was used from sections 3 to 6. A single coat of manual spray resulted in poor curing membrane uniformity, and even a high laboratory ranked curing compound poorly applied can result in poor curing. On the other hand, the CE for

section 1 indicated good curing, even though it was only a single coat application using a low laboratory ranked curing compound. This concludes that uniformity of curing is key to successful curing practice in the field.

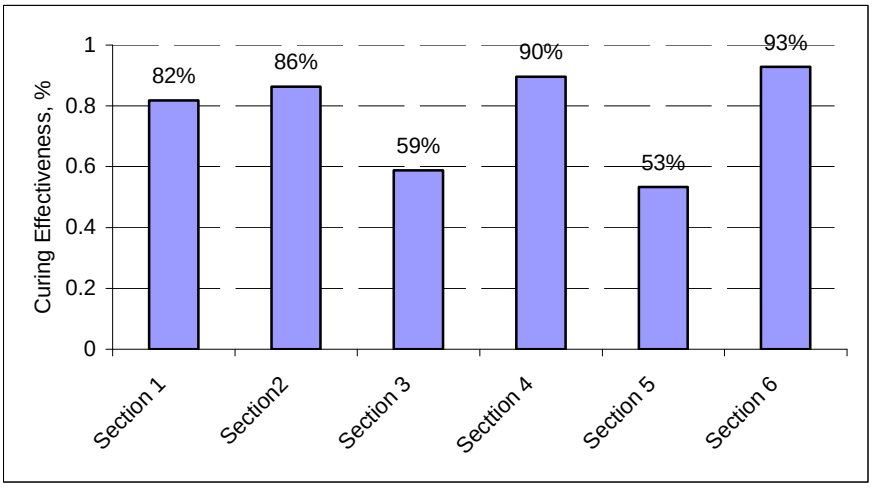

Figure L-12. Cure Effectiveness (I 40, Aug 2006).

APPENDIX M
FIELD TEST AT US 290

A field test was carried out on a US 290 construction site near Fairfield, Texas, during the month of October 2006. Two sections were investigated. The application rate for section 1 was designed to 60 ft^2/gal and was 90 ft^2/gal for section 2. The actual application rates were measured in the field.

AMBIENT CONDITIONS

The ambient weather conditions were characterized by the ACI 308 nomograph shown in Figure 2-7. The PE is shown in Figure M-1. The highest PE was about 0.20 lb/ft^2/hr.

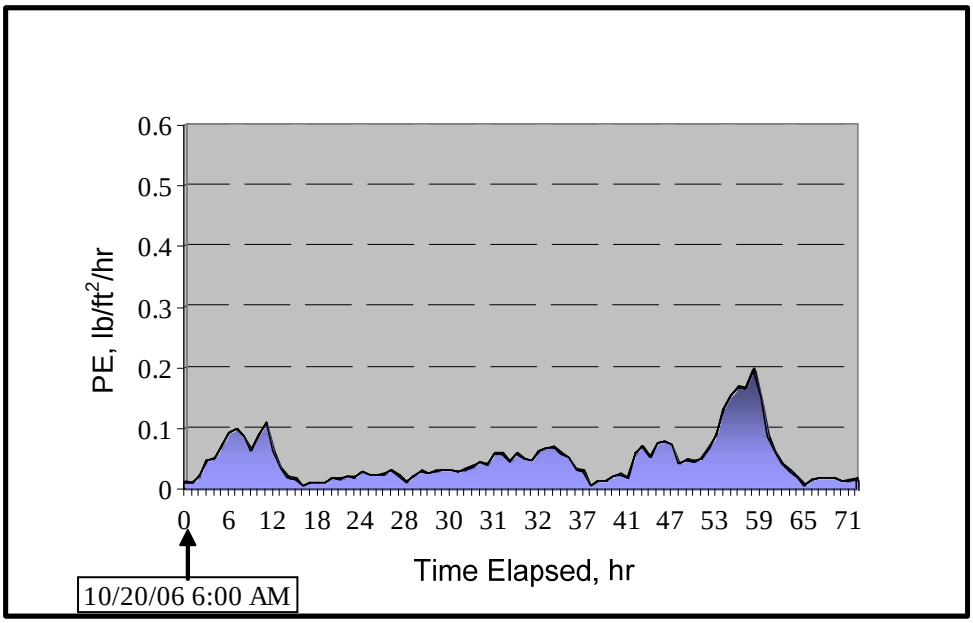

Figure M-1. Potential of Evaporation at US 290.

DATA PRESENTATION

Relative humidity data are presented in Figures M-2 and M-3. Chilled mirror sensors were also inserted in the surface chamber to justify the measurements from the capacitance type of sensor.

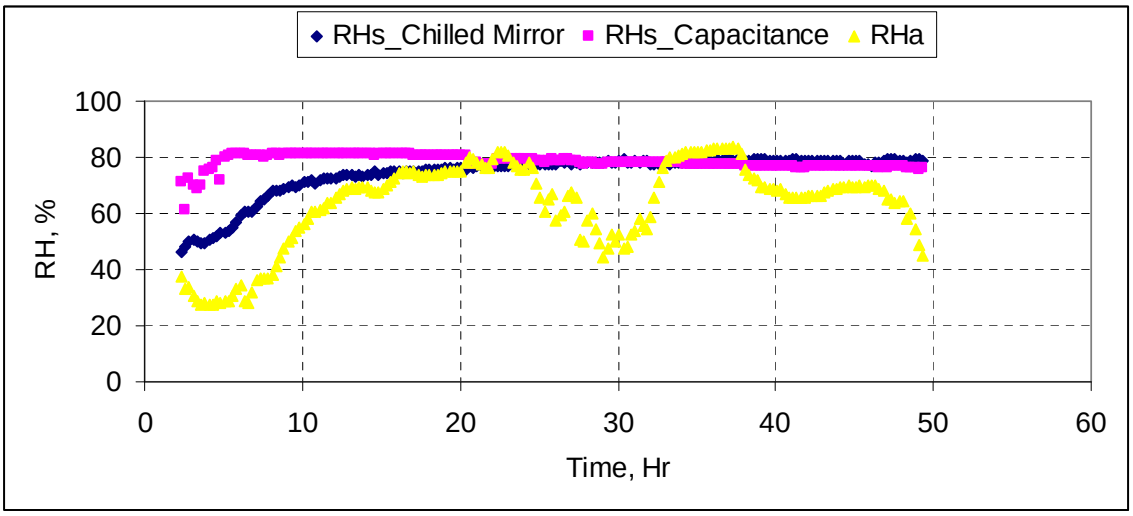

Figure M-2. Relative Humidity Trend for Section 1 (US 290, Oct 2006).

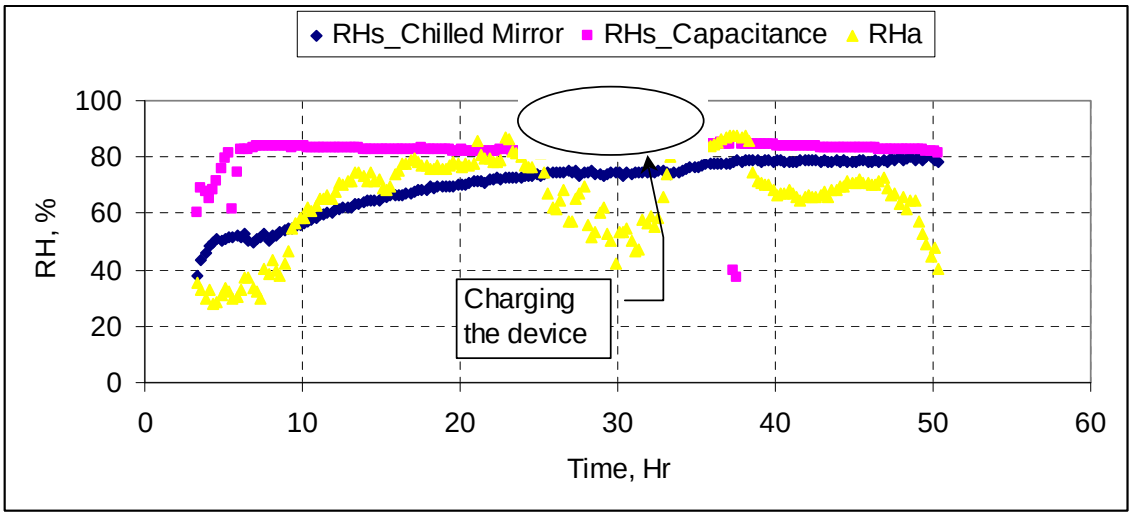

Figure M-3. Relative Humidity Trend for Section 2 (US 290, Oct 2006).

It is observed that chilled mirror measurements started off low, but eventually matched with the measurements from the capacitance sensor. It is believed that the chilled mirror measures the true vapor pressure in the surface chamber. The moisture buildup in the concrete takes time. However, when the moisture content in the air is high, such as when the concrete is fresh, so is the potential for condensation on the sensor. For a capacitance type of sensor, a false reading often results once condensation has taken place; while for a chilled mirror sensor, heating and cooling takes place to

maintain a water membrane on the mirror, thus capable of capturing an accurate assessment of the vapor buildup process.

DC slopes are presented in Figure M-4. Two slopes were obtained for each section. It is observed that the slopes of section 1 are slightly smaller than those of section 2, which means section 1 had better curing.

Application rates were measured in the field. Circular plates were used to collect the curing compound sprayed by the spray machine, as shown in Figure M-5. The weights of plates were taken before and after the curing compound application. Table M-1 is the table to calculate the actual application rate. The application rate of section 1 was approximately 40 ft^2/gal, and the application rate of section 2 was approximately 60 ft^2/gal.

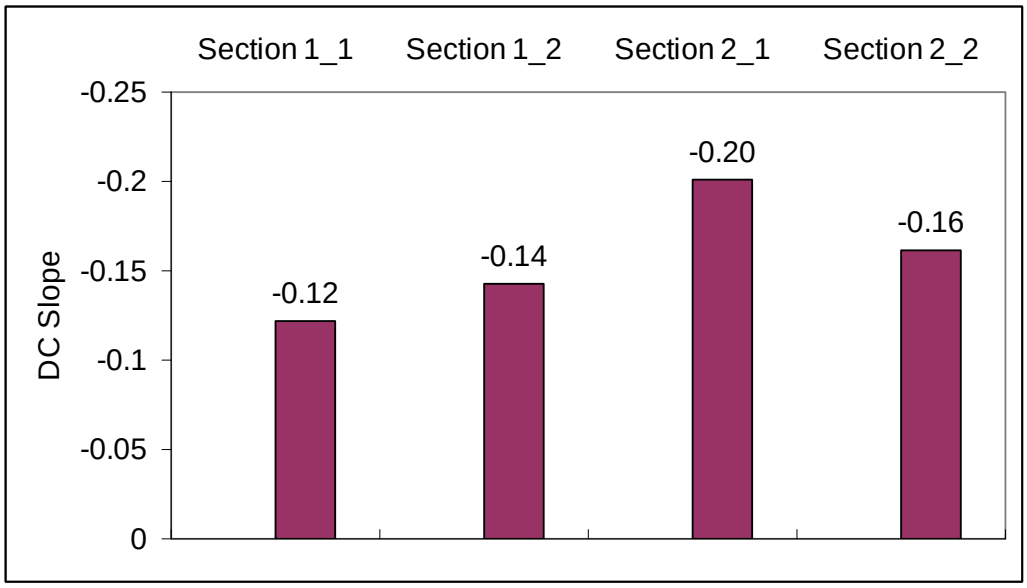

Figure M-4. DC Slopes for US 290 Field Test.

Figure M-5. Collection Plates for Application Rate Determination.

Table M-1. Application Rate Calculations.

	Section 1: 3 coats		Section 2: 2 coats	
Initial Weight, lb	0.0700	0.0700	0.0700	0.0700
Final Weight, lb	0.1100	0.1075	0.0955	0.0975
Net Weight, lb	0.0400	0.0375	0.0255	0.0275
Dry Weight, lb	0.0850	0.0865	0.0800	0.0800
Water Evaporated, lb	0.0250	0.0210	0.0155	0.0175
Area, ft^2	0.1963	0.1963	0.1963	0.1963
Density, lb/gallon	8.3300	8.3300	8.3300	8.3300
Application, gallon	0.0048	0.0045	0.0031	0.0033
Rate, ft^2/gallon	40.8898	43.6158	64.1409	59.4761
Rate per Application, ft^2/gallon	122.6694	130.8473	128.2817	118.9521

Mortar cubes were also prepared for this field test. Strength data and curing effectiveness are presented in Figures M-6 and M-7, respectively. From the strength data, there is not much difference in curing effectiveness for the two sections, which implies that for certain climatic conditions the rate of application can be adjusted to meet the curing needs.

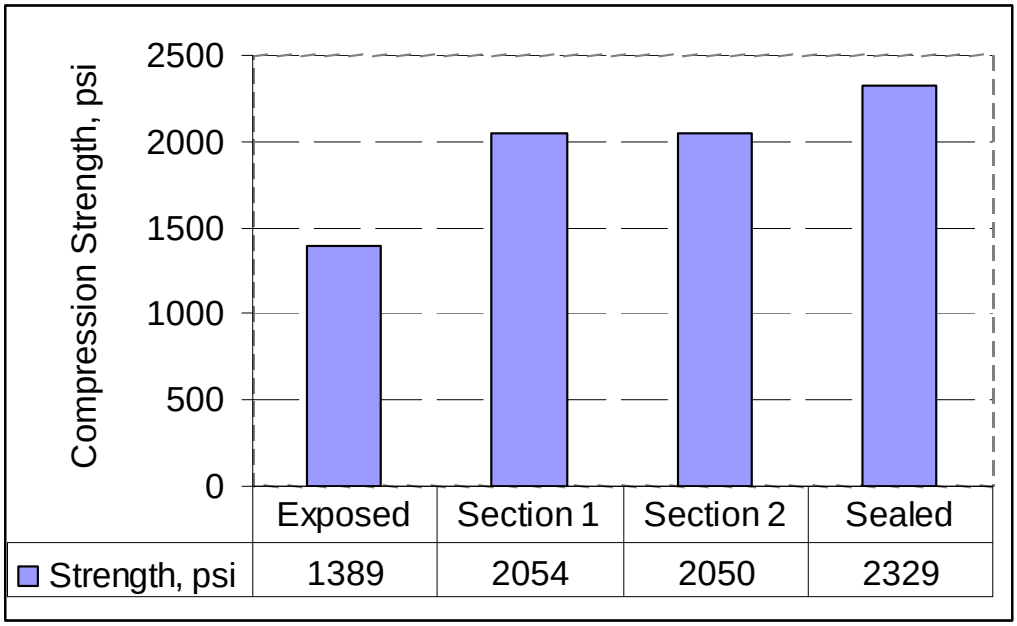

Figure M-6. Mortar Cube Strength (US 290, Oct 2006).

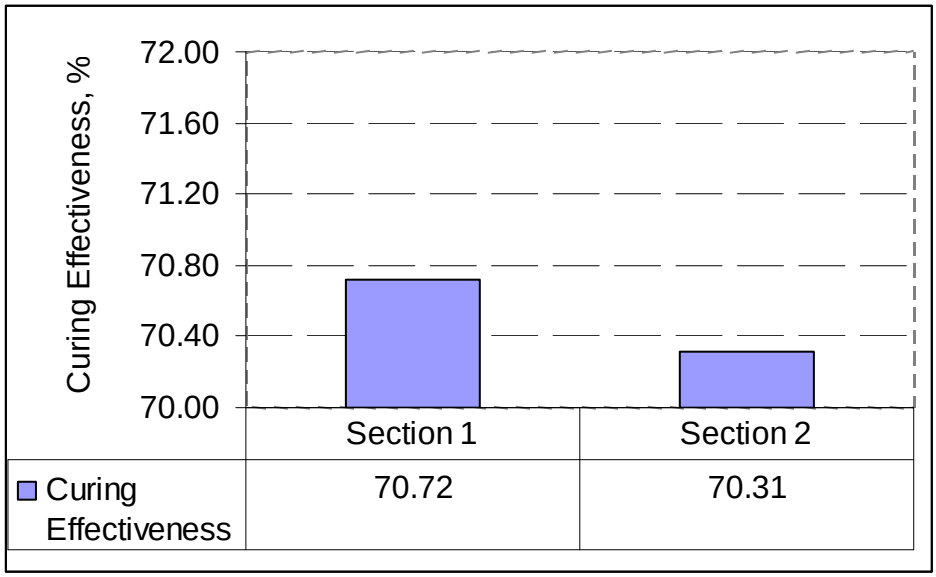

Figure M-7. Curing Effectiveness (US 290, Oct 2006).